1973

Internal Gravity Waves Of Tropospheric Origin

Michael John Curry

MICROFILMED
BY
CENTRAL MICROFILM UNIT
PUBLIC ARCHIVES
OF
CANADA
OTTAWA, ONTARIO

MICROFILMÉ
PAR LE
SERVICE CENTRAL DU MICROFILM
ARCHIVES PUBLIQUES
DU
CANADA
OTTAWA, ONTARIO

DATE

REDUCTION

OPERATOR
OPERATEUR

EXPOSURE
EXPOSITION

CANADA

NATIONAL LIBRARY OF CANADA

CANADIAN THESES

ON MICROFILM

BIBLIOTHÈQUE NATIONALE DU CANADA

THÈSES CANADIENNES

SUR MICROFILM

NL-101(1/66)

INTERNAL GRAVITY WAVES OF TROPOSPHERIC ORIGIN

by

Michael John Curry

Department of Physics

Submitted in partial fulfillment

of the requirements for the degree of

Doctor of Philosophy

Faculty of Graduate Studies

The University of Western Ontario

London, Canada

April 1973

ABSTRACT

Observations of micro-scale fluctuations in atmospheric pressure at the surface of the earth sometimes reveal the occurrence of low-amplitude sinusoidal variations in pressure. A network of three microbarographs has been operated for two years at London, Ontario (81^{o} 15' W, 43^{o} 0' N) and 145 such oscillations recorded. These oscillations are found to be due to internal gravity waves, the properties of which are examined statistically. Using the array of microbarographs as a direction finder, the sources of the waves are located and their characteristics studied. It is shown that internal gravity waves are generated in strongly baroclinic regions of the troposphere, such as frontal systems and areas of strong convection.

It is demonstrated that waves having essentially monochromatic spectra are produced in regions of severe thunderstorm activity. A model is presented of the mechanism by which these waves are generated, and it is shown that the properties of the waves observed are in good agreement with the features of the model.

ACKNOWLEDGEMENTS

The author wishes to thank his supervisor, Dr. R.C. Murty, for his continued and enthusiastic support throughout the course of this work and for his invaluable guidance and criticism during the preparation of this thesis. The author also wishes to thank Dr. D.R. Hay and Dr. J.A. Fulford for their interest and advice, Dr. R.P. Lowe for providing a copy of the Fast Fourier Transform program and for assistance with regard to its use, Dr. J.K.E. Tunaley for enlightening conversations concerning theoretical problems, and Mr. C.W. Colpitts for many interesting discussions concerning the spectral analysis.

This research was supported by the Atmospheric Environment Service (formerly the Meteorological Branch of the Canada Department of Transport). Financial assistance provided by the National Research Council of Canada and by the Government of Ontario is also gratefully acknowledged.

The author would like to express gratitude to Mr. J.L. Roxbrough and the management of Labatt's Ontario Breweries Limited for providing the location for one of the microbarographs and to Mrs. Margaret Meighen for supplying space for another.

Thanks are also due to Mr. Don Scott of the London Weather Office and to the United States Weather Bureau for providing meteorological data necessary for this work.

TABLE OF CONTENTS

LIST OF FIGURES

LIST OF TABLES

LIST OF SYMBOLS

a_n	real part of c_n
b_n	imaginary part of c_n
c	speed of sound
c_n	n^{th} complex Fourier coefficient
d	internal diameter of the microbarograph inlet tubing
e	base of Naperian logarithms
f	a function of time
$\vec{g}$	acceleration due to gravity
i	the imaginary number $\sqrt{-1}$
k	real wave number
m	molecular mass of air
n	index of Fourier components
p	pressure
p_a	ambient pressure
p_c	arbitrary constant pressure correction required during triple cross-correlation
p_i	pressure within the microbarograph chamber numbered i
p_o	amplitude of a sinusoidal pressure signal
Δp	the output of the microbarograph
Δp_+	modified microbarograph output used in triple cross-correlation
$\vec{r}$	radius vector in the x,y,z Cartesian coordinate system
s	surface of a volume of fluid

t	time
t_c	the time for which a synoptic chart was prepared
t_i	time of arrival of a wave at microbarograph number i
t_{ij}	difference in arrival times of a wave at stations i and j
t_o	time of observation of a wave
t_s	time of generation of a wave
Δt	sampling interval of microbarograph data for computer processing
$\vec{u}$	fluid velocity
$\vec{v}$	wave propagation velocity
x,y,z	axes of a Cartesian coordinate system with the z-axis normal to the surface of the earth
A	amplitude
A_n	amplitude of n^{th} Fourier component
A_s	amplitude of the oscillation in the source region
D_i	length of side number i of the triangular array of microbarographs
D_s	distance from the observing region to the source region
E_k	kinetic energy
E_T	thermal energy
F	the Fourier transform of a function f(t)
G	inverted matrix of the coefficients of the linearized perturbation equations
H	the scale height (the height of the homogeneous atmosphere) $\equiv c^2/\gamma g$
K	complex wave number
L	length of the microbarograph inlet tubing
M	mass
N	number of elements in a data vector

Q	source term matrix for the wave generation model
R	radius of the convective cell cap in the wave generation model
R_m	the gas constant
T	temperature; the total length of a data sample
$\vec{U}$	vertical velocity of the convective cell cap in the wave generation model
V	volume
Z	suffix used to denote Greenwich Mean Time (GMT)
α_i	inverse time constant for microbarograph chamber number i
β	angle of arrival of a wave at the microbarograph array
γ	ratio of specific heats
γ_{ij}	the cross-correlation function for records i and j
γ_{123}	the triple cross-correlation function
δ	the unit impulse function
ε	error terms between a data vector and its least squares model
ζ	slope of a linear data model
ζ_ℓ	least squares estimator of ζ
η	intercept of a linear data model
η_ℓ	least squares estimator of η
θ	angle of the geometry of the microbarograph array
κ	the Boltzmann constant
λ	wavelength
μ	coefficient of viscosity
ξ	the Connes apodisation function
ρ	density
σ_{ij}	cross-correlation coefficient for data vectors i and j

σ_{123}	triple cross-correlation coefficient
τ	lag of one data vector with respect to the other during cross-correlation
υ_i	auto-correlation function for record number i
υ_{3i}	triple auto-correlation function for record number i
ϕ_n	phase of n^{th} Fourier component
ψ_n	phase of n^{th} component of microbarograph output
ω	angular frequency
ω_a	cutoff frequency for acoustic waves in an isothermal atmosphere
ω_B	the Brunt-Väisälä frequency
ω_g	the cutoff frequency for gravity waves in an isothermal atmosphere
ω_n	frequency of n^{th} Fourier component
ω_o	center frequency of microbarograph amplitude response curve
ω_s	characteristic frequency of oscillations in the source region
Γ_d	the dry adiabatic lapse rate of temperature
Λ	the value of the determinant of the coefficients of the linearized perturbation equations
Π	the boxcar data window function
T	the mean period of a sinusoidal microbarographic signal
Φ	phase angle of microbarograph output
$\rightarrow$	vector sign
$\hat{}$	denotes Fourier transformed variable
$'$	denotes a perturbation variable
o	as subscript, denotes an unperturbed variable

CHAPTER I

THE FIELD OF ATMOSPHERIC PRESSURE VARIATIONS

1.1 Introduction:

The atmosphere of the earth is a body of fluid in which, because of the effects of the earth's gravitational field, the fluid density is a function of altitude. This density-stratified fluid, possessing an inherent stability which is lacking in a homogeneous fluid (Eckart, 1960), is capable of sustaining motions over a wide range of amplitudes and frequencies. Such motion results in variations in a number of atmospheric variables, including pressure, density, and fluid velocity, but is often most easily detected by measurement of changes in atmospheric pressure.

An empirically derived power spectrum for atmospheric pressure fluctuations was presented by Gossard (1960) who measured changes in pressure at the ground having periods from about 0.2 s to one week. He found that the high frequency variations were due to turbulence while the low frequency spectrum was dominated by the diurnal and semi-diurnal pressure changes, which have amplitudes up to about 5×10^{-4} times the static pressure field (Berry, Bollay, and Beers, 1945). Gossard attributed the content of the mid-frequency spectrum (periods between one minute and one hour, approximately) to pressure changes caused by convective activity and travelling pressure waves.

Pressure variations in the mid-frequency range have

amplitudes up to about 10^{-3} times the ambient field and are most readily detected by means of microbarographs -- sensitive recording barometers having either band-pass or high-pass characteristics so that pressure signals due to macro-scale atmospheric phenomena are rejected. However, pressure changes caused by large-scale motions in storms often have sufficient amplitude to be discernible on conventional barograms. Consequently, such changes, particularly those accompanying local thunderstorms, have been discussed in the literature for a number of years. These pressure traces are generally aperiodic and can be related to vertical flow patterns within the storm cell (Brooks, 1954).

The overhead tropospheric jet stream has been shown, by Herron and Tolstoy (1969) and others, to cause mid-frequency oscillations in atmospheric pressure at the ground. Some such oscillations are pictured in Figures 2 and 3. These pressure structures are typically of several hours duration and are characterized by a power spectrum which exhibits low-pass behaviour (Madden and Claerbout, 1968).

Other signals in the mid-frequency range are recorded which have a much more regular temporal structure. It is well-known, for example, that above-ground nuclear explosions can generate micro-scale pressure waves which can propagate over distances of thousands of miles. Microbarograms of such waves have been published by many authors since they were first reported by Yamamoto in 1954. One of the early records (Yamamoto, 1955) is reproduced here as Figure 1. Typical of these waves are the preliminary long period components followed by oscillations of higher frequency. Pressure waves from nuclear explosions are also characterized by group velocities of the order of the speed of sound (Yamamoto, 1968).

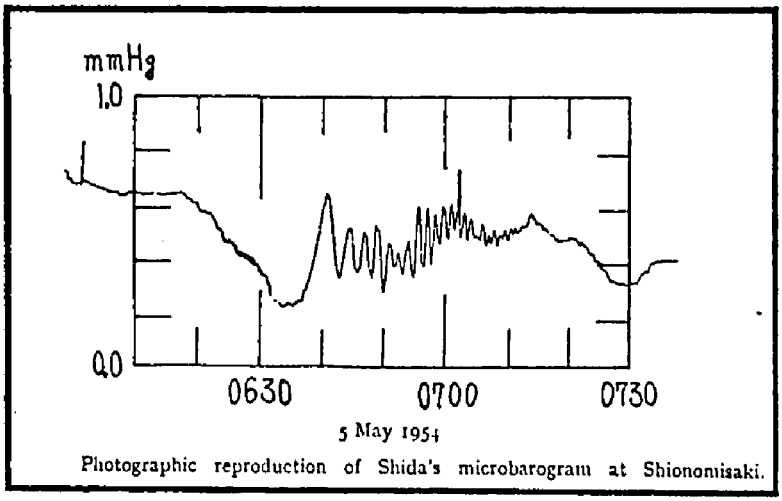

Figure 1. (After Yamamoto, 1955)

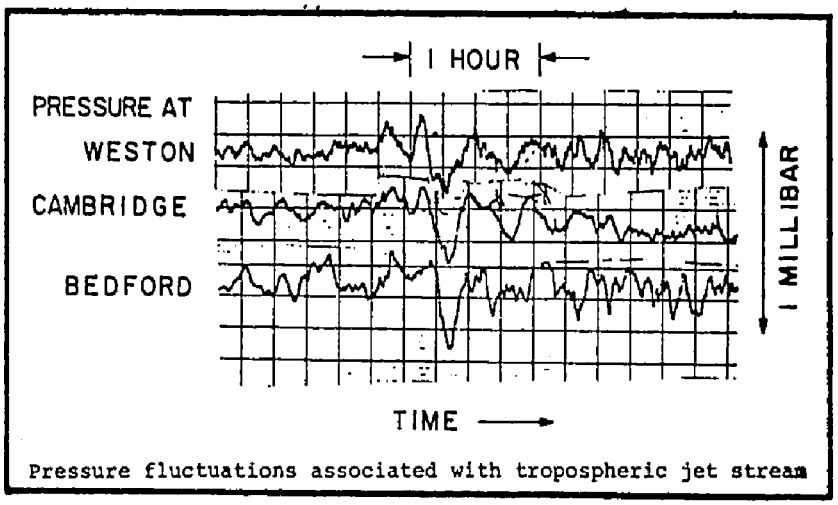

Figure 2. (After Madden and Claerbout, 1968)

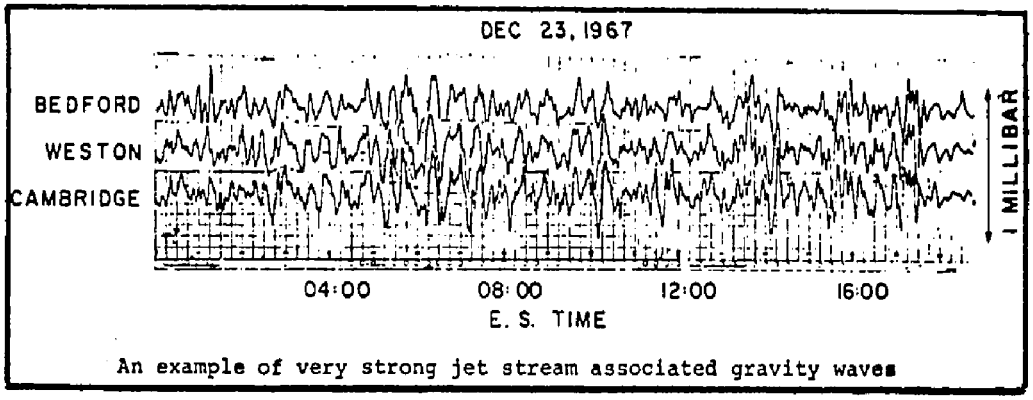

Figure 3. (After Madden and Claerbout, 1968)

This thesis is concerned with a somewhat different type of mid-frequency pressure variation, more sinusoidal in appearance than those produced by either stormy weather or the jet stream. They are of short duration -- typically less than one hour -- and have low amplitude -- usually less than 10^{-4} times the ambient pressure field. They have propagation velocities much less than the speed of sound and, hence, much less than the observed velocities of the waves generated by nuclear explosions. The period of such an oscillation is usually between five and 25 minutes. It is well known that these basically sinusoidal microbarograms are due to atmospheric acoustic-gravity waves -- travelling pressure waves having vertically transverse components. However, it is not clear where the waves originate or what mechanism is responsible for their generation (Beer, 1972).

1.2 Wave motions in the atmosphere:

A body of fluid may admit different types of wave motion. If there exists a surface of discontinuity in the fluid, waves may exist on and propagate along that surface, as do waves on a water surface bounded by air. Such waves are termed surface waves and are characterized by an imaginary wave number in the direction normal to the surface, signifying an exponential decrease in amplitude with distance away from the surface. The bulk of the fluid body may itself contain waves whose horizontal and vertical wave numbers both have real components, so that the waves can propagate throughout the fluid. These are termed body waves or internal waves.

Acoustic waves in the atmosphere are internal waves whose driving forces are those of compression and inertia. They are very

nearly purely longitudinal and propagate with a velocity which is characteristic of the supporting medium. Waves for which the forces of compression and inertia are not significantly greater than forces due to gravity and to the resulting density stratification are no longer essentially longitudinal but have vertically transverse components. Such waves are called acoustic-gravity waves. If the forces due to gravity and density stratification dominate the pressure and inertial forces, the waves are called atmospheric gravity waves, or simply gravity waves.

Other possible wave motions in the atmosphere include Rossby waves, tides, and Lamb waves. Rossby (or planetary) waves are global motions on a scale for which Coriolis forces are important. Tides are atmospheric motions having periods which are multiples or sub-multiples of the solar or lunar day and are driven by gravitational sources external to the earth-atmosphere system. Lamb waves are essentially acoustic surface waves and have been invoked by Bretherton (1969) and others in attempts to understand the propagation of waves from nuclear explosions.

A good deal of effort has been devoted to the study of acoustic-gravity waves, largely because of the suggestion by Hines (1960) that such waves may be responsible for the irregularities observed at ionospheric heights. A summary of previous observations of these waves at the earth's surface follows in section 1.3, while the theory of acoustic-gravity waves is discussed in Chapter II.

1.3 Microbarometric observations of acoustic-gravity waves:

Although small-scale oscillations in pressure at the ground were observed over two hundred years ago (FitzGerald, 1770),

intensive investigation of the oscillations did not commence until the present century. Shaw and Dines (1904) were perhaps the earliest investigators to construct a microbarograph and to attribute to travelling pressure waves the small oscillations observed in the output of the instrument.

The results of subsequent studies have been summarized by Flauraud et al (1954) and by Fullerton (1966) who described the oscillations as being regular, essentially sinusoidal, and basically a fair weather phenomenon. Fullerton gave the range of observed periods as from five to ten minutes, the average velocity as about 10 m/s, and the amplitude range as less than 500 microbars and usually between 50 and 250 microbars. Fullerton went on to describe the oscillations as lasting about one or two hours, on the average, with the extreme duration being about 3.5 hours. He also noted a diurnal variation in the number of oscillations recorded, with the majority arriving at night and the frequency of occurrence dropping sharply around 0800 local time. As a result of his investigations, Fullerton concluded that the majority of the sinusoidal microbarometric traces are due to internal gravity waves. Flauraud et al (1954) conceded that many of the early reports had been concerned with these low amplitude sinusoidal traces but reported that such waves were observed very infrequently during the course of their own investigation. The reason for their failure to observe these sinusoidal microbarograms is not clear.

One significant gap in the published literature on atmospheric gravity waves is the lack of a statistical description of a large number of waves observed in one geographical area. A compilation of data with regard to a sizeable sample of the waves would be of

considerable value in determining the significance of the variations in the parameters describing the waves as observed by various authors.

1.4 Sources of atmospheric gravity waves:

The mechanisms by which gravity waves may be generated have been discussed by many authors. Tolstoy and Herron (1969) showed that the mean power spectrum for ground level pressure changes caused by perturbations in the jet stream could be accounted for through the assumption that gravity waves provided the method for the vertical transfer of energy. The work of Tolstoy and his associates, together with the observations of others, such as Madden and Clearbout (1968), leaves little doubt that the region of the jet stream can generate tropospheric gravity waves. However, the observed waveforms of the pressure fluctuations which correlate with jet stream winds (Figures 2 and 3) are markedly different from the regular microbarograms being discussed here. It is thus unlikely that the essentially sinusoidal pressure variations have their origins in the jet stream region.

Gossard and Munk (1954) observed sinusoidal microbarometric oscillations in southern California and attributed these traces to travelling gravity waves. They noted that the oscillations often occurred after a reversal in the land-sea breeze and were sometimes preceded by a pulse. They did not advance a theory to account for the origin of the waves, other than to suggest a connection between one of their observed oscillations and a tropical storm several days earlier.

Pothecary (1954) examined a sinusoidal oscillation on conventional barograms obtained at some 30 observing stations in southern England. By noting the arrival times of the wave at the various

stations, he was able to trace the progress of the wavefront over the United Kingdom and suggested that the wave originated when a sudden outflow of cold air from an area of severe thunderstorms over Brittany temporarily blocked the previously established easterly flow of air beneath an inversion. He did not, however, study other such waves or discuss in detail the mechanism by which the wave might have been generated.

Pasechnik (1959) published a report of microscale pressure oscillations recorded in the Soviet Union in periods of calm, windless weather prior to the onset of thunderstorm rain. These oscillations had periods between five and 16 minutes, maximum amplitudes of 60 to 500 microbars, and durations of eight to 30 minutes. They were essentially sinusoidal in shape. On the basis of comparison with waves generated by a volcanic eruption, Pasechnik assumed that the waves were generated by an impulsive source but was not able to deduce the precise nature of such a source.

Challinor (1968), working in Australia, recorded sinusoidal micro-scale pressure variations in the period range one to 15 minutes. He divided his period of observation (May 1966 to November 1967) into a total of 1522 temporal units, during which he observed 66 oscillations and 61 local cold fronts. In 37 cases the appearance of the oscillations coincided, to within a few hours, with the approach of a cold front. Challinor concluded that the occurrence of the oscillations was therefore associated with the approach of the cold fronts. However, he neither identified the oscillations as being due to acoustic-gravity waves nor offered any explanation of the generating mechanism.

More recently, Jordan (1972) recorded microbarometric

fluctuations in the lee of the Rocky Mountains in Colorado and observed 13 basically sinusoidal oscillations in the period range two to ten minutes. He stated that these oscillations were due to waves which were apparently caused by locally generated signals from upper tropospheric winds, jet streams, weather fronts, thunderstorms, and severe weather, with shear the principal mechanism. However, his conclusions remain speculative and the nature and origins of the oscillations he observed are not clear.

In 1966, Pierce and Coroniti suggested a mechanism by which thunderstorm activity in the troposphere could propagate energy upwards into the ionosphere. They postulated that air rising rapidly in the updraft column of a strong thunderstorm cell might arrive at an equilibrium height (the tropopause, for example) with sufficient momentum to cause overshooting and a subsequent oscillation about the equilibrium position. They suggested that such an oscillation could generate an acoustic-gravity wave which would propagate freely in the atmosphere. Although the downward propagating wave would be strongly attenuated, Pierce and Coroniti concluded that it might retain sufficient amplitude to be detectable by microbarographs at the surface of the earth. Subsequently, Murty and Curry (1969) reported the observation of a strikingly regular microbarometric oscillation and suggested that this trace could have been due to waves generated by an isolated thunderstorm some 120 miles distant. They had only one observing station, however, and were thus unable to measure the speed or direction of propagation of the wave.

Meanwhile, Hines (1968), investigating possible energy sources for wave motion in noctilucent clouds, found tentative evidence

for suggesting that a front could act as a generator of freely propagating acoustic-gravity waves. He did not, however, draw any firm conclusions regarding the generating mechanism or generalize further from his observations.

Georges (1968), concluding a discussion of the association between short-period ionospheric disturbances and storms in the troposphere, suggested that acoustic-gravity waves could arise in the turbulence associated with strong convective action. A few months later, Baker and Davies (1969) reported a close correlation between stormy weather and ionospheric F-region waves. They too suggested that severe storms might generate upward propagating gravity waves but offered no corroboration of such an hypothesis.

Thus the problem of the origins of the low-amplitude predominantly sinusoidal pressure oscillations observed in many parts of the world remains essentially unsolved.

1.5 Summary:

Microbarograph records frequently contain sinusoidal oscillations of low amplitude and short duration. These oscillations are observed more often at night than during the daylight hours and are usually recorded during fine weather. They have been observed in many different locales, each author reporting somewhat different values for the range of periods observed. However, most periods recorded lie between one and 20 minutes.

It is generally agreed that these oscillations are caused by travelling pressure waves, and it has been suggested that they are probably caused, in particular, by internal gravity waves.

However, although several authors have suggested that tropospheric storms may play an important role in the generation of these waves, this hypothesis has not been experimentally verified.

This thesis discusses (a) the observation of a large number of low-amplitude, sinusoidal microbarometric oscillations, (b) the identification of the type of wave being observed, (c) the statistical properties of the waves, (d) the identification of the sources responsible for the generation of the waves, and (e) a simple source model for the generation of gravity waves by strong convective cells.

The observed characteristics of the waves are presented in Chapter IV and in Appendices B and C. The identification of source regions is discussed in Chapter V, while Chapter VI is concerned with the discussion of source models for acoustic-gravity wave generation by thunderstorms.

CHAPTER II

THE THEORY OF ATMOSPHERIC ACOUSTIC-GRAVITY WAVES

2.1 The isothermal atmospheric model:

The model commonly used for a preliminary development of the theory of acoustic-gravity waves is one in which the atmosphere is assumed to be isothermal, uniform in composition, and stationary in the absence of the waves. The wave motions are assumed to be adiabatic and to have sufficiently small amplitudes with respect to the static field that perturbation methods can be safely used. Under these assumptions, the atmospheric motions are governed by the equations of continuity, motion, and adiabatic state (Hines, 1960; see Appendix E).

The application of perturbation techniques to these equations results in the linear perturbation equations (see Appendix E)

$$\rho_o \frac{\partial \rho'}{\partial t} + u_z' \frac{\partial \rho_o}{\partial z} + \rho_o \nabla \cdot \vec{u}' = 0 \qquad - (1)$$

$$\rho_o \frac{\partial \vec{u}'}{\partial t} = -p_o \nabla p' - p' \nabla p_o - \rho_o \rho' \vec{g} \qquad - (2)$$

$$p_o \frac{\partial p'}{\partial t} + (\vec{u}' \cdot \nabla)\, p_o = c^2 \left[\rho_o \frac{\partial \rho'}{\partial t} + (\vec{u}' \cdot \nabla)\, \rho_o \right] \qquad - (3)$$

which describe the wave motion. It is usual (Hines, 1960; Georges, 1967) to seek wave solutions for the perturbation density, pressure, and velocity of the form

$$A \exp i(\omega t - K_x x - K_z z) \qquad - (4)$$

where the horizontal and vertical wave numbers K_x and K_z are, in general, complex. Thus the following identities apply, where the indicated operations are to be performed on one of the perturbation parameters:

$$\frac{\partial}{\partial t} = i\omega \qquad \frac{\partial}{\partial x} = -iK_x \qquad \frac{\partial}{\partial z} = -iK_z \quad . \qquad - (5)$$

Recalling that the variation of pressure with height in the isothermal atmosphere is given by

$$\frac{dp}{dz} = -\rho g \qquad - (6)$$

one can write the perturbation equations (1), (2), and (3) as (Georges, 1967)

$$\begin{bmatrix} (-iK_x gH) & (0) & (0) & (i\omega) \\ (-iK_z gH - g) & (g) & (i\omega) & (0) \\ (i\omega) & (-i\omega\gamma) & \frac{(\gamma-1)}{H} & (0) \\ (0) & (i\omega) & \left(-\frac{1}{H} - iK_z\right) & (-iK_x) \end{bmatrix} \begin{bmatrix} p' \\ \rho' \\ u_z' \\ u_x' \end{bmatrix} = 0 \qquad - (7)$$

The condition for wave solutions of the perturbation equations to exist then becomes simply that the determinant of the coefficients in (7) shall vanish.

2.2 The dispersion relation for internal waves:

Setting the determinant of the coefficients in the linearized perturbation equations equal to zero yields directly the

dispersion relation (Hines, 1960)

$$\omega^4 - \omega^2 c^2 (K_x^2 + K_z^2) + (\gamma-1) g^2 K_x^2 + i\gamma g \omega^2 K_z = 0 \quad . \quad - (8)$$

It follows from (8) that K_x and K_z cannot both be purely real and non-zero. Since internal gravity waves are observed to propagate horizontally over considerable distances, it seems appropriate to let the horizontal wave number be real: i.e.,

$$K_x = k_x \qquad - (9)$$

This is equivalent to assuming that the wave is not attenuated as it propagates horizontally. This condition then dictates the options available for the vertical wave number K_z, viz:

(i) K_z is purely imaginary. This corresponds to a description of surface waves, or interface waves, which have exponential behaviour with distance away from the surface on which they form. Such waves are discussed in section 2.3.

(ii) K_z is complex. In this case it is easy to show that the condition for a solution of (8) to exist is that

$$K_z = k_z + i \frac{\gamma g}{2c^2} \equiv k_z + i \frac{1}{2H} \quad , \qquad - (10)$$

and, for acoustic-gravity waves which are free to propagate both horizontally and vertically, the dispersion relation becomes

$$\omega^4 - \omega^2 c^2 (k_x^2 + k_z^2) + (\gamma-1) g^2 k_x^2 - \frac{\gamma^2 g^2 \omega^2}{4c^2} = 0 \quad . \quad - (11)$$

Separation of terms in k_x and k_z, together with the definitions

$$\omega_g^2 = (\gamma-1)\, g^2/c^2 \qquad - (12)$$

and

$$\omega_a^2 = \gamma^2 g^2/4c^2 \quad , \qquad - (13)$$

results in the expression

$$\frac{k_x^2}{\frac{\omega^2}{c^2}\left[\frac{1 - (\omega_a/\omega)^2}{1 - (\omega_g/\omega)^2}\right]} + \frac{k_z^2}{\frac{\omega^2}{c^2}\left[1 - (\omega_a/\omega)^2\right]} = 1 \qquad - (14)$$

This equation describes a conic section in the k_x - k_z plane -- an ellipse if $\omega > \omega_a$ and an hyperbola if $\omega < \omega_g$. No real solutions are possible for the case where ω lies between ω_g and ω_a. For the troposphere, ω_a and ω_g correspond to wave periods of about 5.1 and 5.6 minutes respectively.†

The separation of acoustic and gravity modes for internal waves in the isothermal atmosphere is shown clearly in Figure 4. This is the dispersion (or diagnostic) diagram, which consists of a set of contours of constant k_z in the ω - k_x plane. The region indicated in the upper left is the domain of the acoustic waves, while gravity waves are represented in the lower area of the diagram.

2.3 The dispersion relation for surface waves:

The implications pertaining to the propagation of phase and energy which arise because of the split into two distinct groupings

---

† Note that ω_a is always greater than ω_g, since γ is always less than two in the real troposphere.

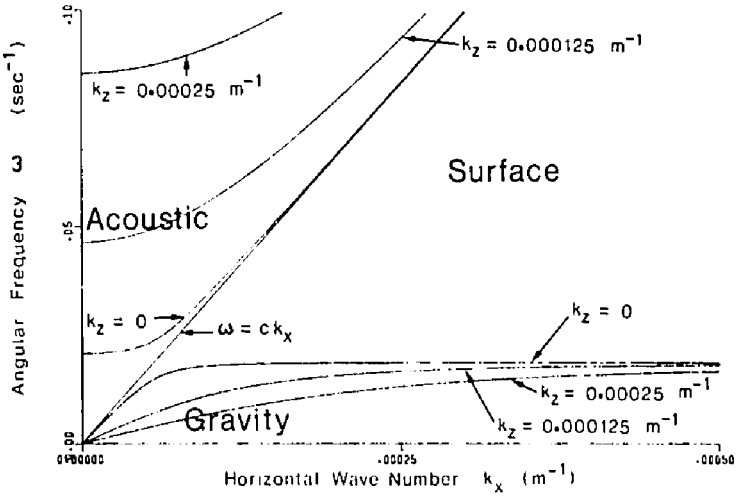

Figure 4. The diagnostic diagram for internal gravity waves.

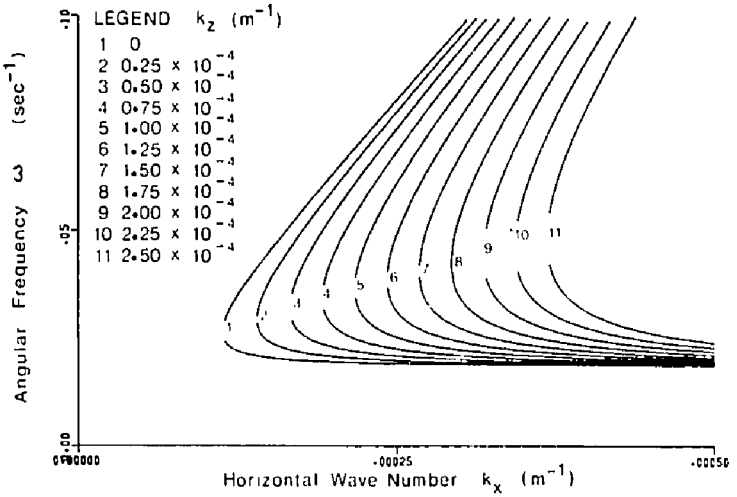

Figure 5. The diagnostic diagram for surface waves, $K_z = -ik_z$.

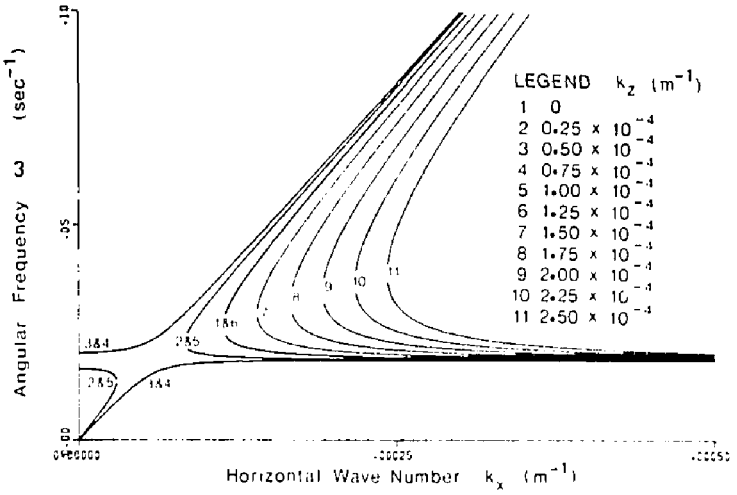

Figure 6. The diagnostic diagram for surface waves, $K_z = +ik_z$.

of waves -- "acoustic" ($\omega > \omega_a$) and "gravity" ($\omega < \omega_g$) -- have been discussed by Hines (1960) and others. It is, in a way, misleading to create such an apparent schism between these groups of waves, for gravitational effects are not absent from the "acoustic" region. Similarly, the "gravity" waves are not entirely unaffected by forces of compression, so that the forbidden region which exists between ω_g and ω_a in the isothermal model must be viewed with some latitude with respect to the real atmosphere.

Further, this range of frequencies is not prohibited for surface waves in the isothermal model. If we write

$$K_z = -ik_z \qquad - (15)$$

and substitute into the dispersion relation (8), we obtain the real dispersion relation for surface waves

$$\omega^4 - \omega^2 c^2 (k_x^2 - k_z^2) + (\gamma-1) g^2 k_x^2 + \omega^2 \gamma g k_z = 0 \quad . - (16)$$

The condition for the existence of real solutions of (16) is

$$\left[-c^2 (k_x^2 - k_z^2) + \gamma g k_z\right]^2 - 4(\gamma-1) g^2 k_x^2 \geq 0 \qquad - (17)$$

which, for $k_z = 0$, becomes

$$k_x \geq 1.1 \times 10^{-4} \ m^{-1} \quad . \qquad - (18)$$

This lower limit on k_x is seen clearly in Figure 5, which shows contours of constant k_z in the $\omega - k_x$ plane for the surface waves defined by (15). A comparison of this diagram with Figure 4 shows that the $k_z = 0$ curves

of Figure 5 approach the $k_z = 0$ curves of Figure 4 for values of k_x greater than about 2.5×10^{-4} m^{-1} and are thus asymptotic to the lines $\omega = ck_x$ and $\omega = \omega_g$.

Thus we find that surface waves in the isothermal atmosphere are subject to restrictions on ω and k_x which confine them to the region of the diagnostic diagram not occupied by the gravity and acoustic modes.

This conclusion is also reached if one admits the possibility of solutions for which

$$K_z = +ik_z \quad , \qquad - (19)$$

in which case the wave amplitude increases exponentially with distance away from the surface. The resulting dispersion curves are shown in Figure 6. The $k_z = 0$ contour is, of course, the same as that of Figure 5 and is also the curve obtained for $k_z = 1.25 \times 10^{-4}$ m^{-1}. The contours numbered 6 to 11 in Figure 6 are identical to the first six k_z curves of Figure 5. The lines for $k_z = 5 \times 10^{-5}$ m^{-1} and $k_z = 7.5 \times 10^{-5}$ m^{-1} are identical and are replicas of the $k_z = 0$ lines of Figure 4. The gaps in the curves of Figures 5 and 6 represent regions where ω is either complex or purely imaginary.

Thus surface waves, having either a positive or a negative exponential behaviour in the z direction, are restricted, in the isothermal model, to that portion of the $\omega - k_x$ plane which is forbidden to the gravity and acoustic waves. While these surface waves may play a prominent role in perturbation phenomena aloft (Naito, 1966), it is difficult to imagine a physical mechanism by which waves which propagate

along an elevated surface of discontinuity and which rapidly decay in amplitude away from that surface could be coupled into wave motions in the bulk of the lower troposphere. Nor is it easy to attach much physical significance to those modes which are amplified as they propagate downwards. It is therefore doubtful whether it is possible for surface waves to appear on microbarograms recorded at the surface of the earth. Georges (1967) leaves the question unanswered, while the work of Fullerton (1966) suggests that internal waves are the most probable cause of the regular microbarometric oscillations observed at the ground.

2.4 Limitations of the isothermal model:

The rather simple picture of the propagation characteristics of acoustic-gravity waves presented in this Chapter applies, strictly speaking, only to an isothermal, windless atmosphere. The effects of temperature and wind variations with height have been discussed by Martyn (1950), Hines (1965), Pierce (1965), Beer (1972), and many others. It appears that the effects of wind, viscous dissipation, and changes in temperature become important in the higher atmosphere but that the isothermal approximation provides a reasonably valid picture of the properties of acoustic-gravity waves in the troposphere. Nonetheless, care should be exercised in interpreting the $\omega = \omega_g$ cutoff for gravity modes as a dictum for observations made in the real atmosphere. It has been suggested (Georges, 1967) that the upper limit of $\omega = \omega_g$ for gravity waves might be replaced by the demarcation

$$\omega = \sqrt{gk_x} \qquad - (20)$$

as a boundary line for the domain of tropospheric gravity waves. However, the dispersion diagram of Figure 4 can be expected to provide a fairly reliable guide to the interpretation of observations of acoustic-gravity waves in the troposphere.

CHAPTER III

OBSERVATIONAL TECHNIQUE

3.1 A brief description of the microbarograph:

The three instruments used in this work for the recording of low-amplitude sinusoidal pressure variations were microbarographs of the type described by Kortschinski, Murty, and Curry (1971). In this device, two copper chambers are separated by a specially mounted brass diaphragm and are open to the atmosphere only through copper capillary tubing. Differences in the physical dimensions of the two chambers and the two inlet tubes cause the instrument to exhibit the characteristics of a band-pass filter, as shown in Figure 7.

The deflection of the center of the diaphragm is proportional to the difference in pressure which exists between the two chambers. Movements of the center of the diaphragm are transmuted into rotational motions of a small mirror about a vertical axis. A beam of light is reflected from the mirror onto a photocell, the output of which is amplified and applied to a chart recorder in such a way that the trace portrays, as a function of time, the pressure differential applied to the diaphragm. Details of the design and construction of the microbarograph were given by Kortschinski (1964) while an analysis of its response characteristics was performed by Curry (1968).

3.2 The response characteristics of the microbarograph:

The effect upon p_i, the pressure within the i^{th} chamber,

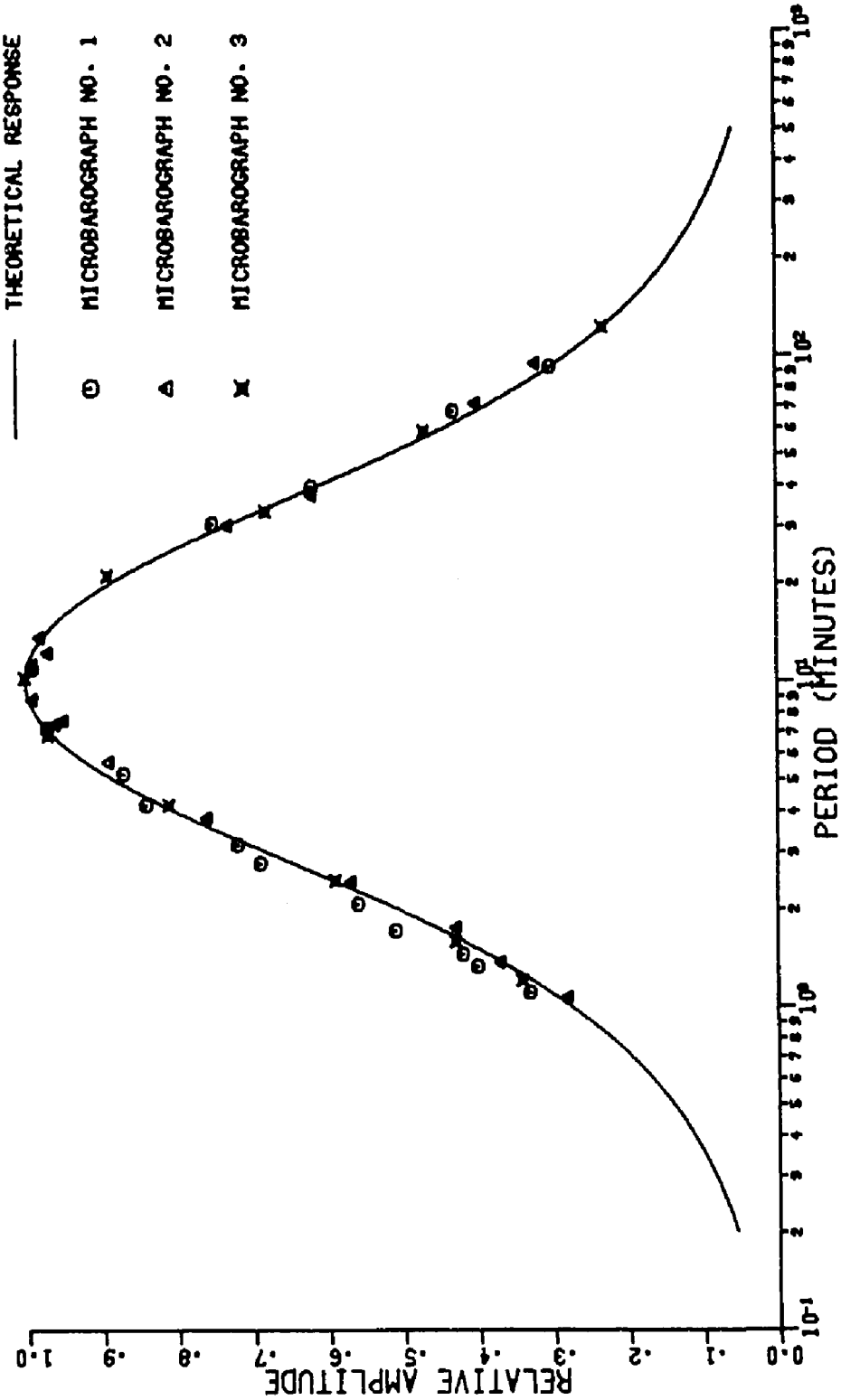

Figure 7. The amplitude response characteristics of the microbarographs.

of a pressure perturbation p_a in the ambient atmosphere is given by

$$\frac{dp_i}{dt} + \alpha_i p_i = \alpha_i p_a \qquad - (21)$$

where α_i, the inverse time constant of the i^{th} chamber-capillary combination, is given by

$$\alpha_i = \frac{\pi}{128} \frac{\kappa}{m} \frac{\rho T}{\mu} \frac{d^4}{V_i L_i} \quad . \qquad - (22)$$

The output of the instrument is then

$$\Delta p = p_1 - p_2 = \alpha_1 e^{-\alpha_1 t} \int p_a e^{\alpha_1 t} \, dt - \alpha_2 e^{-\alpha_2 t} \int p_a e^{\alpha_2 t} \, dt \quad . \qquad - (23)$$

If the perturbation pressure is sinusoidal,

$$p_a = p_o \sin(\omega t) \quad , \qquad - (24)$$

equation (23) can be solved analytically to give

$$\frac{\Delta p}{p_o} = \left(\frac{\alpha_1^2}{\alpha_1^2 + \omega^2} - \frac{\alpha_2^2}{\alpha_2^2 + \omega^2} \right) \sin(\omega t) - \omega \left(\frac{\alpha_1}{\alpha_1^2 + \omega^2} - \frac{\alpha_2}{\alpha_2^2 + \omega^2} \right) \cos(\omega t)$$

$$+ \omega \left(\frac{\alpha_1}{\alpha_1^2 + \omega^2} e^{-\alpha_1 t} - \frac{\alpha_2}{\alpha_2^2 + \omega^2} e^{-\alpha_2 t} \right) \quad . \qquad - (25)$$

The steady-state portion of (25) can be expressed in the form

$$\frac{\Delta p}{p_o} = A \sin(\omega t + \Phi) \qquad - (26)$$

where the amplitude A and the phase angle Φ are given by

$$A = \frac{(\alpha_1 - \alpha_2)\ \omega}{\left[(\alpha_1^2 + \omega^2)\ (\alpha_2^2 + \omega^2) \right]^{\frac{1}{2}}} \qquad - (27)$$

and

$$\Phi = \tan^{-1}\left(\frac{\alpha_1\alpha_2 - \omega^2}{\omega\ (\alpha_1 + \alpha_2)} \right) \qquad - (28)$$

so that the amplitude and phase response characteristics of the microbarograph are determined by the inverse time constants α_1 and α_2.

3.3 Calibration of the microbarographs:

The variable factors in the expression (22) for the inverse time constant are $\rho T/\mu$ and $d^4/V_i L_i$. The former is dependent on the temperature, pressure, and humidity of the air and thus varies with changes in the weather. For ambient temperatures between 19° C and 29° C, relative humidities between 50% and 100%, and ambient pressures between 720 mm Hg and 750 mm Hg, the value of this factor is fairly constant, changing by less than ±2%. Thus the amplitude and phase response characteristics of an individual microbarograph, having known values for V_1 and V_2, are determined solely by the lengths and internal diameters of the two capillary tubes.

Since the basis of analysis in this experiment is a comparison between Δp recordings obtained simultaneously at spatially separated locations, it was necessary to ensure that the response characteristics of the three instruments were closely matched. This was accomplished through careful measurement of the average internal diameter of the copper capillary tubing. With d^4 known, equation (22) could be solved for L_i, the length of tubing required for each particular

chamber (see Appendix F). This method made possible the matching of the three microbarographs to the extent shown in Figure 7. The values of the pertinent parameters are presented in Table I.

The three instruments were operated side by side for several weeks in order to ensure that they would produce identical traces for the same pressure event. A sample of the output obtained during this period is shown in Figure 8. The cross-correlation coefficients between pairs of records for the time period 1945Z to 2023Z (see Appendix A) are

$$\sigma_{32} = 0.997 \qquad \sigma_{31} = 0.990 \qquad \sigma_{21} = 0.992 \quad . \quad - (29)$$

The very nearly identical amplitude spectra for the three traces (see Appendix A) are shown in Figure 9.

3.4 The direction finding array:

The three matched microbarographs were separated to form a direction finding array, the geometry and particulars of which are shown in Figure 10. For a plane wave incident upon this array with angle of arrival β and velocity v, the equations which describe the recording of the wave are

$$\left.\begin{aligned} \cos(\beta - \theta_1) &= \frac{v}{D_1} t_{32} \\ \cos(\beta - \theta_2) &= \frac{v}{D_2} t_{31} \\ \cos(\beta + \theta_3) &= \frac{v}{D_3} t_{21} \end{aligned}\right\} \quad - (30)$$

where

$$\left. t_{32} = t_3 - t_2 \right.$$

TABLE I

MICROBAROGRAPH CALIBRATION PARAMETERS

Center period = 10.0 minutes = $\frac{2\pi}{\omega_o}$

Center frequency = $\omega_o = \sqrt{\alpha_1 \alpha_2} = 0.628 \text{ min}^{-1}$

Bandwidth constant $\equiv \frac{\alpha_1}{\alpha_2} = 5.97$

$\alpha_1 = 1.535 \text{ min}^{-1}$

$\alpha_2 = 0.257 \text{ min}^{-1}$

Half-power points: 3.2 and 32 minutes.

Parameter	Microbarograph Number 1	2	3	Units
Chamber Volume V_1	726 ± 3	738 ± 3	730 ± 3	cm^3
V_2	1451 ± 5	1359 ± 5	1363 ± 5	cm^3
Capillary Diameter:				
d (nominal)	0.020	0.020	0.020	inch
d^4 (nominal)	6.66×10^{-6}	6.66×10^{-6}	6.66×10^{-6}	cm^4
$\overline{d^4}$ (measured)	8.52×10^{-6}	8.14×10^{-6}	8.06×10^{-6}	cm^4
Capillary Lengths:				
L_1	59.4	55.8	55.9	cm
L_2	177.5	181.0	178.7	cm

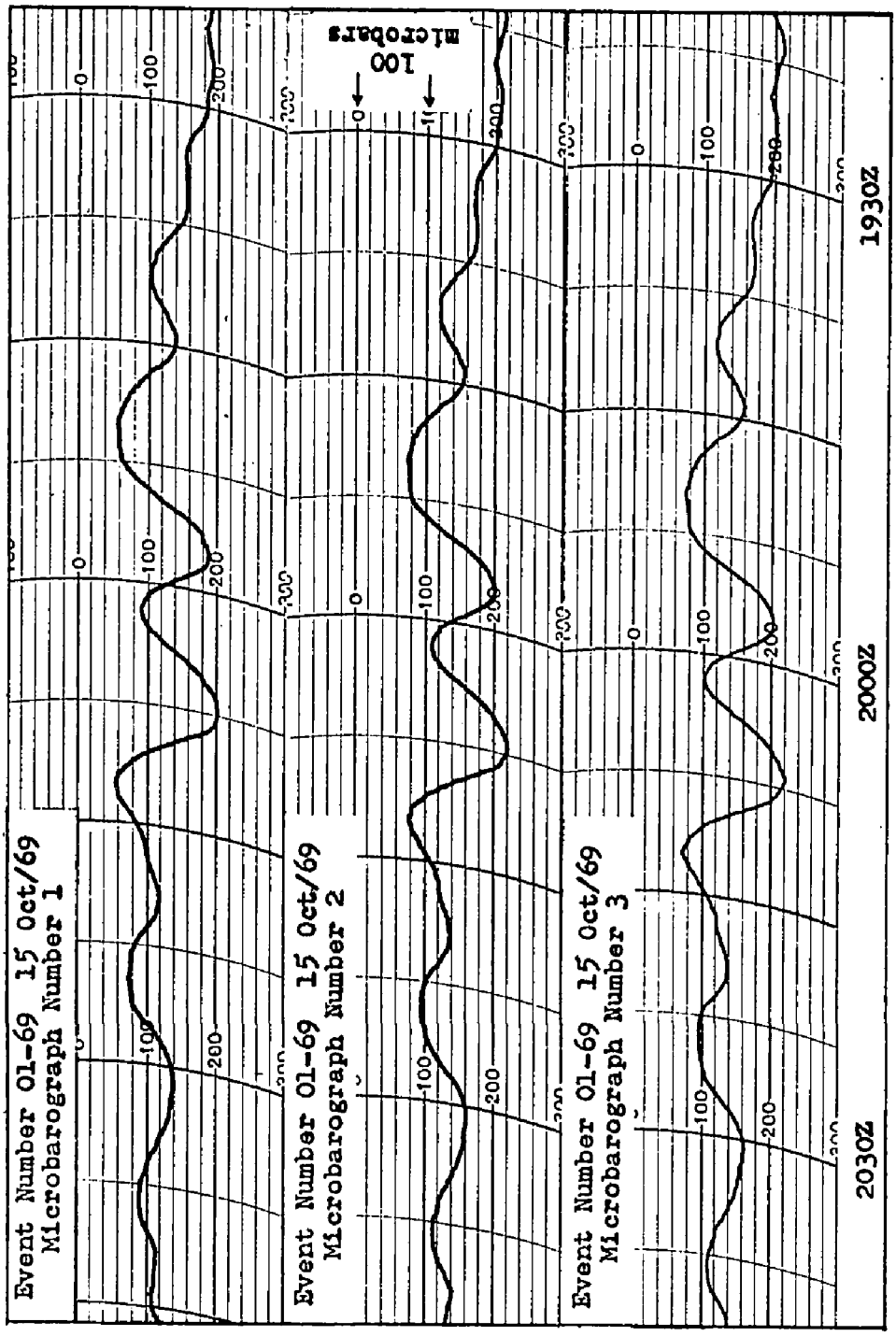

Figure 8. Microbarograms, Event Number 01-69. These traces show the same event as recorded by the three instruments at the same location.

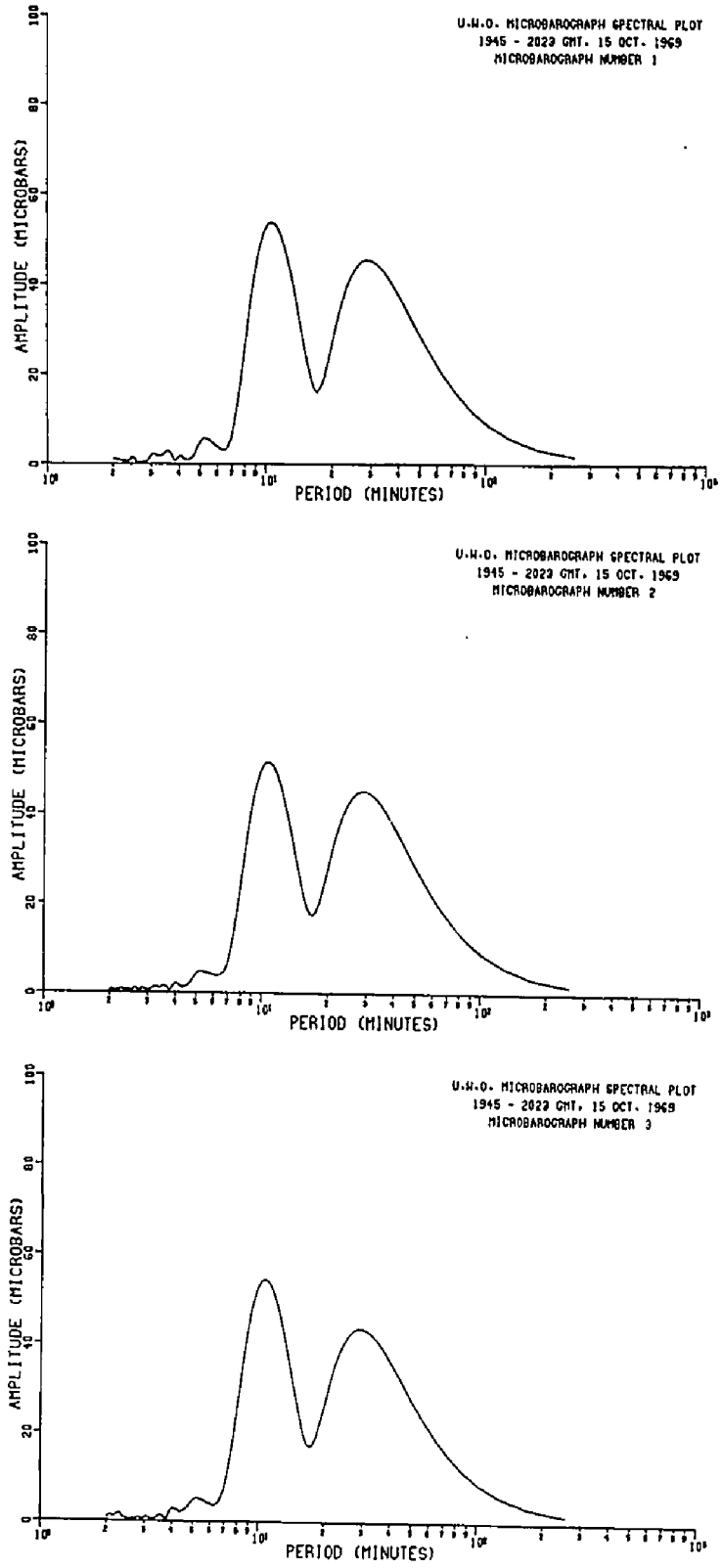

Figure 9. Amplitude Spectra, Event Number 01-69.

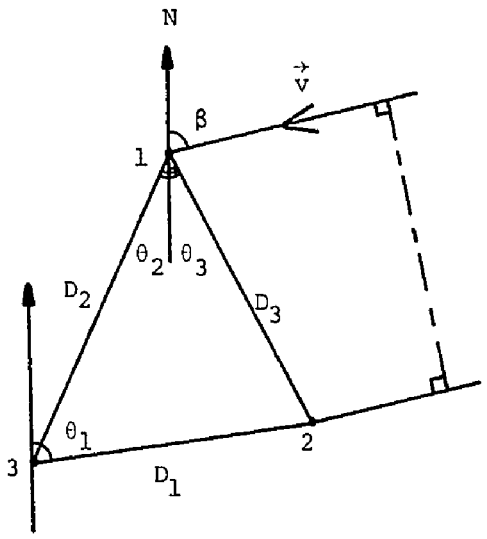

Site No. 1: Room 236, Physics Building, University of Western Ontario, London

Site No. 2: Storage area, Labatt's Ontario Breweries Limited, Simcoe Street, London

Site No. 3: Basement, Private residence, 476 Sherene Terrace, London

D_1 =	4.10 km	θ_1 =	82.8 degrees
D_2 =	4.57 km	θ_2 =	26.5 degrees
D_3 =	4.11 km	θ_3 =	29.0 degrees

(These distances and angles were measured from 1:25,000 scale maps obtained from the Canada Department of Mines and Technical Surveys. The uncertainty in distance is ±0.5% and that in angle is ±0.2 degree.)

Figure 10. The geometry of the microbarograph array.

$$\left.\begin{aligned} t_{31} &= t_3 - t_1 \\ t_{21} &= t_2 - t_1 \end{aligned}\right\} \qquad - (31)$$

and t_i is the time of arrival of the wave at site number i. Although the quantities t_i may be, in practice, difficult to determine accurately, the time difference t_{ij} represents simply the relative displacement in time between the traces recorded by microbarographs i and j caused by the spatial separation of sites i and j. Thus t_{ij} can be determined by noting the relative time displacement at which the correlation between charts i and j is maximum.

The angle of arrival β can then be calculated from equations (30) after re-arrangement into the form

$$(\tan \beta)_1 = -\left[\frac{\frac{t_{32}}{D_1}\cos\theta_2 - \frac{t_{32}}{D_2}\cos\theta_1}{\frac{t_{32}}{D_1}\sin\theta_2 - \frac{t_{31}}{D_2}\sin\theta_1}\right] \qquad - (32)$$

$$(\tan \beta)_2 = -\left[\frac{\frac{t_{32}}{D_1}\cos\theta_3 - \frac{t_{21}}{D_3}\cos\theta_1}{\frac{t_{32}}{D_1}\sin\theta_3 + \frac{t_{21}}{D_3}\sin\theta_1}\right] \qquad - (33)$$

$$(\tan \beta)_3 = -\left[\frac{\frac{t_{31}}{D_2}\cos\theta_3 - \frac{t_{21}}{D_3}\cos\theta_2}{\frac{t_{31}}{D_2}\sin\theta_3 + \frac{t_{21}}{D_3}\sin\theta_2}\right] \qquad - (34)$$

$$\beta = \tan^{-1} \frac{(\tan \beta)_1 + (\tan \beta)_2 + (\tan \beta)_3}{3} \qquad - (35)$$

The velocity v is then found by substitution of β into equations (30). Because the correlations necessary for the determination of the three t_{ij} are done over the entire extent of a wave event, the velocity v is the horizontal component of the group velocity of the wave. However, since the waves are nearly sinusoidal, the group velocity and the phase velocity will not differ greatly so that v is also a good estimate of the phase velocity of the dominant spectral component.

3.5 Summary:

Three microbarographs of the type described by Kortschinski, Murty, and Curry (1971) were assembled and their response characteristics matched to a theoretical response curve having a center period of 10.0 minutes and half-power points of 3.2 and 32 minutes. The instruments were separated to form a triangular array having sides of about four kilometers. By measuring the differences in times of arrival of a pressure wave at the three stations, it is possible to calculate the horizontal velocity and angle of arrival of the wave.

Details concerning the methods of evaluation of the t_{ij} and the accuracies obtainable in practice are discussed in Chapter IV. The particulars of the waves observed are presented in Chapter IV and in Appendices B and C. The sites of the microbarographs themselves are described in Appendix G.

CHAPTER IV

OBSERVATIONS OF INTERNAL GRAVITY WAVES

4.1 The data sample:

In order that a sizeable number of low-amplitude sinusoidal pressure oscillations might be obtained, microbarograms were recorded continuously at all three locations over a period of nearly two years -- from 14 November 1969 to 10 November 1971. The charts were manually scanned for the occurrence of wave events, defined as regular oscillations incident upon the entire array. This means that the wave event must (a) be apparently sinusoidal or nearly so, (b) appear and be identifiable on all three charts, (c) last for at least one complete period, and (d) have sufficient amplitude with respect to the background noise to permit a meaningful correlation between pairs of records. Over the two year period, 145 such events were recorded.

Since data from all three stations are necessary for the determination of the angle of arrival β and the velocity v of the wave, a malfunction in any of the instruments resulted in the complete absence of usable data for the duration of the problem. Details concerning the effective hours of operation of the system as a whole are given in Table II.

The data discussed in this chapter are tabulated in detail in Appendix B.

TABLE II

EFFECTIVE HOURS OF OPERATION OF THE MICROBAROGRAPH SYSTEM

Month	Number of Hours in Month	Hours of Successful Operation	Hours of Missing Data
Nov/69	456	427.3	28.7
Dec/69	744	637.0	107.0
Jan/70	744	739.7	4.3
Feb/70	672	666.3	5.7
Mar/70	744	702.9	41.1
Apr/70	720	606.2	113.8
May/70	744	567.4	176.6
Jun/70	720	447.3	272.7
Jul/70	744	603.9	140.1
Aug/70	744	697.1	46.9
Sep/70	720	413.0	307.0
Oct/70	744	558.0	186.0
Nov/70	720	406.8	313.2
Dec/70	744	731.7	12.3
Jan/71	744	157.5	586.5
Feb/71	672	249.0	423.0
Mar/71	744	672.5	71.5
Apr/71	720	643.0	77.0
May/71	744	592.8	151.2
Jun/71	720	402.3	317.7
Jul/71	744	374.1	369.9
Aug/71	744	713.0	31.0
Sep/71	720	517.8	202.2
Oct/71	744	731.0	13.0
Nov/71	240	240.0	0.0

Total elapsed time:	17496 hours	
Total of successful operation:	13497.6 hours	(77.1%)
Total of missing data:	3998.4 hours	(22.9%)

4.2 The seasonal variation in the number of waves recorded:

The monthly distribution of the observations of wave events is presented in Table III. The frequency of occurrence of events, as actually observed, suggests that the waves tend to occur more often during the winter months than during warmer seasons. However, if a simple linear correction is made to the frequency of occurrence to allow for the periods of time when the system as a whole was not operational (Table II), this apparent seasonal bias is reduced considerably (Table III).

It is therefore concluded that no significant seasonal variation in the frequency of occurrence of the waves can be established on the basis of these observations.

4.3 The direction finding analysis:

The evaluation of the three quantities t_{ij}, necessary for the determination of β and v, could be achieved in three possible ways:

(i) Overlaying the three charts on a light-table, adjusting them for the best apparent match among records, and measuring the relative displacements of the charts at this position of maximum correlation.

(ii) Performing three cross-correlations between pairs of records and noting the relative chart displacements for which each cross-correlation coefficient is maximum (see Appendix A).

(iii) Performing a simultaneous cross-correlation among all three records and noting the relative chart displacements at maximum correlation (see Appendix A).

It was ascertained that, since the cross-correlation coefficient is, in practice, always less than unity, method (ii) gave

TABLE III

SEASONAL DISTRIBUTION OF WAVE OBSERVATIONS

Months	Number of Waves Observed	Projected Number with no Instrument Failures
Apr - Sep	63	87
Oct - Mar	82	94
May - Oct	64	85
Nov - Apr	81	96
Jan - Mar	38	46
Apr - Jun	31	41
Jul - Sep	32	46
Oct - Dec	44	48
TOTAL	145	181

unreliable results, producing values for the three t_{ij} which did not satisfy the condition (see equation (31), Chapter III)

$$t_{31} = t_{32} + t_{21} \quad . \qquad - (36)$$

Accordingly, method (ii) was not used.

Analysis of microbarograms obtained when the three instruments were situated together revealed that the uncertainties in the t_{ij} resulting from all sources -- fluctuations in chart recorder speed, drift in the microbarograph amplifiers, errors in digitizing the records, roundoff errors in computation, and changes introduced by the microbarographs -- amounted to about ±0.15 minute when method (iii) was used and that the resulting uncertainties in β and v, for typical values of the t_{ij}, would be about $\pm 6^{o}$ and ±12% respectively. Further study of typical records, some obtained when the instruments were located together and some when they were spatially distant, showed that a trained observer using method (i) could achieve accuracies which resulted in uncertainties of $\pm 12^{o}$ in β and ±25% in v.

A sample consisting of 12 of the 145 events was chosen for machine analysis using method (iii) while all 145 events were analyzed under method (i). The results of the two methods for the 12 selected events are presented in Table IV. It is evident that the two methods give results which agree, in general, within the stated limits of accuracy and that the discrepancies are in practice usually considerably less than these limits might imply.

The results of the direction finding analysis are shown in Figures 11 and 12. The histogram of Figure 11 gives the distribution of the horizontal component of the group velocity of the waves. The mean

TABLE IV

COMPARISON OF METHODS OF SOLVING THE DIRECTION FINDING EQUATIONS

Event Number	Date	Method (i) β (deg) ±12°	Method (i) v (m/s) ±25%	Method (iii) β (deg) ±6°	Method (iii) v (m/s) ±12%
16-70	15 Feb/70	285	26	288	30
18-70	15 Feb/70	207	19	226	25
24-70	19 Mar/70	301	37	292	35
31-70	18 Apr/70	222	22	216	23
42-70	27 May/70	280	52	275	43
43-70	19 Jun/70	211	38	224	41
49-70	16 Jul/70	145	18	149	20
50-70	18 Jul/70	318	13	317	13
58-70	6 Sep/70	270	43	277	52
60-70	24 Sep/70	283	26	275	23
62-70	26 Sep/70	221	35	218	30
74-70	21 Dec/70	223	35	225	37

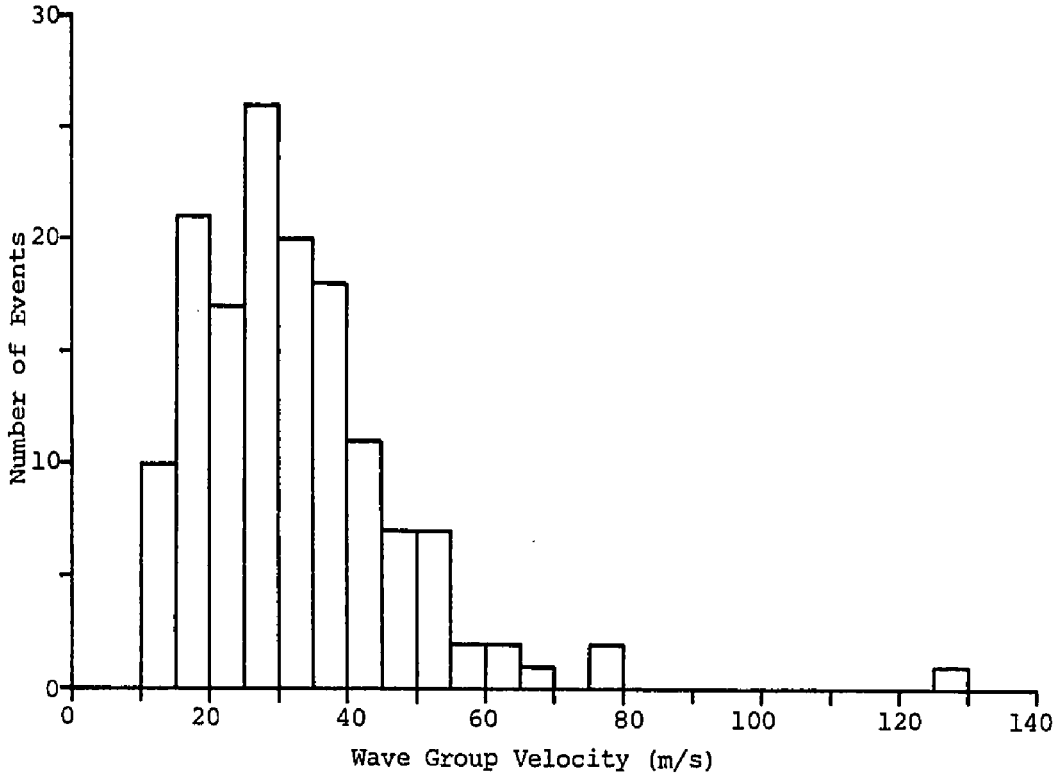

Figure 11. The distribution of the horizontal velocity of the waves.

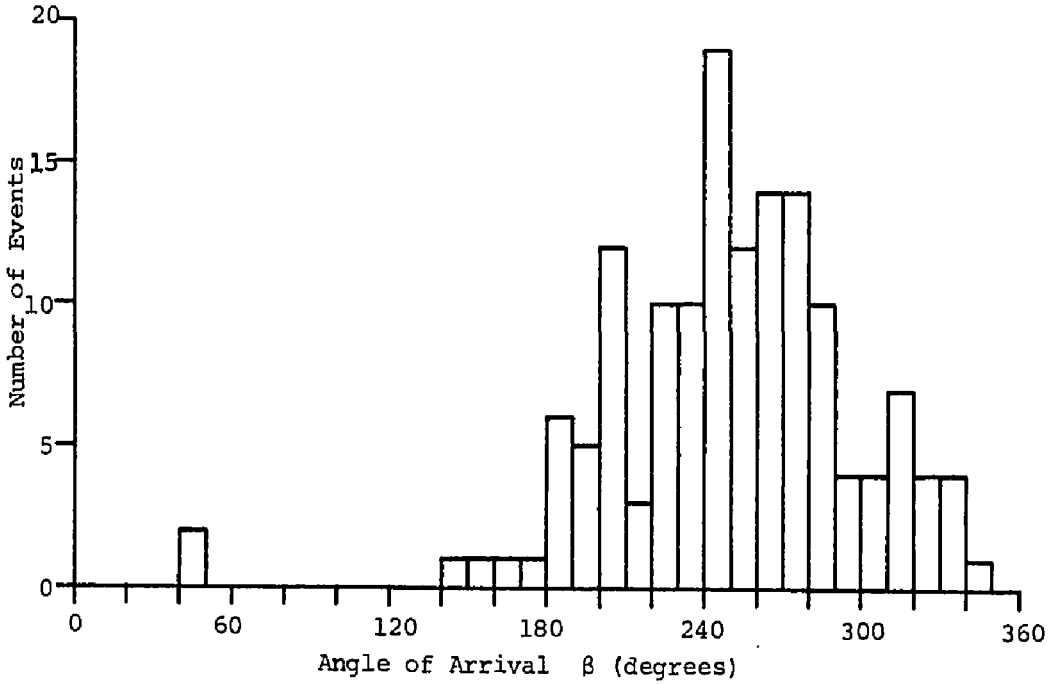

Figure 12. The distribution of the angle of arrival of the waves.

value of the velocity is 32.2 m/s and the median about 30 m/s. The observed velocities thus average about one-tenth of the speed of sound and are typical of gravity wave propagation velocities.

The distribution in the angle of arrival β (Figure 12) shows that all but a few of the waves were incident upon the receiving array from the southwest, west, or northwest. Only six of the 145 waves have a value of β less than 180°. The mean and median values of angle of arrival are both 250°.

Thus the waves are, in general, observed to approach the receiving region from westerly directions at a mean velocity of about 30 m/s.

4.4 The characteristics of the waves:

The average period of each wave observed was determined by measuring the distances between wave peaks and troughs on the three charts and taking the average of these values. The distribution of these periods is shown in Figure 13. The mean and median values are both about 10 minutes. Only 11 of the 145 waves had dominant periods less than 5.6 minutes, the cutoff period for the gravity wave modes in an isothermal atmosphere (Chapter II).

A portion of the microbarograph amplitude response curve (Figure 7) is also plotted in Figure 13. It is evident that the distribution in period falls off much more rapidly than does the instrument response curve, so that it is unlikely that the range of periods observed was significantly limited by the pass-band of the microbarographs.

The angular frequency ω, wavelength λ, and horizontal

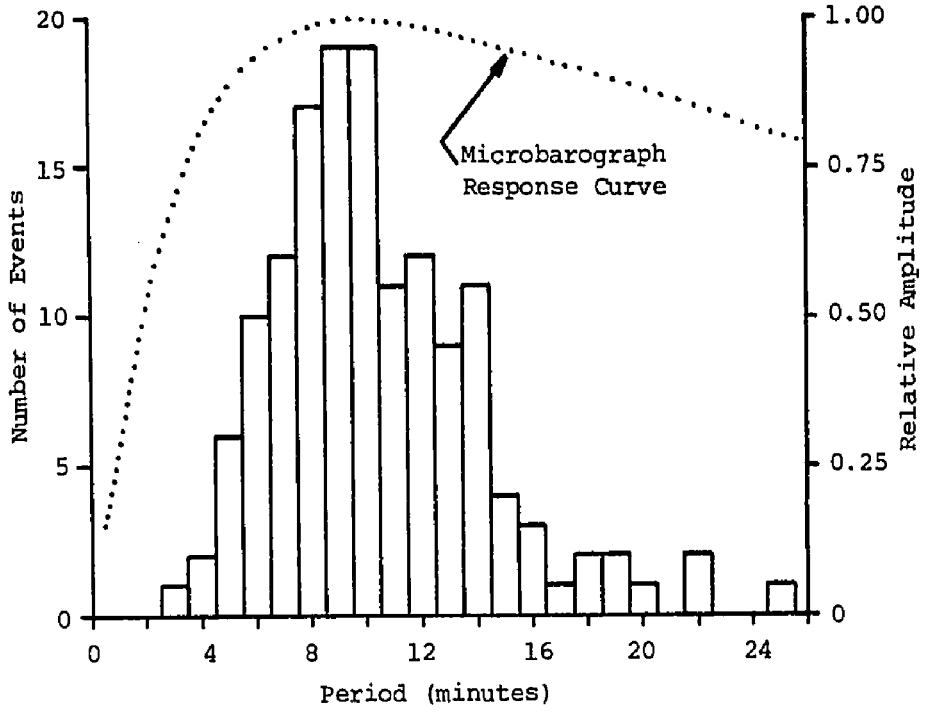

Figure 13. The distribution in mean period of the waves.

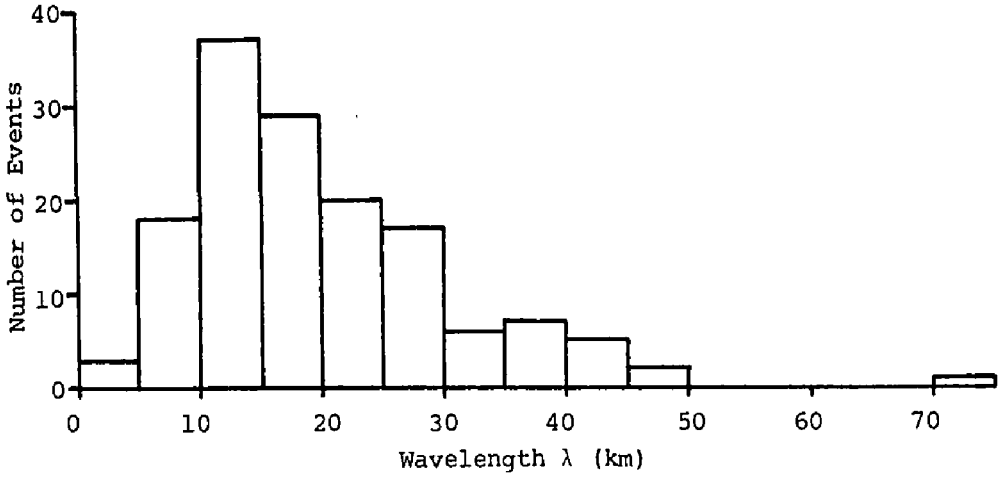

Figure 14. The distribution in wavelength of the waves.

wave number k_x were determined for each wave using the relations

$$\left.\begin{aligned} \omega &= 2\pi/T \\ \lambda &= vT \\ k_x &= 2\pi/vT \end{aligned}\right\} \qquad - (37)$$

where T is the average period of the waveform. The distribution in wavelength is shown in Figure 14. The mean value of λ is 19.8 km and the median is 16.1 km. Most of the waves have wavelengths from two to six times the longest dimension of the microbarograph array, and it is therefore not surprising that the wave events should correlate well among the three stations (see Appendix C).

The angular frequencies and horizontal wave numbers for the 145 events are plotted in Figure 15. Also shown are the lines $\omega = ck_x$, the dispersion relation for Lamb waves, and $k_z = 0$, the cutoff line for gravity waves in the isothermal atmosphere (see Figure 4, Chapter II). Eleven of the waves lie in the surface wave region of the diagram while the remaining 134 fall into the gravity wave region.

It is not certain whether the 11 waves for which $\omega > \omega_g$ are in fact surface waves in an isothermal or nearly isothermal atmosphere or rather gravity waves in an atmosphere having a non-zero vertical temperature gradient. It should be noted in this regard that all the waves lie well beneath the alternate gravity wave cutoff line $\omega = \sqrt{gk_x}$ suggested by Georges (1967).

In any case, it is evident that the pressure oscillations observed are due, in general, to internal gravity waves which travel at about 0.1 c and which approach the observing region from predominantly westerly directions.

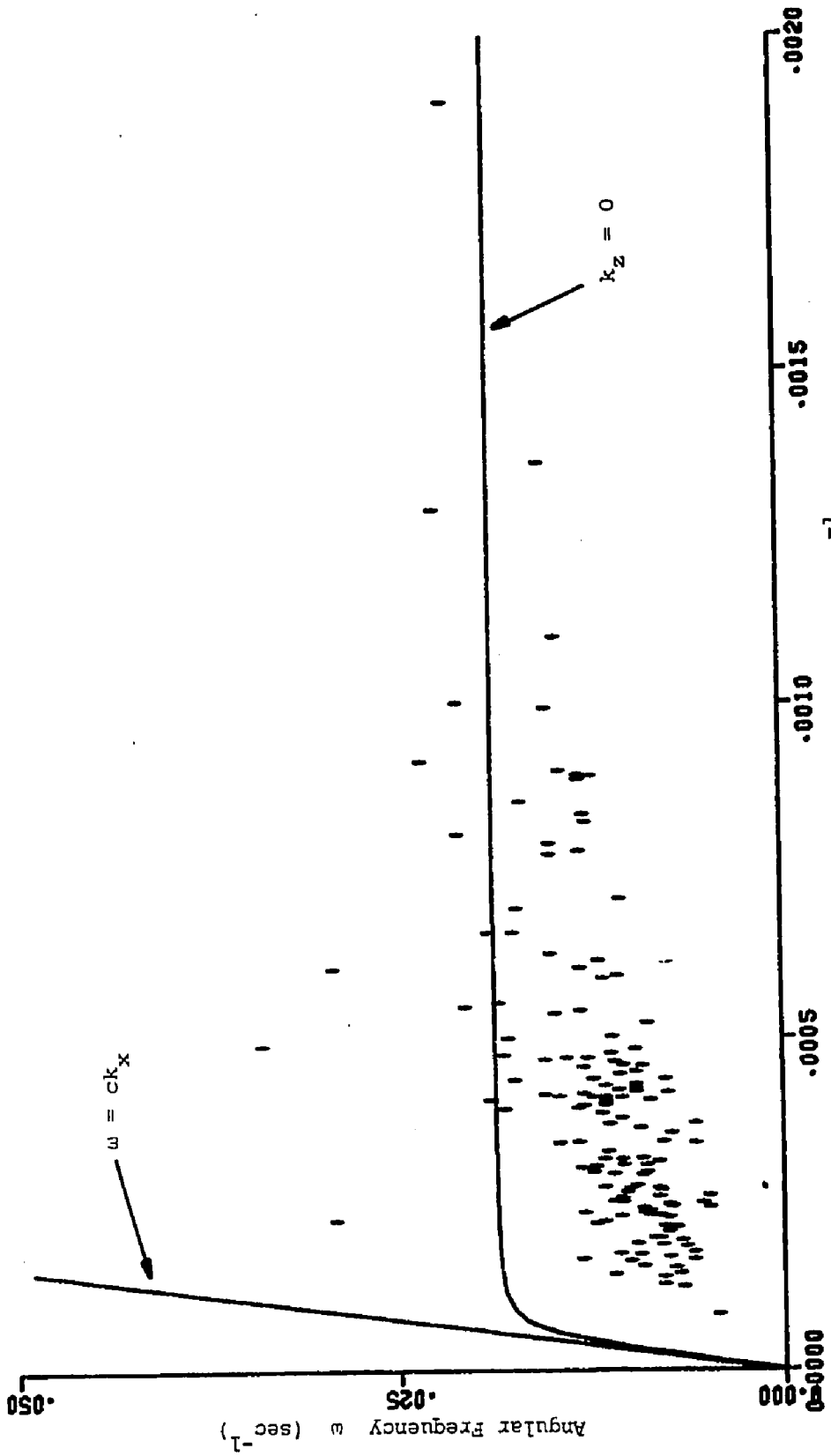

Figure 15. The dispersion or diagnostic diagram for the observed waves.

4.5 Surface weather in the observing region:

The distribution of the angles of arrival for the observed gravity waves (Figure 12) suggests a connection between the waves and weather disturbances, which usually approach the observing region from westerly directions. Accordingly, it is of interest to investigate the weather conditions prevailing over southwestern Ontario at the times when the waves were received.

The local weather conditions (Appendix B) were evaluated using the records of hourly surface weather observations made at the London Weather Office (station code XU) situated about 10 km to the east of the microbarograph array.

Figure 16 represents the total cloud cover, in tenths, observed at the times when waves were recorded. The average cloud cover at such times was 6.0 tenths, 46 of the waves being recorded under completely overcast skies, the majority of which were due to stratiform clouds (see Appendix B). Most of the waves were recorded in the absence of clouds of vertical development (Table V).

The data summary presented in Table VI clearly demonstrates that the observations of the waves are inversely correlated with stormy weather conditions at the receiving location. Fully 60% of the waves were recorded in the absence of any atmospheric obstruction to vision. Another 30% were observed during periods of fog or haze which, as are stratiform clouds, are indicators of stability in the troposphere (Saucier, 1955).

Hourly observations at the London Weather Office using a 3.5 cm radar, having a maximum range of about 150 miles, were examined for the periods during which waves were observed. It was found that

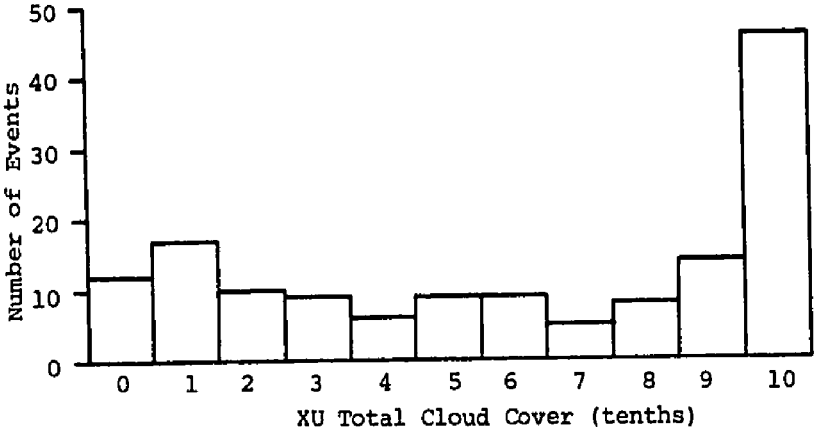

Figure 16. Local cloud cover when waves were observed.

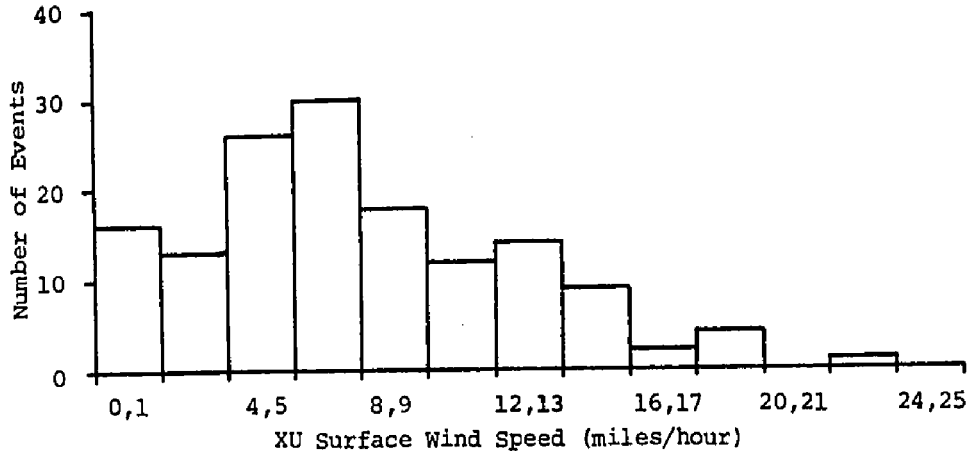

Figure 17. Local wind speed when waves were observed.

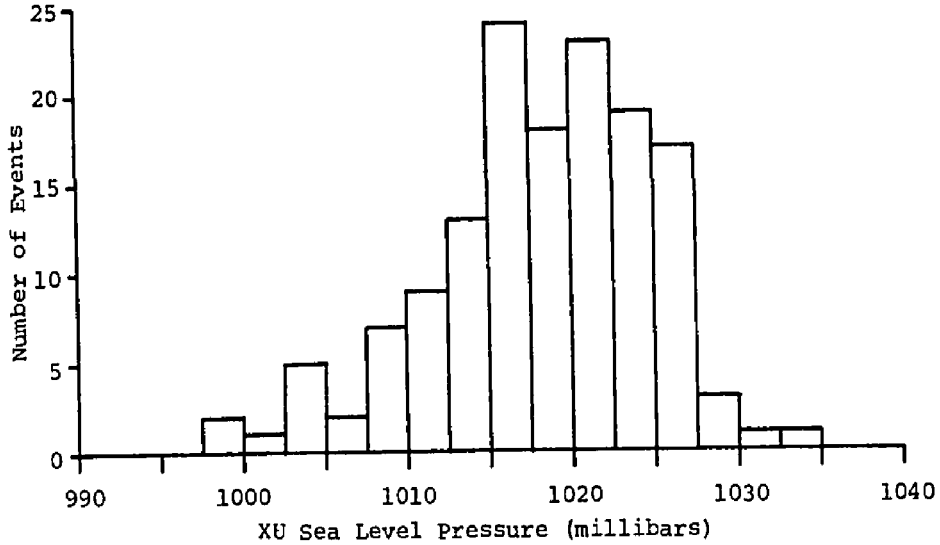

Figure 18. Local barometric pressure when waves were observed.

TABLE V

VISIBLE CLOUD TYPES, STATION XU, AT THE TIME OF OBSERVATION OF THE WAVES

Type of Cloud		Number of Events
Low Level Cloud:		
Stratus	ST	6
Stratocumulus	SC	53
Stratus Fractus	SF	7
Nimbostratus	NS	0
Medium Level Cloud:		
Altostratus	AS	8
Altocumulus	AC	47
High Level Cloud:		
Cirrus	CI	38
Cirrostratus	CS	15
Clouds of Vertical Development:		
Cumulus	CU	11
Cumulonimbus	CB	2
No Visible Cloud Reported:		16

TABLE VI

LOCAL WEATHER, STATION XU, AT THE TIME OF OBSERVATION OF THE WAVES

Weather Condition	Symbol	Number of Events
Fog	F	26
Haze	H	27
Smoke	K	1
Rain	R	0
Rain, light or very light	R-, R--	8
Snow	S	2
Snow, light or very light	S-, S--	9
Thunder (audible)	T	1
Drizzle, light	L-	1
No visible weather or obstruction to vision		87
F and/or H only		36
K only		1
S without F and/or H		2
S with F and/or H		0
S- without F and/or H		4
S- with F and/or H		5
R- without F and/or H		3
R- with F and/or H		5
T with F and/or H		1
L- with F and/or H		1
No visible weather or obstruction to vision		87

only 22% of the waves were recorded when there were any precipitation echoes observed on the radar screen.

The distribution of surface wind speeds at the times when waves were recorded (Figure 17) reveals that 50% of the waves arrived during times when the local wind speed was less than 7 miles/hour while only 21% were recorded when the surface winds exceeded 12 miles/hour. The mean wind speed at times of wave observation was also about 7 miles/hour.

The mean sea level pressure at station XU when waves were recorded was 1018 mb, the distribution having the form shown in Figure 18. In Figure 19, this value is indicated by the dashed line while the dotted line at 1015 mb indicates the average sea level pressure over the two-year observing period. The symbols Δ and ∇ mark, respectively, the maximum and minimum corrected sea level pressures observed during a given month. The circles indicate the average pressure at the times when waves were recorded during individual months while the squares indicate the monthly mean sea level pressures at station XU. There clearly exists a tendency for the waves to be recorded during periods of high barometric pressure.

It has been shown in this section that the waves, while not necessarily a fair-weather phenomenon, are associated with quiet weather characterized by high barometric pressure, light winds, lack of local storm activity, and generally stable atmospheric conditions in the observing region. It is therefore unlikely that the waves are of local origin.

4.6 The diurnal variation in the number of waves recorded:

The frequency of observation of the waves is presented as a function of local time of day in Table VII. It is evident that there is a distinct diurnal bias, nearly twice as many waves being recorded

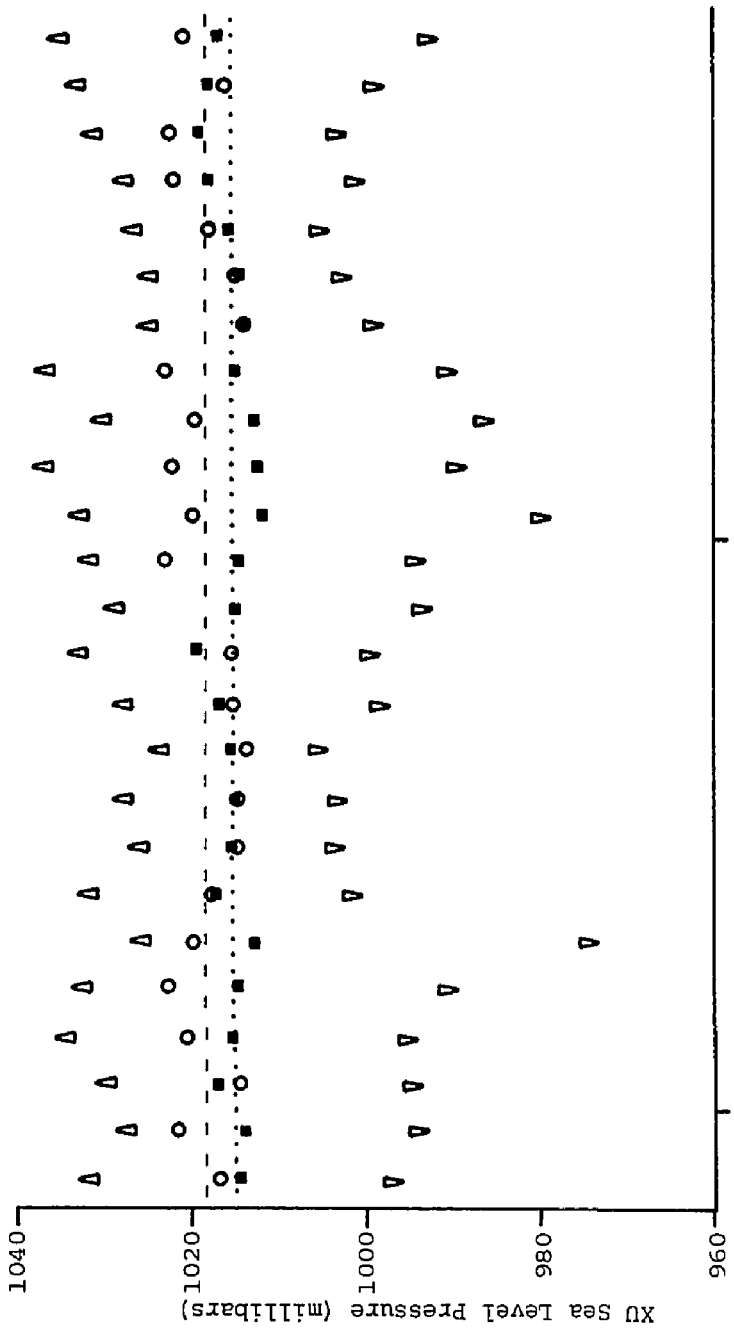

Figure 19. Corrected sea level pressure extremes, London Weather Office.

TABLE VII

DIURNAL DISTRIBUTION OF WAVE OBSERVATIONS

Time Interval (Local Standard Time)	Number of Events
0001 - 0300	25
0301 - 0600	28
0601 - 0900	16
0901 - 1200	17
1201 - 1500	9
1501 - 1800	17
1801 - 2100	15
2101 - 2400	16
0001 - 0600	53
0601 - 1200	33
1201 - 1800	28
1801 - 2400	31

Median time of arrival ≈ 0950 LST

during the early morning hours as in the afternoon.

The conclusions discussed in section 4.5 above suggest that this diurnal variation is also a bias toward stable conditions, waves being observed more often in the relatively stable night-time conditions afforded by the absence of insolation than in the afternoon when solar heating perturbs the lower troposphere. It is not considered that the observed diurnal variation is characteristic of the waves themselves.

4.7 Summary:

During an observing period of nearly two years, 145 low-amplitude sinusoidal pressure variations were observed. These were identified as being due to internal gravity waves not of local origin. The properties of the waves are summarized in Table VIII.

TABLE VIII

OBSERVED CHARACTERISTICS OF THE WAVES

1.	Waveform:	Very regular and essentially sinusoidal
2.	Amplitude:	Between 20 and 250 microbars; mean about 60 microbars
3.	Period:	Between 3 and 25 minutes; mean about 10 minutes
4.	Wavelength:	Between 3 and 74 km; mean about 20 km
5.	Velocity:	Average about 30 m/s
6.	Duration:	Average about 30 minutes; extreme 75 minutes
7.	Direction of Travel:	Predominantly from westerly directions
8.	Number of periods in waveform:	Average 3; most usual value 3
9.	Diurnal variation:	Maximum frequency of occurrence in early morning, minimum in afternoon
10.	Seasonal variation:	No significant seasonal variation observed
11.	Synoptic weather at time of observation:	
	Cloud cover:	Average six-tenths
	Cloud types:	Predominantly stratiform
	Visible Weather:	Predominantly fog or haze
	Precipitation:	Usually none
	Surface winds:	Usually light; mean about seven miles/hour
	Surface pressure:	Usually high; mean 1018 millibars
	Weather radar echoes:	Usually none

CHAPTER V

THE ORIGINS OF THE WAVES

5.1 The definition of a source region:

A gravity wave carries energy as it propagates. Therefore the mechanism which generates a gravity wave must be capable of supplying it with energy. The search for sources for the waves observed in this experiment then amounts to a search for regions where there is energy available for the generation of the waves.

The amount of energy necessary for the generation of acoustic-gravity waves can be estimated in a number of ways. It is well known, for example, that the energy released suddenly by a lightning discharge, about 10^{10} joules (Vonnegut, 1963), results in the production of acoustic waves. The figures given by Wood (1968) concerning the Great Siberian meteorite of 1908, which was observed to have generated pressure waves (Georges, 1967), imply a kinetic energy before impact of the order of 10^{12} joules. These numbers are approximately of the same order of magnitude as the estimate of 10^{10} joules made by Pierce and Coroniti (1966) as the kinetic energy of the oscillations which might generate acoustic-gravity waves at the tops of cumulus clouds. Thus one is led to expect that energies of perhaps 10^{8} or 10^{9} joules are necessary for the generation of tropospheric internal gravity waves. Further, one would expect that a not inconsiderable fraction of this energy should be available for vertical motions.

A tropospheric source region for the generation of gravity waves must therefore be a region where there is (a) a large amount of energy available, and (b) the possibility of strong vertical motion. These conditions are clearly not met under the quiescent conditions observed in the region of the microbarograph array when the waves were recorded. However, they are met in regions in which there are frontal zones or precipitating systems.

A source region, then, is an area in which there is such an energy source and which lies in a geographical location appropriate for the generation of the observed wave.

5.2 The method of source location:

Because location by triangulation is not possible with a single-station direction finder as used in this experiment, it is not possible to uniquely define a source region for each specific wave. It is, however, possible to identify a time locus of potential source regions which lie in the direction β at distances given by

$$D_s = v\,(t_o - t_s) \qquad - (38)$$

where t_o is the time of observation of the wave and t_s is the time of its generation. An examination of synoptic data then reveals whether the time history of observed tropospheric phenomena is such that a potential source of energy inhabited any of the possible source regions at an appropriate time.

This method was applied to all 145 wave events. The primary source of synoptic data lay in the surface charts prepared by the Central Analysis Office of the Canadian Weather Service. These

charts are issued for the hours 0000Z, 0600Z, 1200Z, and 1800Z daily and are polar stereographic projections drawn to a scale of 1:20,000,000. They cover the major portion of the North American continent. Also of value were 1:10,000,000 scale surface charts compiled at the Toronto Weather Office for the synoptic situation at 1800Z daily. United States Weather Bureau daily maps were also available in some instances.

The charts were carefully scanned for events of meteorological significance in the region defined by β, D_s, and $t_s = t_c$, the time for which the chart was drawn. Interpolation between charts was possible in most cases. If one of the possible source regions coincided in time and space with a region in which there was an appropriate source of energy, that region was identified as the source of that particular wave event. If no such coincidence was found, the wave was identified as having no apparent source.

Particulars of the sources located in this manner are given in Appendix B.

5.3 Example 1: A wave with no apparent source:

The wave recorded at approximately 2115Z on 19 March 1970 (Figure 20) was the longest observed during the two year period. At 1500Z the London Weather Office had reported a ceiling of 800 feet with a cloud cover of 4/10 stratus fractus. The visibility was three miles in haze, the wind was from the east at 11 miles/hour, and the temperature and dew point were 36° F and 29° F respectively. By 2100Z (1600 LST) the cloud had modified to 1/10 cumulus and the cloud base had lifted to 3500 feet. The visibility was essentially unlimited, the wind was still from the east at 15 miles/hour, and the temperature and dew point were

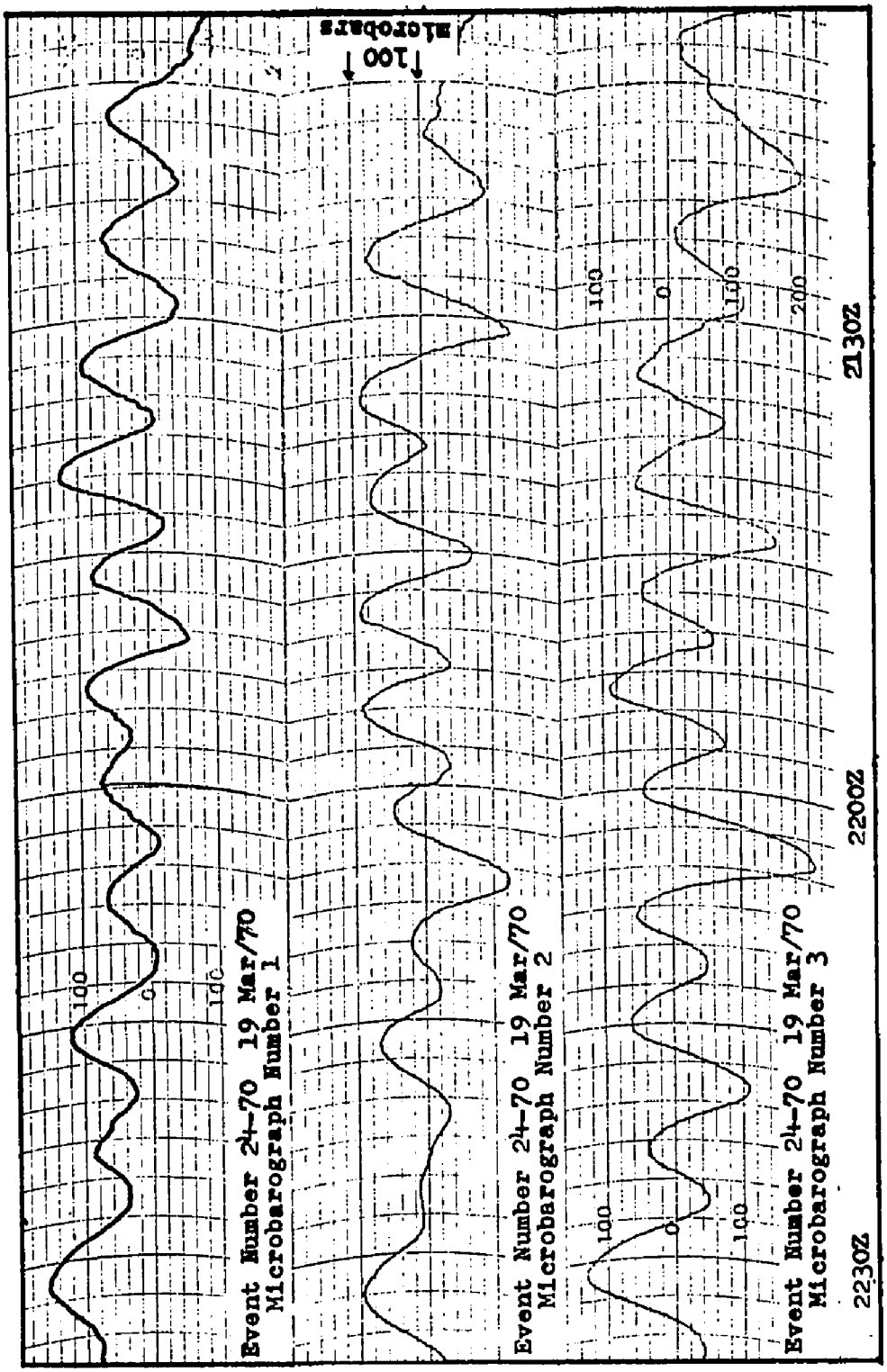

Figure 20. Microbarograms, Event Number 24-70.

46^{o} F and 29^{o} F respectively. The wave was thus recorded under quiescent local conditions.

The maximum cross-correlation coefficients for the microbarograms of Figure 20 are (see Appendix A) $\sigma_{32} = 0.869$, $\sigma_{31} = 0.749$, and $\sigma_{21} = 0.728$, indicating that the wave maintained its structure fairly well over the dimensions of the receiving array. The values of v and β, as determined using method (iii) (Chapter IV), are 35 m/s ± 12% and $292^{o} \pm 6^{o}$. The average period T of the wave, as determined by measuring the distances between peaks and troughs on the charts, was found to be 7.2 ± 0.7 minutes. The amplitude spectra (Figure 21) show a dominant component at a period of about 7 minutes, having a mean amplitude of about 60 microbars. The values of ω and k_x, computed for this seven minute component, are 1.5×10^{-2} s^{-1} and 4.2×10^{-4} m^{-1} respectively, so that the wave falls well within the gravity wave region of Figure 15.

The plotting of the locus of source regions is done in the manner shown in Figure 22, where the shaded areas indicate possible source regions for 0300Z, 0900Z, and 1500Z. The size of each shaded area is determined by the uncertainties in β and v. The errors involved in plotting directions as straight lines on the polar stereographic projection are not large for the range of distances involved in this work, as evidenced by Figure 23. A true bearing of $292^{o} \pm 6^{o}$ is shown by the curved unbroken lines. The straight line approximation is indicated by the dashed lines. The distance scale is the same as that of Figure 22.

The quantities selected for study using the synoptic charts included pressure, wind speed and direction, amount of cloud,

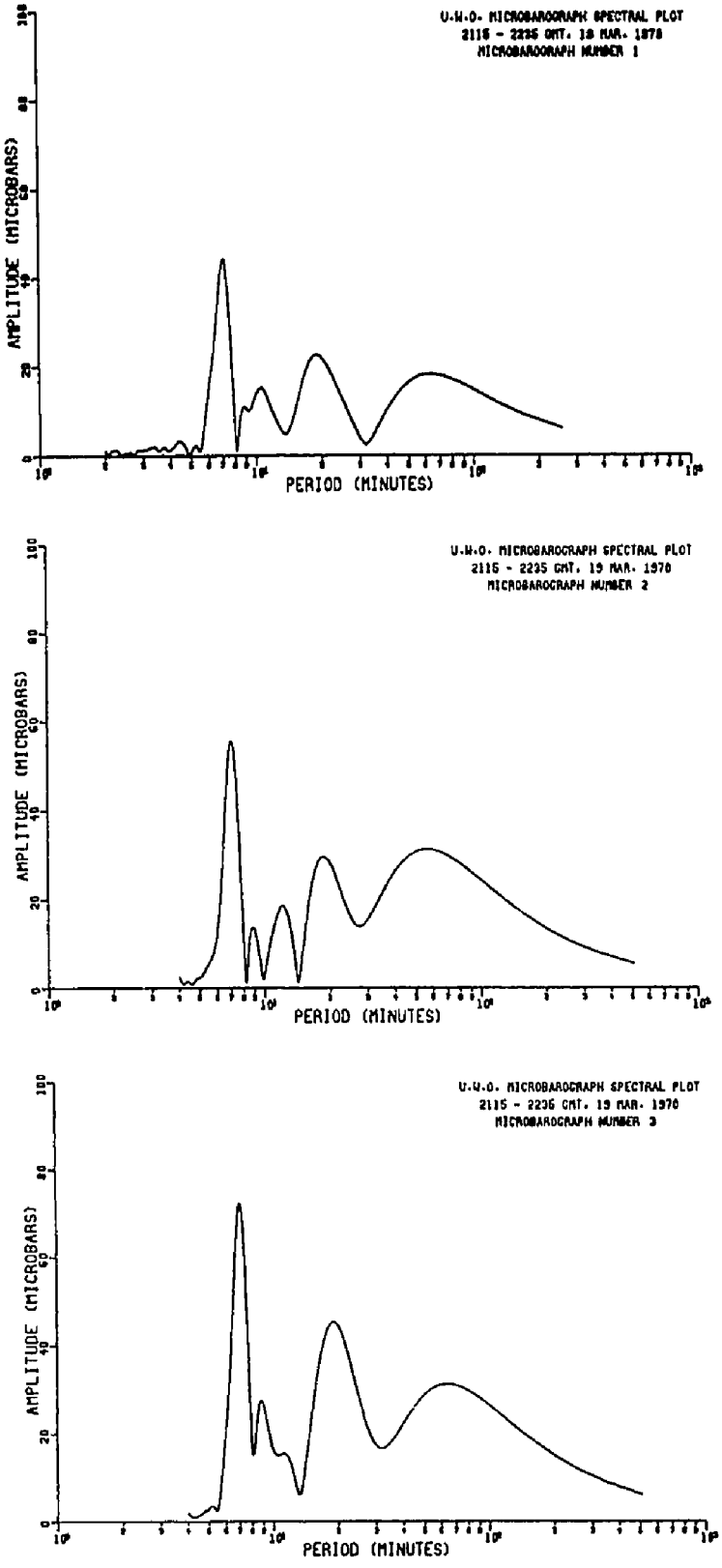

Figure 21. Amplitude spectra, Event Number 24-70.

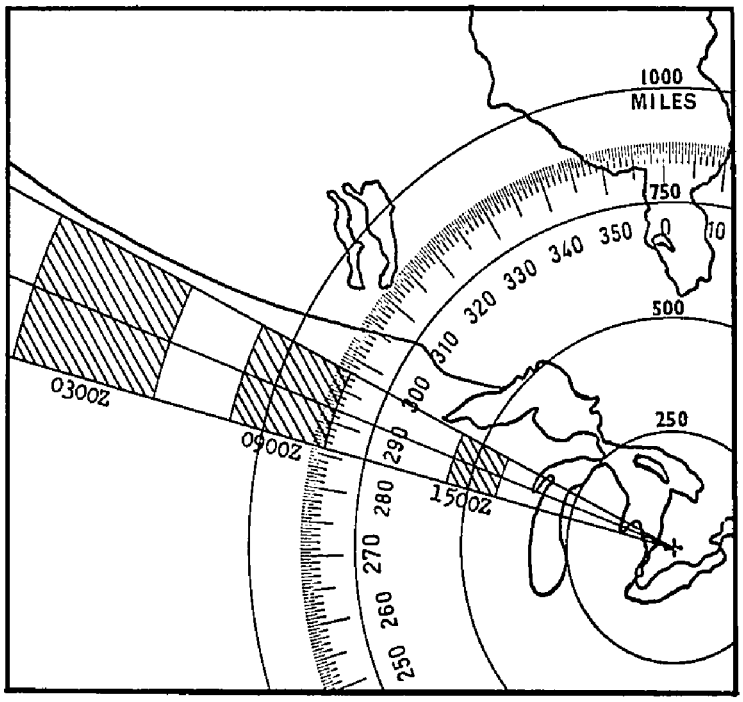

Figure 22. The plotting of possible source regions.

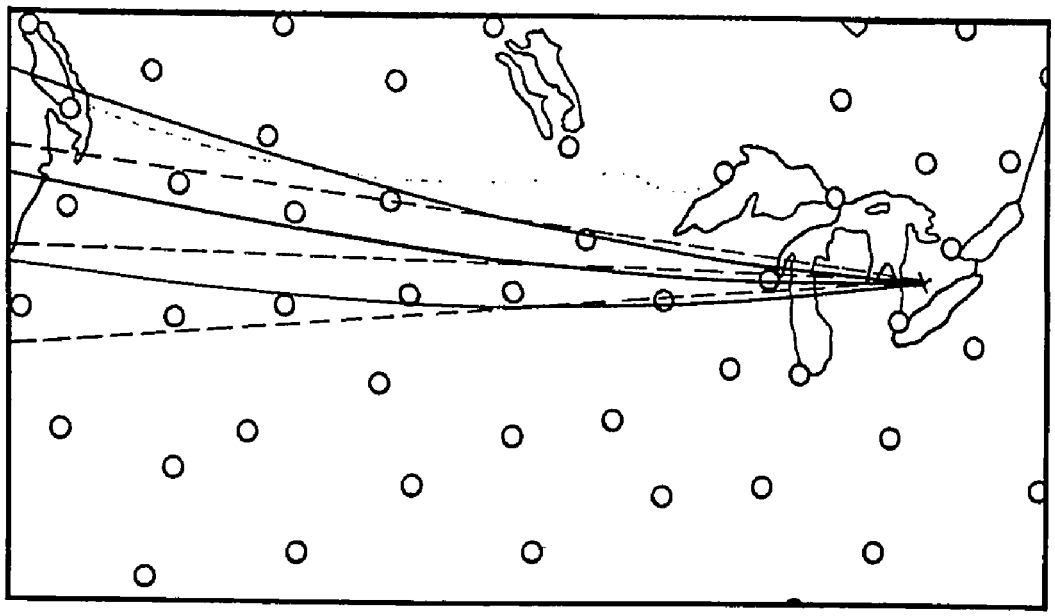

Figure 23. The plotting of directions on the polar stereographic chart.

precipitation and obstructions to vision (shown in the plotting symbols as present weather and recent weather), and the positions of frontal zones. This information for Event Number 24-70 is shown in Figures 24 to 27 which give synoptic data for the period 0000Z to 1800Z on 19 March 1970. Although cyclogenesis along the Maritime front resulted in stormy weather in the southern United States, the locus of possible source regions passes through anticyclonic conditions over the prairie regions of the northern U.S. Light winds, predominantly clear skies, high surface pressures, and a lack of precipitation are found within the possible source regions. Thus no tropospheric source of energy for the generation of the wave is evident and the event is labelled "No Apparent Source" (see Appendix B).

5.4 Example 2: Waves generated near a frontal zone:

A somewhat different situation emerges in the case of the waves of 12 September 1971 (Figure 28). Three waves, Event Numbers 44-71, 45-71, and 46-71, were recorded at 0550Z, 0640Z, and 0730Z respectively. Analysis using method (i) gave the wave velocities as 15 m/s, 15 m/s, and 14 m/s (± 25%) respectively and the angles of arrival as 204°, 201°, and 195° ($\pm 12^{\circ}$) respectively. These values suggest the possibility that the three waves may have had a common origin.

The synoptic data for 1800Z on 11 September (Figure 29) show that a ridge of high pressure covered much of the central part of North America but that strong vertical motions, indicated by the presence of a frontal zone, thunderstorms, and showers, were occurring several hundred miles to the south of the observing region. It is this active region which is identified as the source of the three waves, as

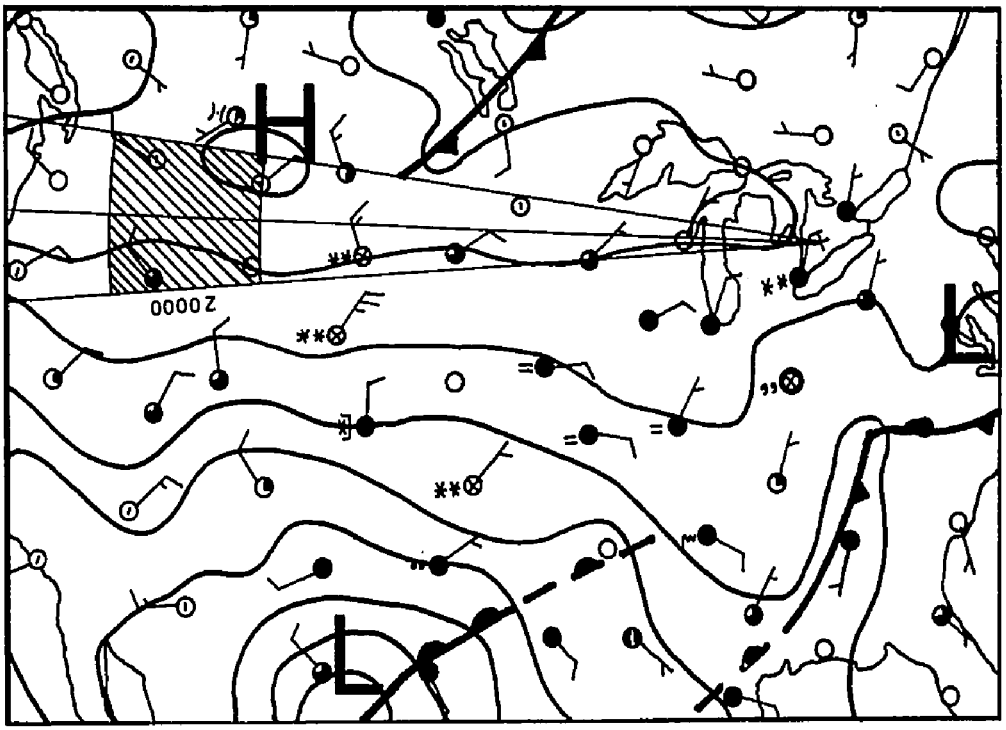

Figure 24. The surface chart, 0000Z 19 March 1970.

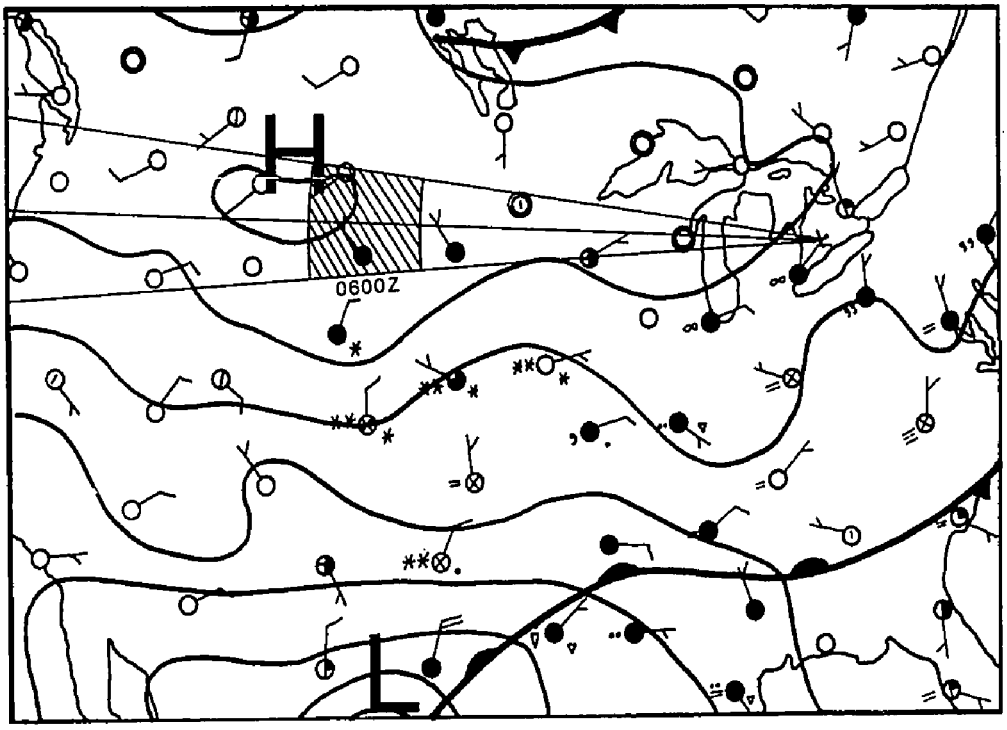

Figure 25. The surface chart, 0600Z 19 March 1970.

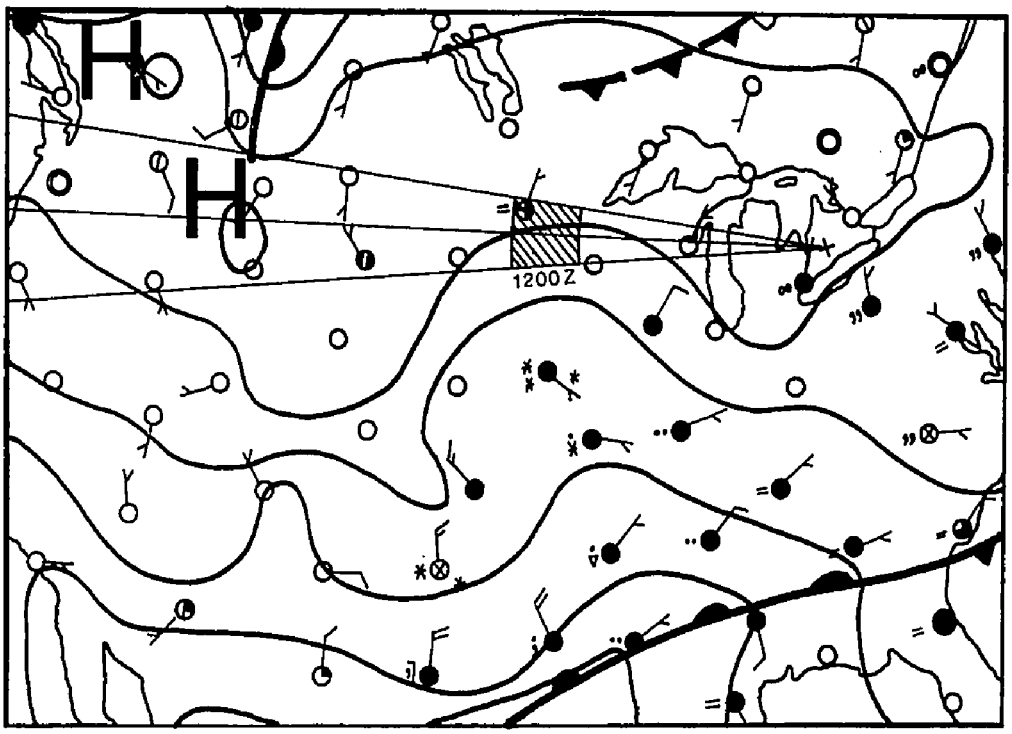

Figure 26. The surface chart, 1200Z 19 March 1970.

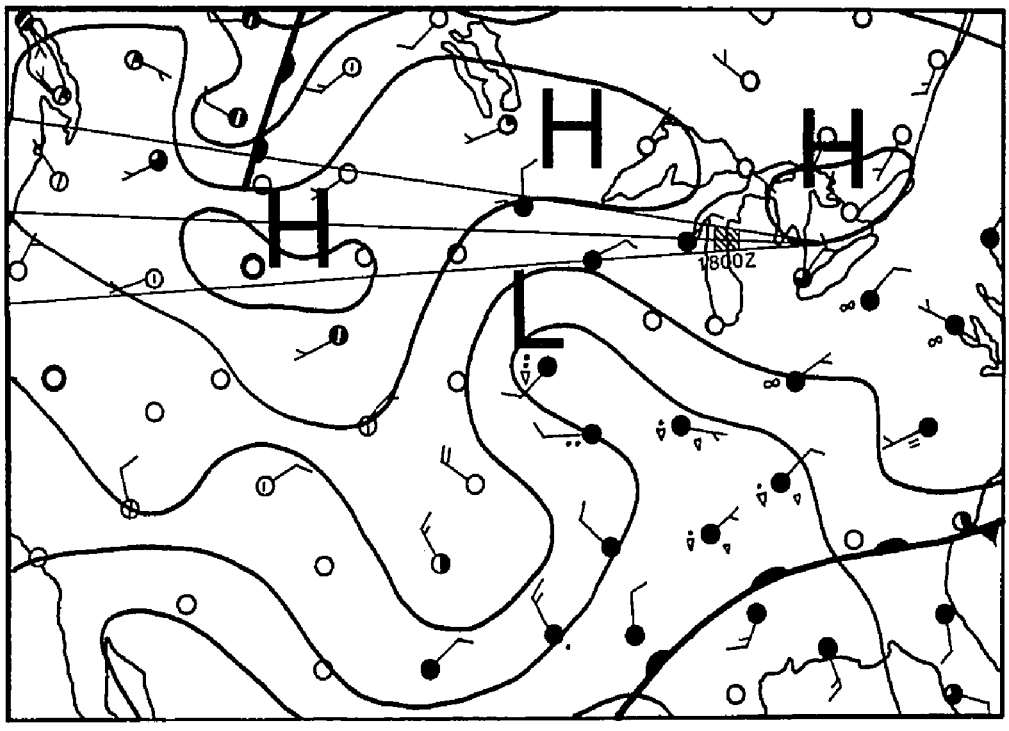

Figure 27. The surface chart, 1800Z 19 March 1970.

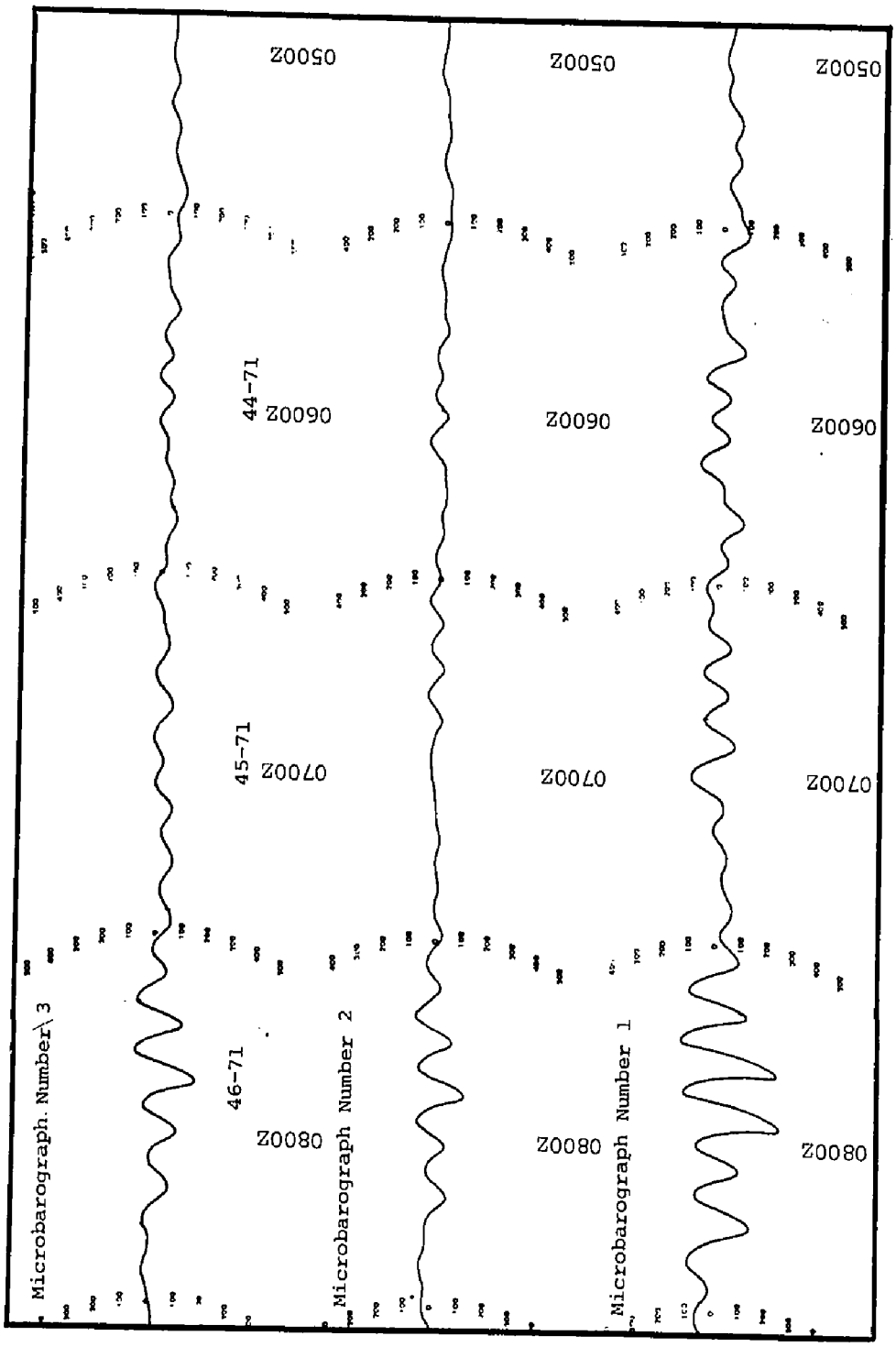

Figure 28. Microbarograms, 12 September 1971.

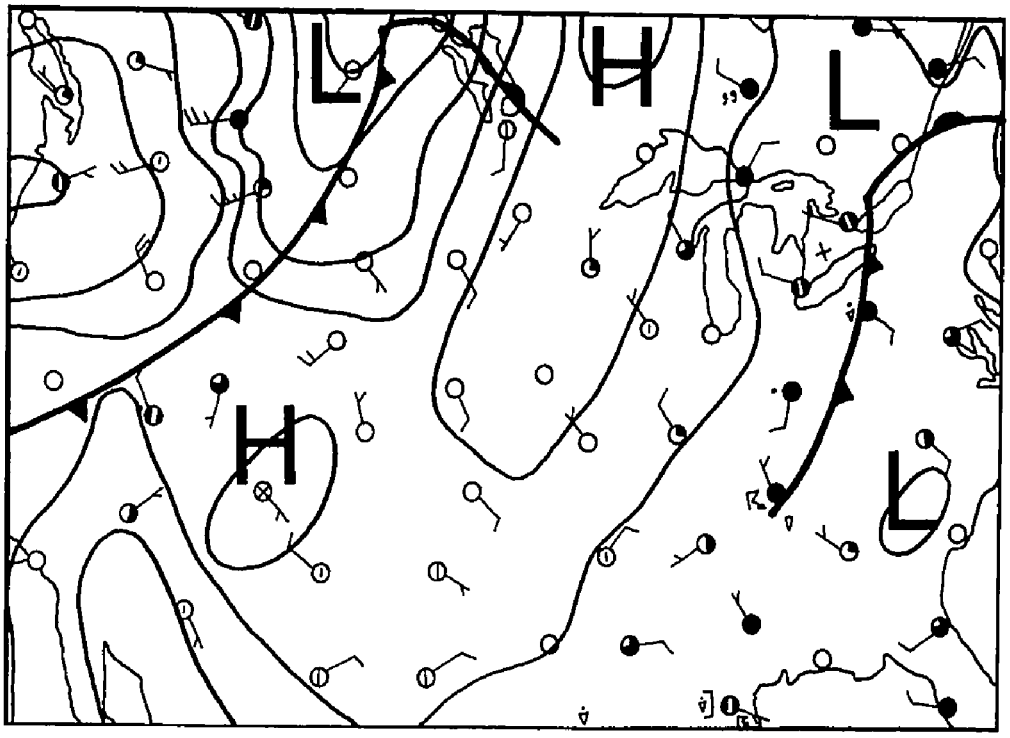

Figure 29. The surface chart, 1800Z 11 September 1971.

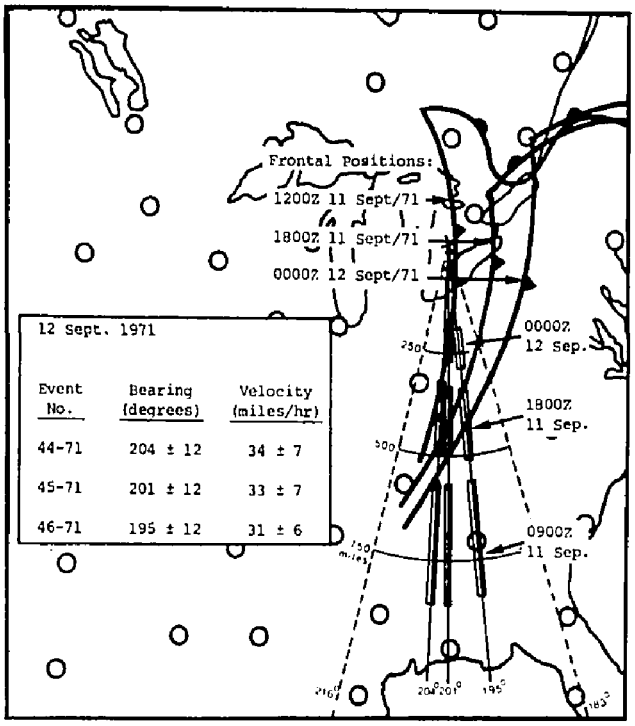

Figure 30. Identification of the source region for the waves of 12 September 1971.

shown in Figure 30 where bars are used to delineate the extent of some possible source regions along the lines drawn in the directions of the three β values. The dashed lines indicate the uncertainty limits in β of 204 + 12 degrees and 195 - 12 degrees. The heavy solid lines mark the frontal positions at 1200Z and 1800Z on 11 September and at 0000Z on 12 September.

It is apparent that all three waves could have originated in or near the frontal region within a few hours of 1800Z on 11 September. Although the front is identified on the synoptic charts as a cold front, it is clear that its motion was slow between 1800Z and 0000Z so that it may have had a somewhat different character for a time. The formation of thunderstorms in the area is indicative of a considerable input of energy and strong vertical motion which presumably could act as a wave generator, possibly in the manner suggested by Pierce and Coroniti (1966).

Thus a source region is identified, having the following characteristics (see Appendix B): (a) Cold front, (b) Not near cyclonic wave, (c) Generally receding (although perhaps very slightly) from the receiving array, (d) Near a low pressure area, (e) Thunderstorms and showers in the area, and (f) Mean distance about 450 miles.

Although the identification of individual sources in this manner is somewhat circumstantial, similar analyses applied to the 145 wave events produce interesting correlations which are discussed in detail in Chapter VI.

5.5 Waves generated by thunderstorms:

Event number 49-70 (Figure 31) was recorded at approxi-

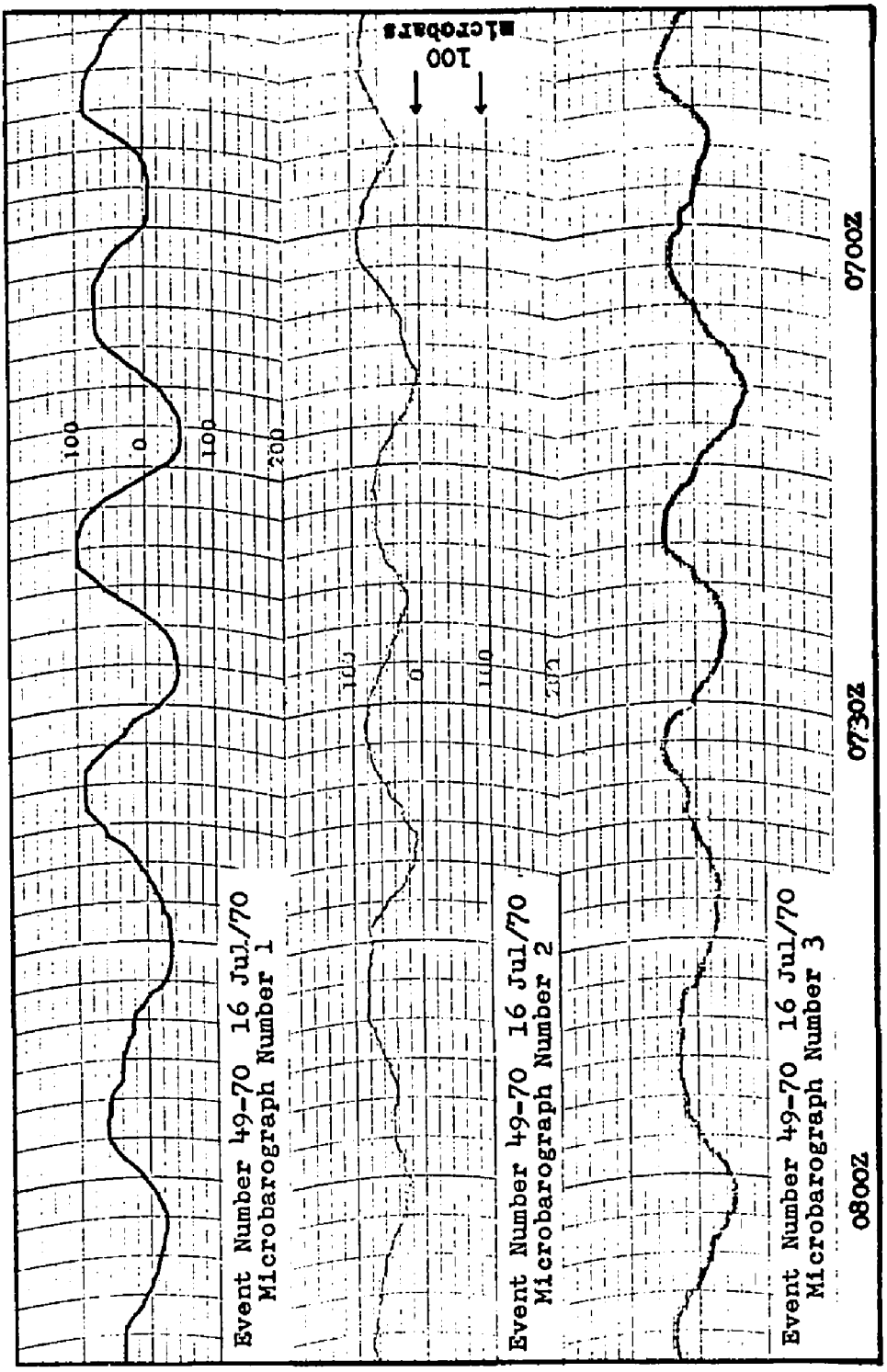

Figure 31. Microbarograms, Event Number 49-70.

mately 0645Z on 16 July 1970. The waveform is most regular in chart number 1 but maintains a clearly identifiable structure over the extent of the microbarograph array. The maximum cross-correlation coefficients between pairs of records for this event are $\sigma_{32} = 0.824$, $\sigma_{31} = 0.908$, and $\sigma_{21} = 0.761$. Analysis by method (iii) produced values for v and β of 21 m/s ± 12% and $149^{\circ} \pm 6^{\circ}$ respectively. The amplitude spectra (Figure 32) show that the wave consisted essentially of a single component having a period of about 16 minutes and a mean amplitude of about 45 microbars.

The locus of possible source regions (Figure 33) leads directly to a storm system to the southeast of Lake Erie. The London Weather Office radar observations for 16 July report an area of echoes of moderate strength from showers and thunderstorms at 0245Z at a mean distance of about 100 miles. By 0345Z the echoes had intensified and moved slightly to the east. Strong echoes from thunderstorm activity were observed. By 0445Z the area of activity had diminished to a region 20 miles in diameter at a distance of about 140 miles. The track of the storm system and the locus of possible source regions intersect at about 0415Z.

It is therefore concluded that Event number 49-70 had its origins in a region of strong thunderstorm activity. Other examples of the generation of gravity waves by thunderstorms were also found, most notably Events 50-70 and 60-70 (see Appendices B and C). The most probable source for Event number 50-70, recorded at 0345Z on 18 July 1970, was found to lie in a region of strong thunderstorm activity ahead of an advancing cold front as shown in Figure 34. The probable time of origin is about 0100Z and the distance to the source region is

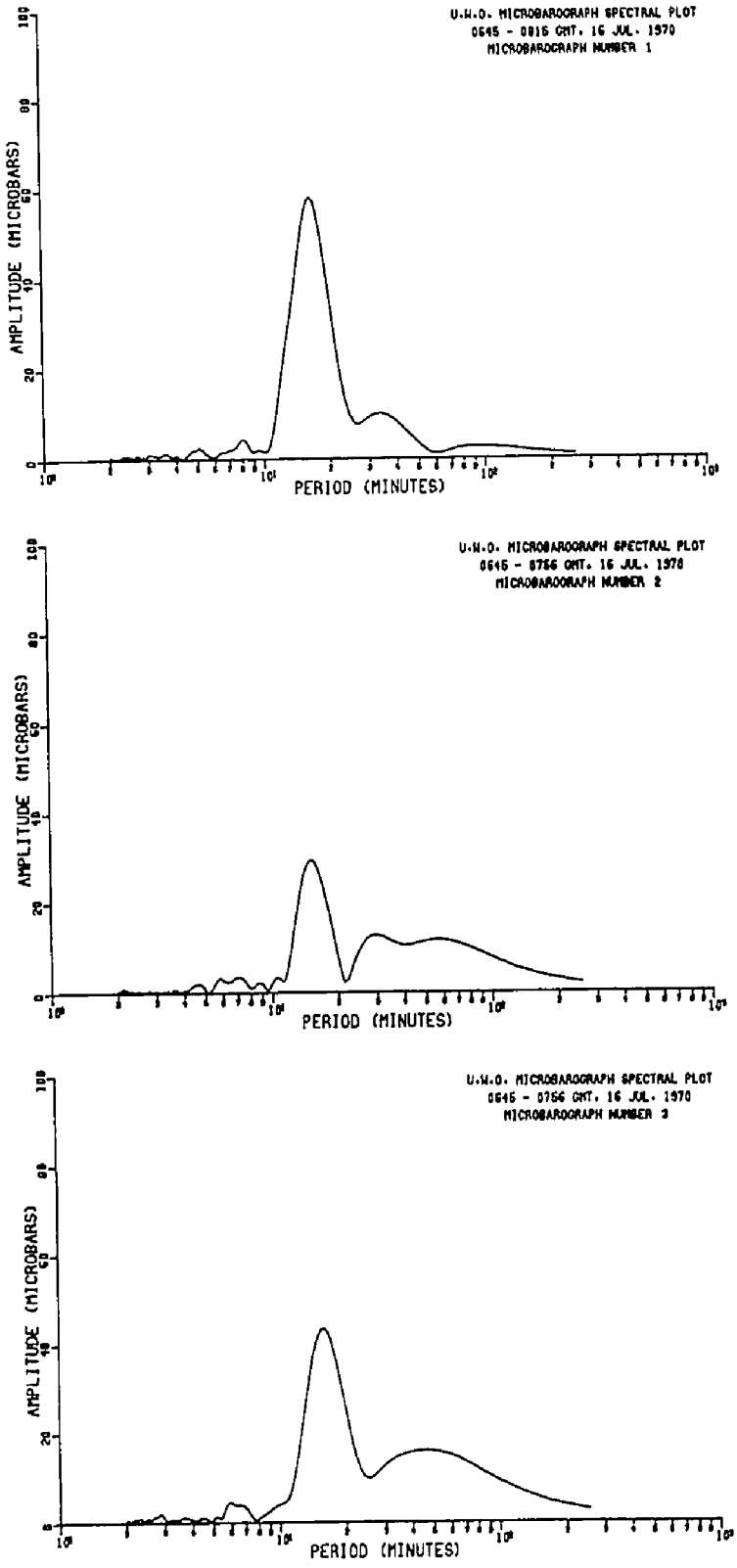

Figure 32. Amplitude Spectra, Event Number 49-70.

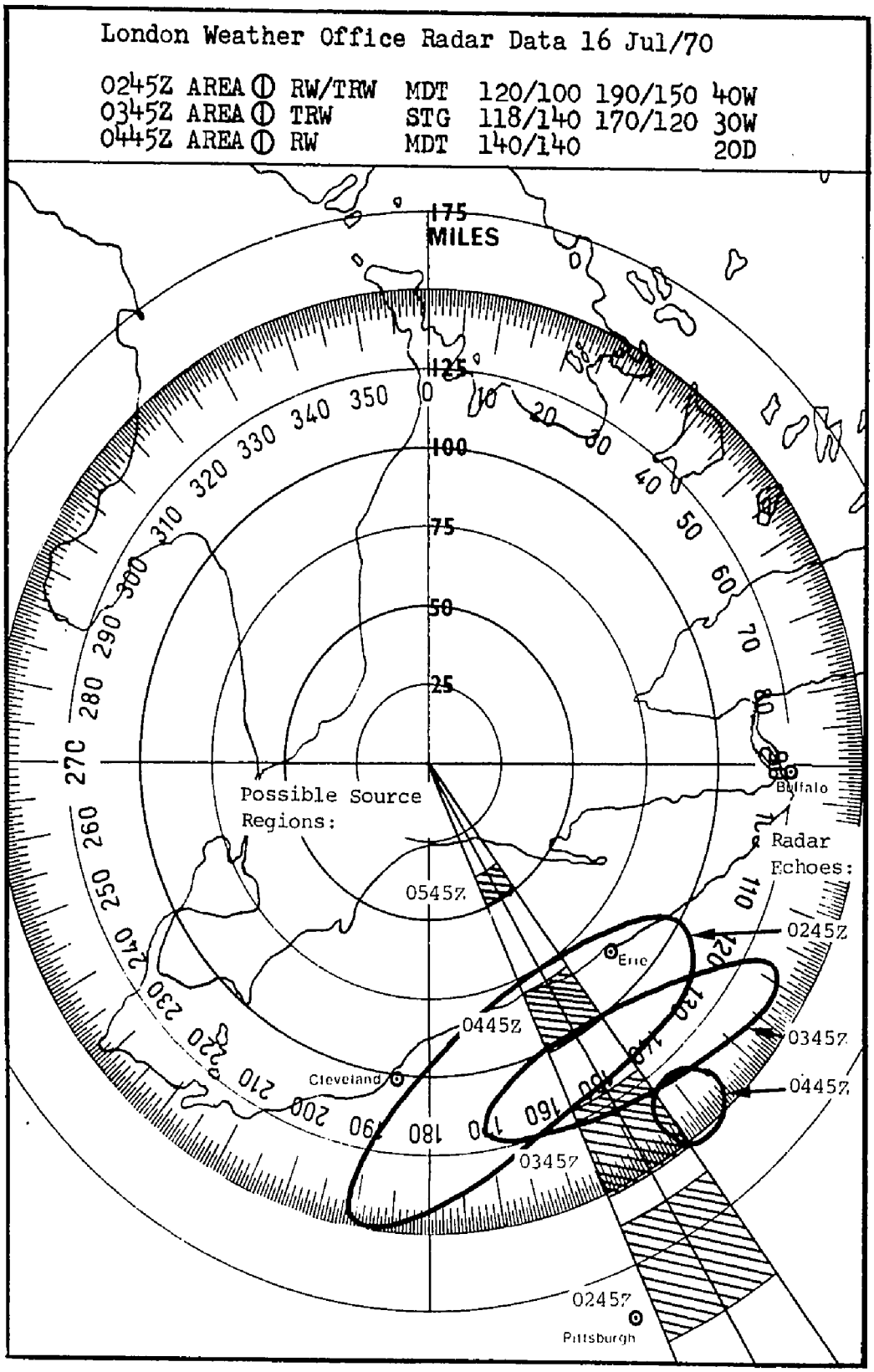

Figure 33. Source location, Event Number 49-70.

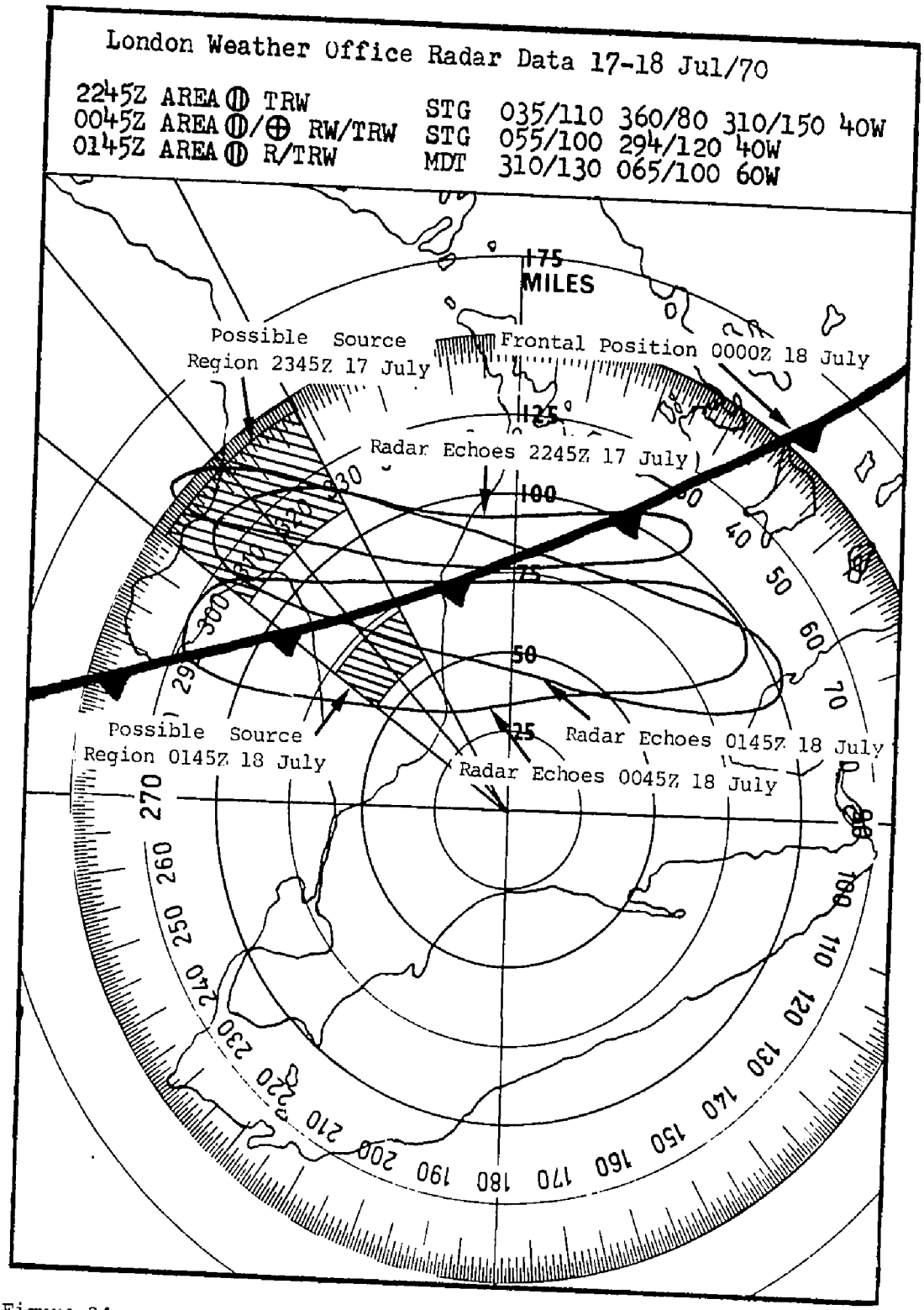

Figure 34. Source location, Event Number 50-70.

about 75 miles. The height of the echo tops was reported as 30,000 feet, indicating strong vertical motions in the region. Event number 60-70 is also attributed to a cold front thunderstorm system. A study of the radar observations (Figure 35) suggests two possible sources -- an area of thundershower activity at 1845Z at a distance of about 100 miles and a line of strong thunderstorm cells at a range of about 50 miles at about 1945Z. The latter is considered to be the more likely source. In either case, it is highly probable that the wave was generated in a region of strong thunderstorm activity.

Thus three of the 145 waves were clearly identified as having been generated by strong thunderstorms. Another 35 were found to have been generated in regions where there was thunderstorm activity, although the distances involved and the uncertainties in v and β make it impossible to conclude that these waves were generated by thunderstorms.

5.6 The blocking of the waves by frontal zones:

None of the sources which were located for 128 of the 145 waves were found in regions such that the waves would have had to travel through a frontal zone to reach the microbarograph array. This suggests that a frontal zone acts as a barrier to the propagation of the waves.

The case of Event number 30-71 is an example of a not uncommon occurrence. The wave was recorded at 0200Z on 18 May 1971. Subsequent analysis showed that its most probable source lay in a region of thunderstorm and shower activity near an advancing cold front (Figure 36). A warm front was situated between the source region and the microbarograph array.

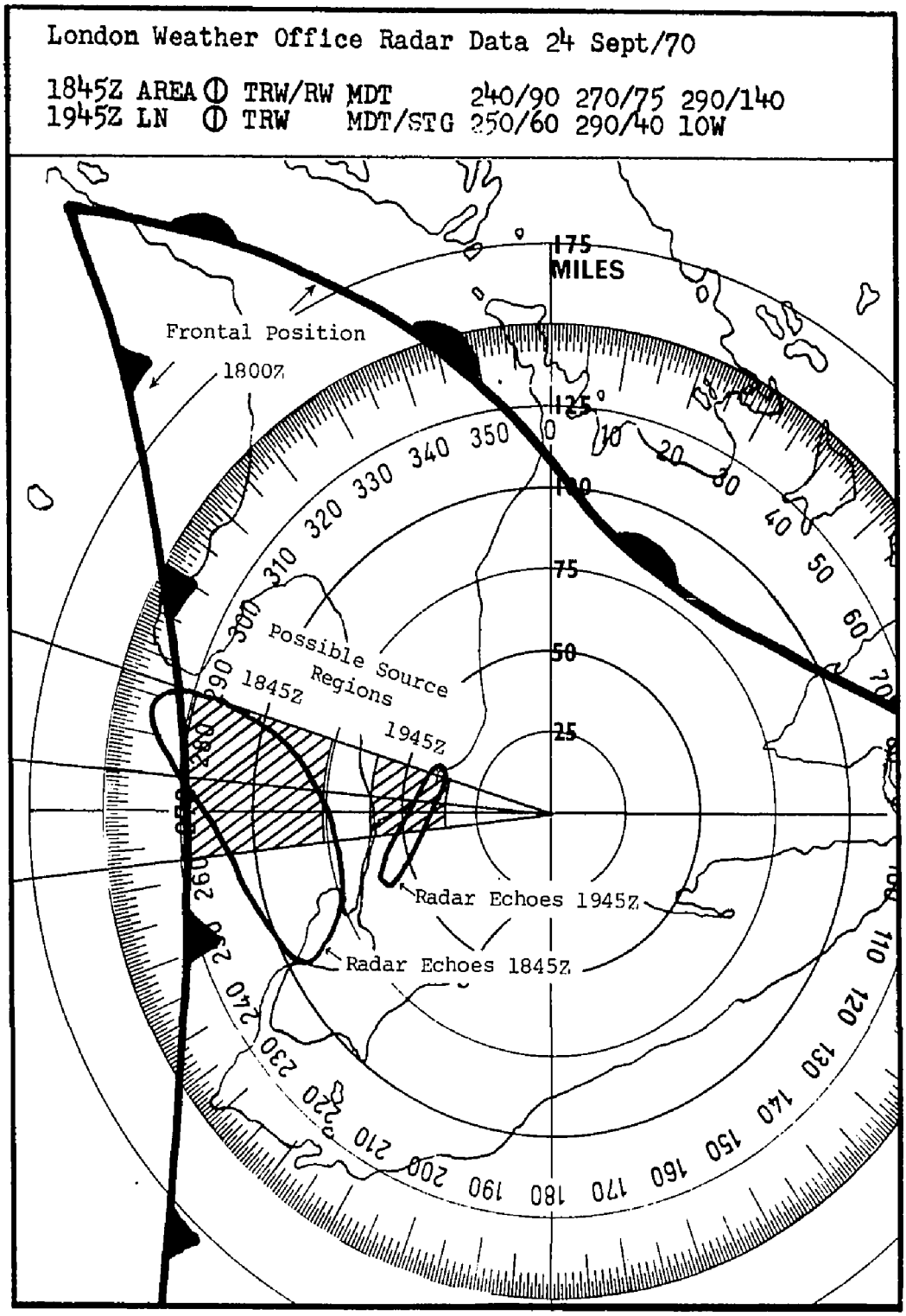

Figure 35. Source location, Event Number 60-70.

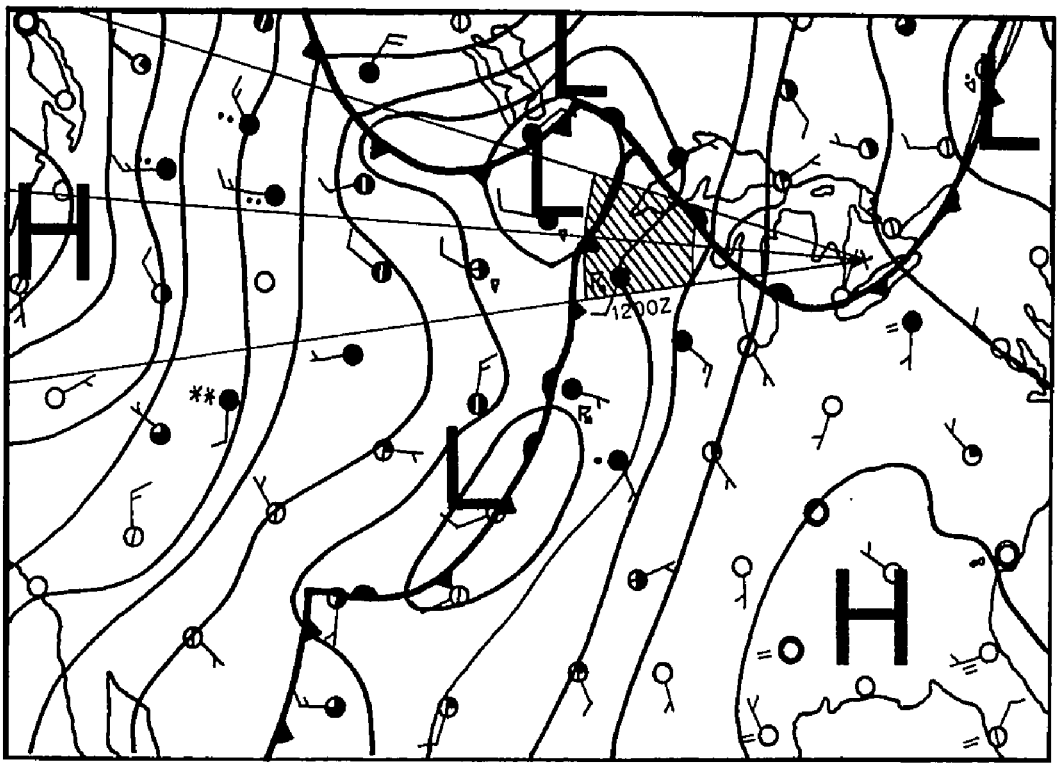

Figure 36. The surface chart, 1200Z 17 May 1971.

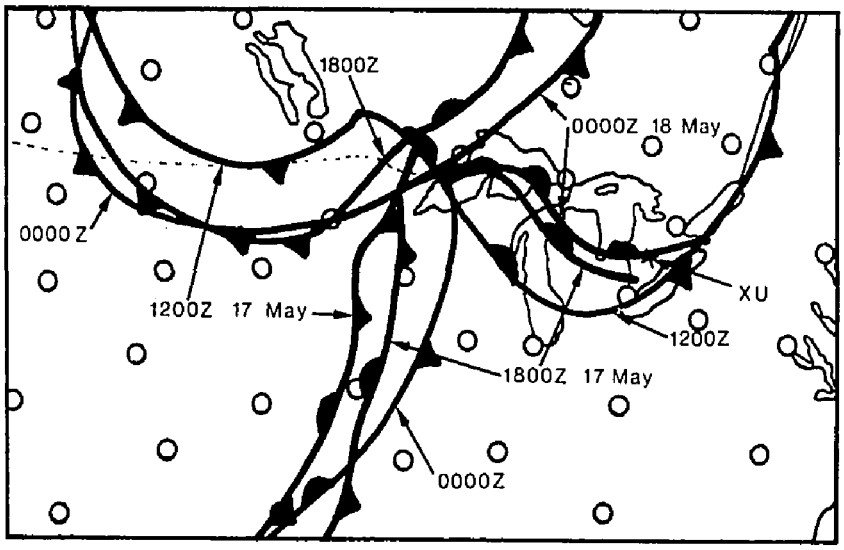

Figure 37. Frontal positions, 17-18 May 1971.

However, the motion of this warm front was such that it had passed over the receiving array by 0000Z on 18 May so that the wave propagation path did not pass through the frontal zone (Figure 37).

The analysis of the entire set of 128 waves for which sources were located thus suggests that internal gravity waves do not propagate through frontal zones.

5.7 Diurnal variation in the generation of the waves:

After sources have been located for the waves, it is possible to assign an approximate time of generation to each event, assuming that the velocity of the wave remained essentially constant between the source and observing regions. The distribution of these times of origin is given in Table IX. It is evident that there is no significant diurnal effect involved in the generation of the waves.

5.8 Summary:

For 128 of the 145 waves recorded in this experiment, it was possible to identify source regions in which tropospheric energy was available for the generation of a gravity wave. The characteristics of these source regions are described in Appendix B and summarized in Table X. Three of the waves were attributed to strong thunderstorm activity while a total of 38 were found to have been generated in regions in which there were thundershowers. Evidence was found to suggest that internal gravity waves cannot propagate through frontal zones. It was found that there was no diurnal variation in the frequency of generation of the waves.

TABLE IX

DIURNAL DISTRIBUTION OF WAVE GENERATION

Time Interval (Local Standard Time)	Number of Events
0001 - 0300	22
0301 - 0600	11
0601 - 0900	17
0901 - 1200	16
1201 - 1500	19
1501 - 1800	15
1801 - 2100	18
2101 - 2400	10
0001 - 0600	33
0601 - 1200	33
1201 - 1800	34
1801 - 2400	28

Median time of generation ≈ 1154 LST

TABLE X

THE ORIGINS OF THE WAVES

Total number of waves recorded:	145
Number with no apparent source:	17
Number with source identified:	128

	Cold Front	Warm Front	Total
Number of sources associated with fronts:	42	63	105
(a) At or near cyclonic wave:	21	43	64
(b) Not near cyclonic wave:	21	20	41

	Low	High	Mid-range
Pressure system in source region:	73	16	39

Number for which precipitation was observed in the source region:

Rain:	73
Snow:	31
Thunderstorms:	38
None indicated:	28

Number clearly remaining in the same air mass:	119
Number observed to have travelled between air masses:	0

CHAPTER VI

THE GENERATION OF INTERNAL GRAVITY WAVES

6.1 The validity of the identification of source regions:

The search for the sources of the waves studied in this work was necessarily a search for regions of the troposphere where kinetic or potential energy was available to produce the motions necessary for the generation of a gravity wave. In view of the fact that the single-station location technique cannot provide a range measurement, it is prudent to inquire whether the fact that such energy sources could be located in 88% of the cases studied is a significant one. This is tantamount to asking, "What is the probability of finding such a source region for a random wave event?".

Accordingly, a fictitious sample of 25 randomly chosen events was compiled, using tables of random numbers, in the following way. A three-digit random variable, ranging between 1 and 365, was used to select a day of the year for the fictitious observation, and a separate binary random variable assigned each such observation to one of the two years during which data were obtained. A third randomly chosen number, between 0 and 2400, was converted to hours and minutes in the 24-hour system and was rounded to the nearest five minutes to give the time of arrival of the wave. Two more random variables provided values of β and v, with the restriction that the distributions in these quantities should bear the general features of those shown in Figures

11 and 12, Chapter IV. The resulting simulated events, tabulated in Table XI, were subjected to the same source analysis as were the 145 observed waves. The results, presented in Table XII, indicate that it is quite unlikely that the identification of sources for the observed gravity waves is due to chance and that one is, therefore, justified in assuming a correlation between the postulated sources and the observed waves.

6.2 The nature of the sources:

The characteristics of the source regions presented in Table X suggest that the most probable generator of the type of internal gravity wave observed in this experiment lies in a precipitating low pressure system near the warm front side of a cyclonic wave, a region in which potential energy is being transformed into horizontal and vertical kinetic energy. Only 23 of the 128 sources were associated not with frontal activity but rather with isolated areas of convection and precipitation. The fact that 57% of the sources were found in or near regions of low barometric pressure while only 12.5% were associated with high pressure systems is also indicative of a correlation between the production of the waves and conditions of tropospheric instability.

The conditions prevalent in the source regions can be, in general, specified by noting that they exist in regions of strong baroclinity -- regions of the troposphere where the virtual isotherms and isobars are not parallel in cross-section. Baroclinity is strong in the region of the frontal zone, in the jet stream core, and in any region of strong convection. Thus the most general statement of the results of the present experiment is that internal gravity waves have been observed

TABLE XI

THE CHARACTERISTICS OF THE RANDOMLY CHOSEN SIMULATED WAVES

	Date	Time (GMT)	β (deg)	v (mph)
1.	24 Nov/69	1430	194	40
2.	8 Jan/70	0520	229	95
3.	14 Feb/70	0100	195	130
4.	10 Mar/70	2025	311	85
5.	17 Mar/70	1635	206	30
6.	19 Mar/70	1535	266	40
7.	23 Jun/70	1245	333	60
8.	29 Jun/70	1240	248	70
9.	3 Aug/70	0255	298	40
10.	5 Sep/70	0535	276	70
11.	15 Oct/70	1205	328	85
12.	31 Oct/70	1200	195	100
13.	2 Dec/70	2335	241	95
14.	16 Dec/70	1205	357	30
15.	24 Feb/71	0315	298	60
16.	27 Feb/71	0625	281	60
17.	20 Mar/71	2120	257	50
18.	30 Mar/71	1035	242	50
19.	14 Apr/71	0700	222	70
20.	23 Apr/71	0000	259	50
21.	6 Jun/71	0205	267	85
22.	10 Aug/71	1015	205	120
23.	8 Sep/71	0150	193	60
24.	9 Sep/71	0205	268	70
25.	7 Oct/71	1625	248	40

TABLE XII

STATISTICS OF THE LOCATIONS OF SOURCES

	Observed Waves	Simulated Waves
Total number of waves:	145	25
Number with source identified:	128 (88%)	8 (32%)
Number with no apparent source:	17 (12%)	15 (60%)
Doubtful cases:	0	2 (8%)

to have been generated in strongly baroclinic regions in the troposphere.

The fact that the waves were not observed to travel through a frontal zone implies that the strongly baroclinic atmosphere is a barrier to the propagation of the waves, presumably through a process of energy dissipation, and may indicate a reason for the absence of observed waves during periods of local stormy weather.

6.3 The production of gravity waves by thunderstorms:

The results of the present work have clearly established that low-amplitude internal gravity waves are generated by strong thunderstorm systems. It is therefore of interest to examine a simple model of the generating mechanism (Figure 38). The top of the developing thunderstorm cell is assumed to be a hemispherical cap of radius R rising with velocity $\vec{U}$. The rising cap is assumed to reach a position of stability at or near the tropopause and to create there an oscillation at a characteristic frequency ω_s. The kinetic energy carried into the source region by the cap is then

$$E_k = \frac{\pi}{3} R^3 U^2 (\rho_a + \rho_w) \qquad - (39)$$

where ρ_a is the density of the air and ρ_w is the mass density of suspended hydrometeors.

The rising cap will also carry thermal energy, since the air within the updraft portion of a thunderstorm cell is everywhere at a higher temperature than air at the corresponding altitude in the ambient atmosphere (Malan, 1963). The amount of excess thermal energy carried into the source region is given by

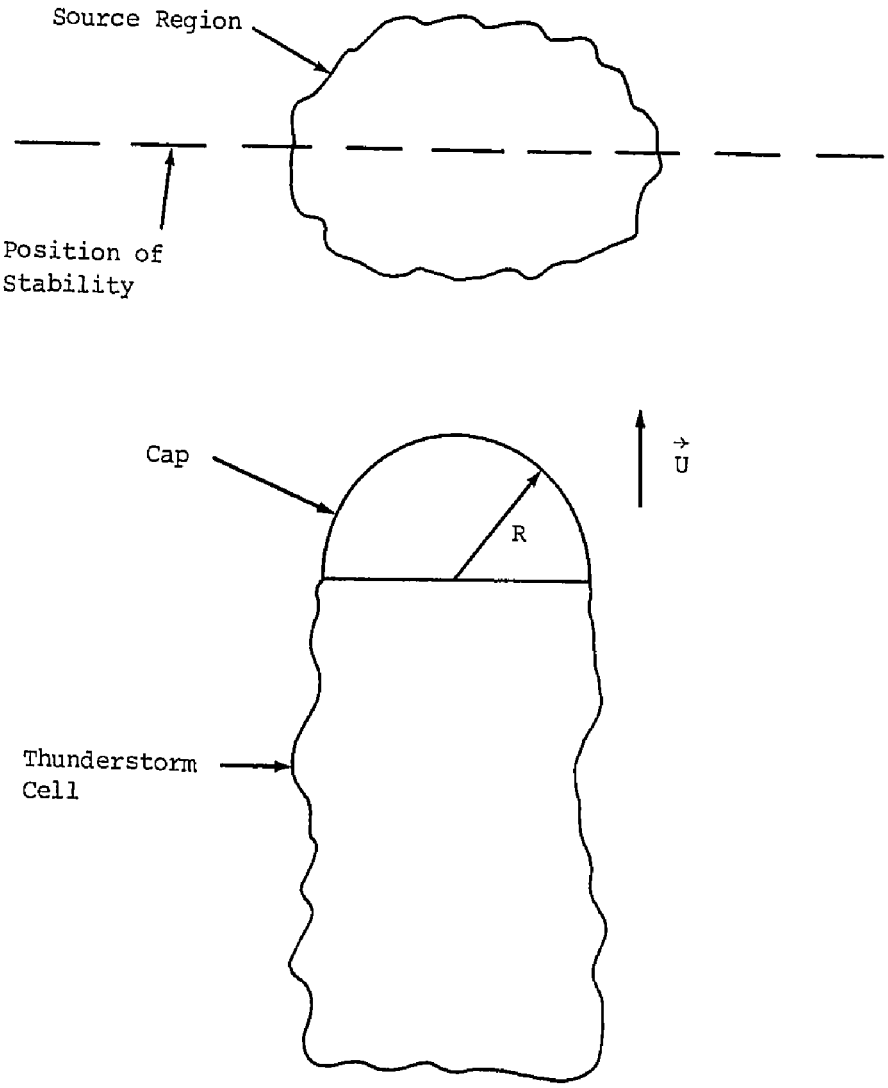

Figure 38. Sketch of a simple model for the generation of internal gravity waves by a developing thunderstorm.

$$E_T = \frac{2\pi}{3} R^3(\rho_a + \rho_w)\ C\ \Delta T \qquad - (40)$$

where C is the specific heat and ΔT is the difference in temperature between the cap and its surroundings. It is easily shown that $E_k >> E_T$ so that the energy available for the generation of waves, while thermodynamic in origin, is kinetic in the source region.

An order of magnitude calculation of the value of E_k can be made making use of the values

ρ_w	$= 10^{-5}$ kg/m^3	(Atlas, 1963)
ρ_a	$= 0.5$ kg/m^3	(Berry, Bollay, and Beers, 1945)
R	$= 5 \times 10^2$ m	(Malan, 1963)
U	$= 10$ m/s	(Cunningham, 1958; Marwitz and Auer, 1968)

which result in a value of $E_k \simeq 5 \times 10^9$ joules, a figure which is comparable to the energy figures given in Chapter V for other sources of waves. The values of R and U used in this calculation are typical of convective cells of moderate strength and could be expected to be larger for severe thunderstorms.

In order to investigate the spectral behaviour of such a model, we observe that the operations indicated by equations (4) and (5) of Chapter II, operations which lead to the dispersion relation (8), are equivalent to performing Fourier transforms on the perturbation variables such that, for instance,

$$\hat{p}'(\omega,\vec{K}) = \int_{-\infty}^{+\infty}\int\int p'(t,\vec{r})\, e^{-i\omega t}\, e^{iK_x x + iK_z z}\, dt\, dx\, dz \qquad - (41)$$

where the symbol ^ denotes the transformed variable. Recalling that the Fourier transform of the time derivative of a function is simply iω times the Fourier transform of the function itself, we can immediately obtain equation (7) by transforming the hydrodynamic equations (1) to (3) such that, for example, (see equation (E14), Appendix E)

$$\rho_o \frac{\partial u_x'}{\partial t} = -p_o \frac{\partial p'}{\partial x} \qquad - (42)$$

becomes

$$-gH\, iK_x\, \hat{p}'(\omega,\vec{K}) = -i\omega\, \hat{u}_x' \quad . \qquad - (43)$$

Similar transformations of the other three perturbation equations admit the matrix equation

$$\begin{bmatrix} (-iK_x gH) & (0) & (0) & (i\omega) \\ (-iK_z gH - g) & (g) & (i\omega) & (0) \\ (i\omega) & (-i\omega\gamma) & \frac{(\gamma-1)}{H} & (0) \\ (0) & (i\omega) & -\frac{1}{H} - iK_z & (-iK_x) \end{bmatrix} \begin{bmatrix} \hat{p}' \\ \hat{\rho}' \\ \hat{u}_z' \\ \hat{u}_x' \end{bmatrix} = \begin{bmatrix} \hat{Q}_1 \\ \hat{Q}_2 \\ \hat{Q}_3 \\ \hat{Q}_4 \end{bmatrix} \qquad - (44)$$

where the vector on the right hand side is a source term vector. We shall include the source model by rewriting the energy equation as

$$p_o \frac{\partial p'}{\partial t} + (\vec{u}'\cdot\nabla)p_o - c^2\left[\rho_o \frac{\partial \rho'}{\partial t} + (\vec{u}'\cdot\nabla)\rho_o\right] = Q_3(t,\vec{r}) \qquad - (45)$$

where the source term Q_3 must have the dimensions of energy/time/volume. If the oscillatory motion aloft is given by

$$z - z_s = A_s \sin(\omega_s t) \qquad - (46)$$

and the kinetic energy of the motion is

$$E_k = \frac{1}{2} M \left(\frac{dz}{dt}\right)^2 \qquad - (47)$$

then the source term is

$$Q_3 = \frac{1}{V}\frac{\partial E_k}{\partial t} = - \rho A_s^2 \omega_s^3 \cos(\omega_s t) \sin(\omega_s t) \qquad - (48)$$

and the Fourier transformed source term is

$$\hat{Q}_3 = i \frac{\pi}{2} \rho A_s^2 \omega_s^3 \left[\delta(\omega - 2\omega_s) - \delta(\omega + 2\omega_s)\right] . \qquad - (49)$$

It is clear that the propagation of energy takes place at a frequency $\omega = 2\omega_s$, indicating that the pressure amplitude of the wave varies at frequency ω_s.

The mechanism by which such a wave is generated is examined with reference to a particular example in section 6.4.

6.4 Case study of wave generation by a thunderstorm:

It has been shown in section 5.5 that Event number 49-70 was generated in a thunderstorm system over Pennsylvania at about 0415Z on 16 July 1970. The source region identified for this wave was located approximately 75 miles north of Pittsburgh, 40 miles south of Erie, and

120 miles east of Cleveland. The United States Weather Bureau stations at these three cities reported thundershower activity and distant lightning on July 15 and 16. The station at Erie recorded wind, lightning, and flood damage with additional reports of hail and tornado damage. The summary of radar observations for the northeastern United States issued by station MKC in Kansas City for 0045Z on 16 July reported a line of severe thundershowers 15 miles wide located 50 miles west of Allentown, Pennsylvania, and 40 miles northwest of Baltimore. Clearly, there existed severe storm conditions over the state of Pennsylvania for the whole of 15 July and the early part of 16 July.

Figure 39 shows a tephigram of data obtained from a radiosonde probe at Pittsburgh at 2315Z on 15 July 1970 (Table XIII). The lines marked T and T_D are the plots of temperature and dewpoint, respectively. This sounding is assumed to be typical of the state of the atmosphere over Pennsylvania for several hours before and after 2315Z.

An indication of the stability of the troposphere at the time of the radiosonde ascent is provided by the Showalter index, obtained graphically by considering a parcel of air at 850 mb to be lifted dry adiabatically to its condensation level and then moist adiabatically to 500 mb. The value of the index is the difference in centigrade degrees between the temperature of the ambient air and the temperature of the parcel at the 500 mb level. Petterssen (1956) considers that showers are possible when the index is less than 3, thunderstorms when it is less than 0, and heavy thunderstorms when it is less than -3. The Showalter index for the sounding of Figure 39 is -1.2.

A parcel at 850 mb in the atmosphere represented by this sounding, if lifted dry adiabatically from 850 mb, reaches its lifting

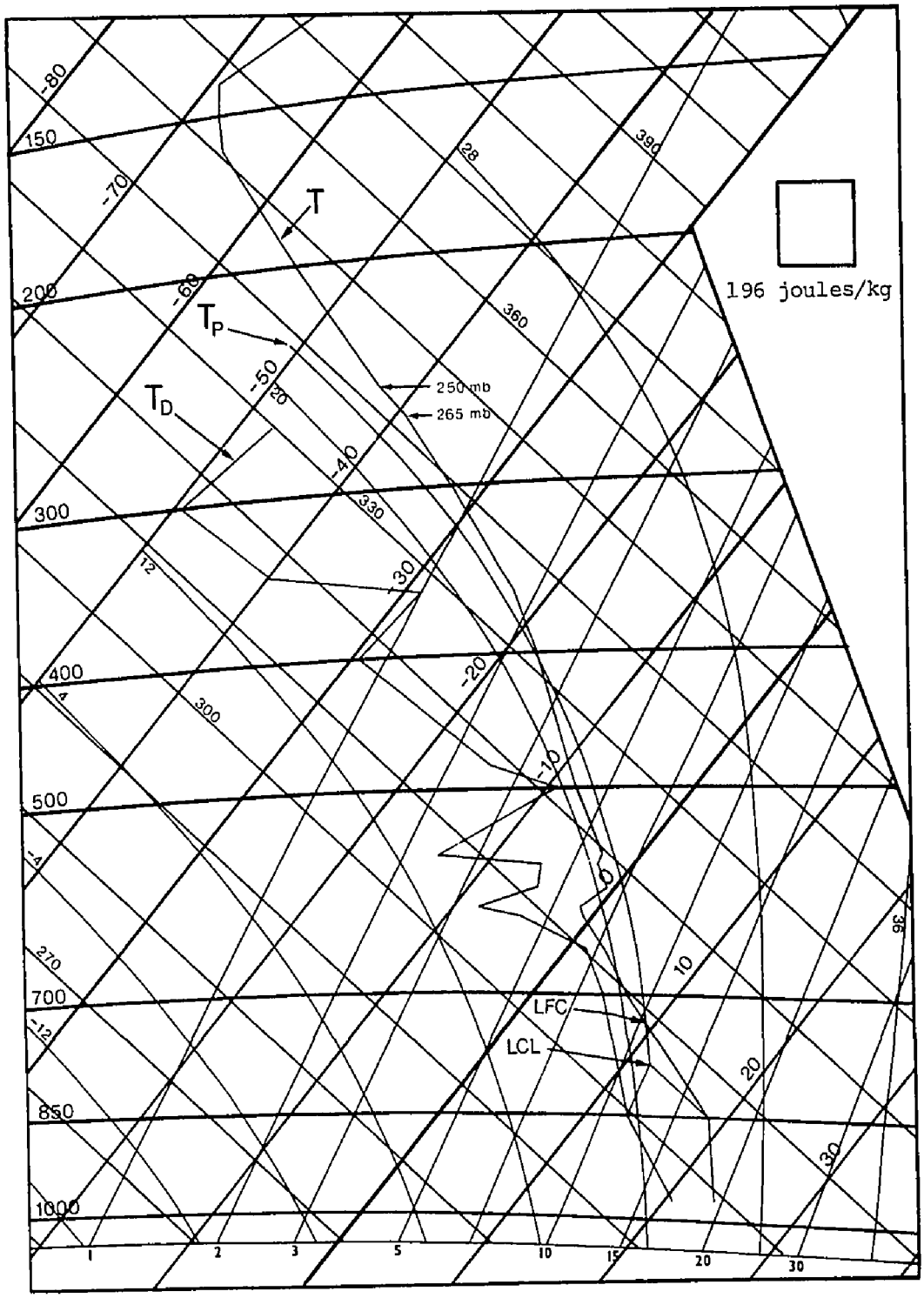

Figure 39. Tephigram, Pittsburgh, Pennsylvania, 2315Z 15 July 1970.

TABLE XIII

UPPER AIR DATA, PITTSBURGH, 2315Z 15 JULY 1970

Pressure (millibars)	Height (meters)	Temperature (degrees C)	Dewpoint (degrees C)	Relative Humidity (%)
970	360	23.3	20.4	84.5
850	1508	18.5	12.9	68.4
700	3142	6.5	4.9	88.7
652	3722	2.7	1.3	93.0
619	4141	-0.7	-4.8	75.0
609	4271	-1.3	-8.1	60.3
590	4524	-0.5	-5.2	68.7
568	4827	-2.6	-6.3	75.4
558	4968	-2.7	-13.8	41.3
500	5831	-8.0	-9.4	86.0
482	6115	-9.9	-15.0	65.7
400	7533	-17.9	-29.5	35.0
359	8334	-22.9	-28.8	58.8
345	8624	-25.0	-39.9	24.1
300	9625	-32.5	-49.5	10.8
265	10488	-39.1	-47.7	37.9
250	10884	-42.8		
200	12351	-54.7		
160	13743	-65.6		
150	14133	-67.8		
141	14504	-69.5		
119	15528	-64.6		
107	16176	-65.6		
100	16590	-63.2		
83	17737	-62.7		
72	18623	-58.2		

condensation level (LCL) at 782 mb. If lifted further, it follows the moist adiabat labelled T_p and reaches its level of free convection (LFC) at 731 mb. At this point the parcel experiences a net upward force and will spontaneously continue to rise.

The total energy imparted to the parcel by the net upward acceleration is found, by measuring the area enclosed by the curves T and T_p between 731 mb and 405 mb, to be approximately 200 joules/kg, corresponding to a vertical velocity of about 20 m/s at the 405 mb level. At this level, the parcel experiences neutral buoyancy, while above 405 mb the net acceleration on the parcel is downward. Thus the parcel will continue to rise above 405 mb but will decelerate until its kinetic energy has been totally changed into hydrostatic potential energy.

The loss of kinetic energy can be determined by measuring the area between the curves T and T_p above 405 mb. Between 405 mb and 265 mb, the parcel loses about 155 joules/kg, while the area enclosed by the T and T_p curves between 405 and 250 mb corresponds to an energy loss of about 215 joules/kg. It follows that the parcel will come to rest at some level between 265 mb and 250 mb.

If the parcel of air which has thus risen from 850 mb to about 260 mb were an isolated bubble, it would then be accelerated downward along T_p and eventually execute damped vertical oscillations about the 405 mb level. However, in the present model the parcel represents the cap of a rising column of air in the thunderstorm updraft system. Therefore, the parcel will not subside but will be trapped at the 265 - 250 mb layer by the continuing upward flow of air from lower levels. This trapping effect should result in two observable phenomena:

(a) An increase in moisture content in the 265 mb region, since the mixing ratio is larger at low levels than at higher altitudes, and

(b) A damped vertical oscillation centered approximately about the 260 mb level. This oscillation will be one of the ambient air which has been displaced by the cap of the updraft column, since the air of lower origin cannot rise above this level. In this respect, the 265 - 250 mb layer can be viewed as a region where the rate of loss by the rising cap of kinetic energy with height is large. The result is an almost impulsive transfer of kinetic energy and momentum from the cap to the ambient air in the source region. It is this air, displaced dry adiabatically from its stable position in the source region, which oscillates about that position of stability. The gravity wave which is generated by this oscillation should then have a frequency equal to the Brunt-Väisälä frequency for the ambient air in the source region.

The accumulation of moisture at the 265 mb level is shown in Figure 40, in which the ordinate scale, although not strictly logarithmic in pressure, is linear in height. The circles indicate the values of relative humidity derived from the radiosonde observations as presented in Table XIII. The rise in relative humidity from about 11% at 300 mb to 38% at 265 mb is a marked increase in moisture content which is considered to be due to the trapping effect discussed above.

The characteristic frequency of free vertical oscillations in the atmosphere, the Brunt-Väisälä frequency, is given by (Brunt, 1927)

$$\omega_B = \left[\frac{g}{T}\left(\Gamma_d + \frac{dT}{dz}\right)\right]^{\frac{1}{2}} \quad . \qquad - (50)$$

The corresponding Brunt period is then equal to $2\pi/\omega_B$. The variation

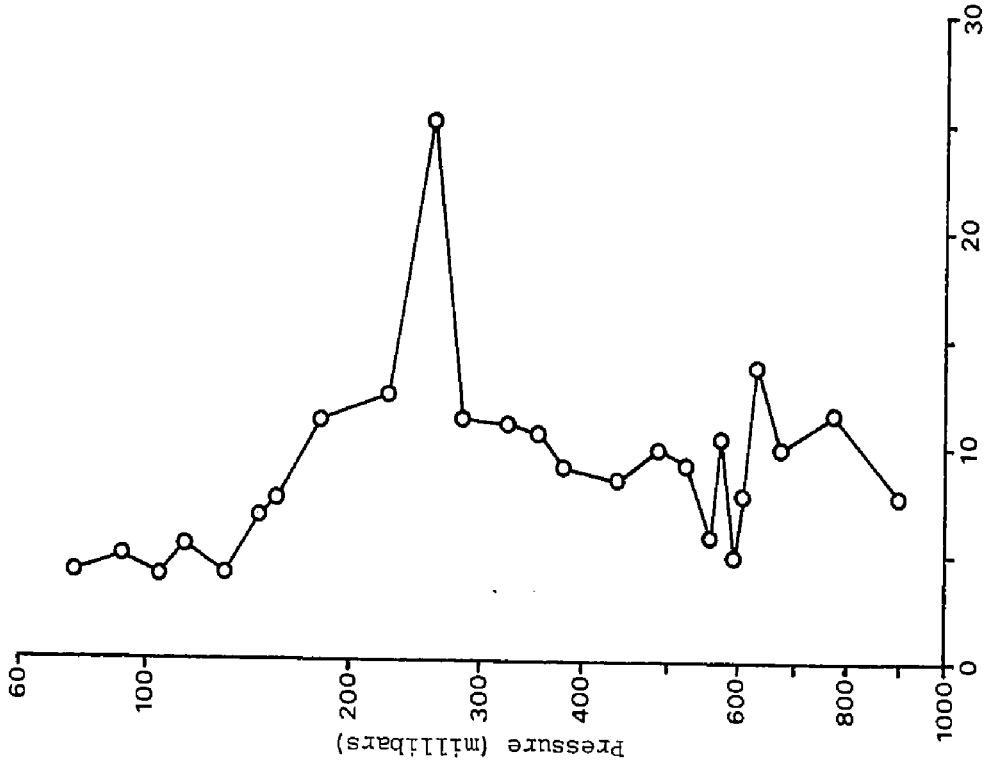

Figure 41. The variation of Brunt period with height, Pittsburgh, 2315Z, 15 July 1970.

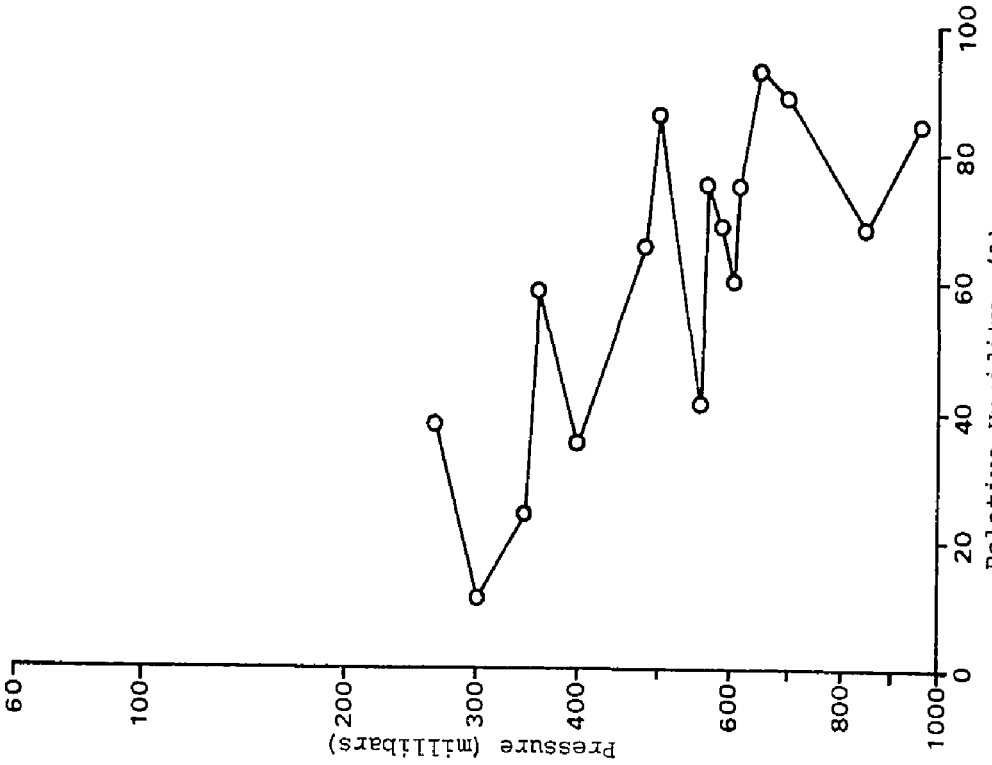

Figure 40. The vertical structure of moisture content, Pittsburgh, 2315Z 15 July 1970.

of Brunt period with height for the atmosphere represented by Figure 39 is shown in Figure 41, where the plotted values represent averages over the layers between the pressure readings shown in Table XIII. For the 265 - 250 mb layer, Δz = 396 m, ΔT = -3.7 ^{o}C, T = 232 ^{o}K, and the Brunt period is 25.0 minutes. This is somewhat larger than the observed mean period of the waveform of Event number 49-70 (Figure 32, Chapter V). However, the Brunt period is a strong function of dT/dz when the lapse rate is large, an uncertainty of about 6% in $\Delta T/\Delta z$ being sufficient to account for the difference between the computed Brunt period and the observed wave period in the present example.

It appears certain, then, that the wave observed as Event number 49-70 was generated when the updraft region of a strong thunderstorm cell impulsively perturbed stable air at about the 260 mb level, in accordance with the model presented in section 6.3. The kinetic energy of the rising cap at the 265 mb level in this model is found to be approximately 6 x 10^{9} joules, which is of the same order of magnitude at the energy estimate made in section 6.3.

The other waves which were observed to have been generated in thunderstorm systems, Events 50-70 and 60-70, also have spectra which are characterized by the presence of a single dominant component (see Appendix C). In addition, Event number 58-70, whose spectra also exhibit the dominance of a single frequency (Appendix C), was observed to have been generated in a region in which there was thunderstorm activity (Appendix B), although it is not possible to associate the wave with a particular storm system.

6.5 The far-field pressure response:

In the foregoing sections, it has been shown that the generation of internal gravity waves by the convective column model is energetically possible, that the resulting wave should be monochromatic, and that the observed parameters concerning Event number 49-70 are in good agreement with the predictions of the model. It should then be possible to calculate the properties of the ensuing pressure perturbation as a function of time and distance from the source.

The solution of equation (44) for the transformed perturbation pressure $\hat{p}'$ is obtained from the matrix equation

$$\begin{bmatrix} \hat{p}' \\ \hat{\rho}' \\ \hat{u}_z' \\ \hat{u}_x' \end{bmatrix} = \frac{\left[G_{ij}\right]}{\Lambda} \begin{bmatrix} 0 \\ 0 \\ \hat{Q}_3 \\ 0 \end{bmatrix} \qquad - (51)$$

where Λ is the value of the determinant of the 4 x 4 matrix of equation (44) and $\left[G_{ij}\right]$ is its inverted matrix (see Appendix D). The far-field perturbation pressure $p'(t,\vec{r})$ can then, in principle, be found by performing the inverse Fourier transform given by

$$p'(t,\vec{r}) = \frac{1}{(2\pi)^3} \int_{-\infty}^{+\infty}\int\int \hat{p}'(\omega,\vec{K})\, e^{i\omega t}\, e^{-iK_x x - iK_z z}\, d\omega\, dK_x\, dK_z \qquad - (52)$$

In practice, however, the solution of (52) is a formidable task, even for the simple source model discussed above.

The waves which have their origins in or near frontal systems often have more complex spectra than those shown for the waves

of thunderstorm origin, so that the simple mono-frequency source model would seem to be inadequate in such cases. The solution of (52) would then be correspondingly more difficult. However, Liu and Yeh (1971) have formulated the far-field response problem in a fairly general way and have calculated the response of the distant atmosphere to an impulsive point source. They found that the acoustic mode predominates for $t < 11$ minutes but that the gravity mode dominates at times of several hours after the impulse. Their results suggest that a good deal of caution should be exercised with regard to the choice of a model for the production of internal gravity waves by tropospheric sources of a general nature.

6.6 Suggestions for further research:

The data and conclusions presented in this thesis suggest several areas of merit for future investigation. The expansion of the microbarograph array to include more observation points would permit the calculation of range as well as bearing for the source regions of the observed waves, although the distance over which microbarograms from different locations could be profitably correlated may be limited by the fact that waves are not observed to propagate through regions of strong baroclinity. The addition of more microbarographs would also increase the reliability of the system as a whole. The automatic digital recording of data from all of the microbarographs would greatly facilitate the spectral analysis of a large number of waves in order that the sources might be studied in detail in terms of their spectral behaviour.

A search should be made for additional gravity waves

which are clearly generated by thunderstorms so that the particulars of the generating mechanism discussed in this chapter might be investigated in detail. This study would require upper air data which might be difficult to obtain. Nonetheless, observations of microbarometric oscillations over a period of several years should provide enough waves of thunderstorm origin for which atmospheric soundings are available for the source region so that the particulars of the generating mechanism could be investigated in some detail.

Perhaps the most important question left unanswered by the present work is why internal gravity waves are not observed to be generated by all thunderstorm systems. In this regard, it would be of interest to study a large number of thunderstorms at distances between 50 and 150 miles from the observing region in order to determine what physical criteria are necessary for the generation of gravity waves by strong convective cells. It is hoped that such a study would provide valuable information concerning the physical processes which occur within and above a thunderstorm.

APPENDIX A

COMPUTER PROGRAMS AND METHODS OF ANALYSIS

A.1 Spectral Analysis:

The power spectrum analysis of the microbarograph data is based on a program called TFRAP1 (Transformée de Fourier Rapide) which is derived from a program described by Forman (1966) and was adapted by M. Gabriel Otis of Université Laval. TFRAP1 performs a Fast Fourier Transform (FFT) of a uniformly sampled time record, using the computation algorithm of Cooley and Tukey (1965). TFRAP1 differs from some other FFT routines in that the input and output series both appear in natural order. This form of the FFT algorithm has been attributed to T.G. Stockham (both by Forman, 1966, and by Cochran et al, 1967) and has the disadvantage that an additional complex storage array is required during computation, since "in place" calculation is not possible. This is not a serious limitation in the present work, however, since a computer with 32k of core provides ample room for the processing of several hours of microbarograph data.

The FFT algorithm simply provides an efficient way of computing the complex Fourier coefficients c_n such that the output of the microbarograph can be expressed as

$$\Delta p(t) = \sum_{n=n_1}^{n_2} c_n \, e^{in\omega_n t} \qquad \text{- (A1)}$$

FORTRAN PROGRAM TFRAP1 PAGE 1

```
1  C     TFRAP1 (TRANSFORMEE DE FOURIER RAPIDE) IS A FAST
2  C     FOURIER TRANSFORM ROUTINE USING THE COOLEY-TUKEY
3  C     METHOD TO EFFECT A TRANSFORM (DIRECT OR INVERSE)
4  C     OF A DISCRETE SERIES OF DATA POINTS FORMED BY THE
5  C     UNIFORM SAMPLING OF A CONTINUOUS FUNCTION OF TIME
6  C     OR OF FREQUENCY.
7  C
8  C     IF THE INPUT VECTOR CONSISTS OF N POINTS SPACED
9  C     DX APART, THE VALUES IN THE TRANSFORM ARE OF
10 C     NECESSITY SPACED DY=1/(DX*N) APART.
11 C
12 C     N MUST BE STRICTLY EQUAL TO AN INTEGER POWER OF
13 C     2. IN GENERAL, THEREFORE, IT IS NECESSARY TO
14 C     TRUNCATE OR TO AUGMENT (BY, FOR EXAMPLE, THE
15 C     ADDITION OF ZEROS) THE INPUT VECTOR SO THAT THIS
16 C     CONDITION IS SATISFIED.
17 C
18 C     ON INPUT, THE VECTORS TR1 AND TI1 SHOULD CONTAIN,
19 C     RESPECTIVELY, THE REAL AND IMAGINARY PARTS OF THE
20 C     FUNCTION SERIES TO BE TRANSFORMED. IF THIS FUNC-
21 C     TION IS REAL, THE ENTIRE TI1 VECTOR SHOULD BE
22 C     INITIALIZED TO ZERO.
23 C     ON OUTPUT, THE VECTORS TR1 AND TI1 CONTAIN,
24 C     RESPECTIVELY, THE REAL AND IMAGINARY PARTS OF THE
25 C     COMPLEX FOURIER COEFFICIENTS OF THE TRANSFORM
26 C     SERIES.
27 C
28 C     THE VECTORS TR2 AND TI2 REMAIN INTERNAL TO THE
29 C     SUBROUTINE AND NEED NOT BE INITIALIZED TO ZERO.
30 C     THEY ARE AVAILABLE FOR USE OUTSIDE TFRAP1.
31 C
32 C     L IS SET EQUAL TO 1 FOR THE DIRECT TRANSFORM
33 C     (TIME TO FREQUENCY) AND TO -1 FOR THE INVERSE
34 C     TRANSFORM (FREQUENCY TO TIME).
35 C     NMAX IS THE NUMBER OF POINTS IN THE TRANSFORM.
36 C     (EG.  32, 64, 128, 256, 512, 1024, ......)
37 C     NMIN=NMAX/2
38 C
39 C     IN ORDER TO ENSURE CORRECT PHASE INFORMATION
40 C     RETRIEVAL, IT IS NECESSARY TO ENTER REAL AMPLI-
41 C     TUDE DATA INTO TFRAP1 IN SUCH A WAY THAT THE
42 C     INPUT FUNCTION SERIES IS CONTINUOUS AT THE ENDS
43 C     OF THE RECORD -- I.E. IT IS STRICTLY PERIODIC.
44 C     THIS IS ACCOMPLISHED BY SPLITTING THE RECORD
45 C     INTO HALVES AND EXCHANGING THEIR POSITIONS.
46 C     IF IT IS NECESSARY TO AUGMENT THE RECORD BY THE
47 C     ADDITION OF ZEROS, THEY SHOULD BE ADDED TO THE
48 C     MIDDLE OF THIS MODIFIED INPUT VECTOR.
49 C
50 C     THE PHASE ANGLE DETERMINED BY THE COMPONENTS OF
```

```
51  C     THE COMPLEX FOURIER COEFFICIENTS IS THE PHASE
52  C     OF THE CO-SPECTRUM WITH RESPECT TO THE START OF
53  C     THE INVERTED INPUT VECTOR.
54  C
55  C     FOR EXAMPLES OF THE USE OF TFRAP1, SEE PROGRAMS
56  C     PSPEC AND PSPEC1.
57  C
58  C     TFRAP1 IS DERIVED FROM A PROGRAM WRITTEN BY
59  C     MICHAEL L. FORMAN (J. OPT. SOC. AMER., VOL. 56,
60  C     P.978, JULY 1966) AND WAS ADAPTED BY G. OTIS.
61  C
62  C
63        SUBROUTINE TFRAP1(TR1,TI1,TR2,TI2,NMAX,NMIN,L)
64        DIMENSION TR1(NMAX),TI1(NMAX),TR2(NMIN),TI2(NMIN)
65        JHALF=NMAX/2
66        XJHAL=JHALF*L
67        IHALF=JHALF
68        KHALF=NMAX/4
69        PIJHAL=3.14159265/XJHAL
70     34 IF(IHALF)65,65,37
71     37 JP=0
72        WR=1.0
73        WI=0.0
74        ANG=IHALF
75        ANG=PIJHAL*ANG
76        DR=COS (ANG)
77        DI=SIN (ANG)
78        DO 81 I=1,JHALF
79        IF(IHALF-1)38,38,39
80     38 JK=I-1
81        IF(JK)481,48,481
82     39 IMOD=I-(I/IHALF)*IHALF
83        IF(IMOD)48,48,41
84     41 JK=I-IMOD
85        IF(JK-JP)48,48,43
86     43 JP=JK
87    481 ANG=WR
88        WR=ANG*DR-WI*DI
89        WI=ANG*DI+WI*DR
90     48 IP=JK+I
91        IQ=IP+IHALF
92        AR=TR1(IP)
93        AI=TI1(IP)
94        BR=TR1(IQ)*WR-TI1(IQ)*WI
95        BI=TR1(IQ)*WI+TI1(IQ)*WR
96        IF(I-KHALF)51,51,53
97     51 IU=I+KHALF
98        TR2(I)=AR+BR
99        TI2(I)=AI+BI
100       TR2(IU)=AR-BR
```

```
101         TI2(IU)=AI-BI
102         GO TO 81
103      53 IL=I-KHALF
104         IU=IL+JHALF
105         TR1(IL)=AR+BR
106         TI1(IL)=AI+BI
107         TR1(IU)=AR-BR
108         TI1(IU)=AI-BI
109      81 CONTINUE
110         JJJ=KHALF+1
111         DO 83 IK=JJJ,JHALF
112         JJMK=IK-KHALF
113         JJPK=IK+KHALF
114         JJPJ=IK+JHALF
115         TR1(IK)=TR1(JJMK)
116         TI1(IK)=TI1(JJMK)
117         TR1(JJPJ)=TR1(JJPK)
118         TI1(JJPJ)=TI1(JJPK)
119         TR1(JJMK)=TR2(JJMK)
120         TI1(JJMK)=TI2(JJMK)
121         TR1(JJPK)=TR2(IK)
122      83 TI1(JJPK)=TI2(IK)
123         IHALF=IHALF/2
124         GO TO 34
125      65 CONTINUE
126         RETURN
127         END
```

The conditions under which equation (A1) is valid have been discussed at length by Blackman and Tukey (1958). If the bandwidth of the system is such that (A1) is a good approximation to the function $\Delta p(t)$, then Parseval's theorem states that the quantity

$$\sum_{n=n_1}^{n_2} |c_n|^2 \qquad \text{- (A2)}$$

is a measure of the power content of $\Delta p(t)$ over one complete period -- i.e. over the length of the record.

Writing the complex Fourier components as

$$c_n = a_n + ib_n \quad , \qquad \text{- (A3)}$$

it follows that the amplitude and phase of the n^{th} Fourier component are given by, respectively,

$$A_n = \sqrt{a_n^2 + b_n^2} \qquad \text{- (A4)}$$

$$\phi_n = \tan^{-1}\left(\frac{b_n}{a_n}\right) \quad . \qquad \text{- (A5)}$$

The output coefficients of TFRAP1 as it is used in the present work are A_n and ψ_n where the phase angle ψ_n is chosen such that the microbarograph output function can be expressed as

$$\Delta p(t) = \sum_{n=1}^{N} A_n \sin(\omega_n t + \psi_n) \quad . \qquad \text{- (A6)}$$

The coefficients A_n and ψ_n thus represent, respectively, the amplitude and phase spectra of the output of the microbarograph.

FORTRAN PROGRAM PSPEC1 PAGE 1

```
C     THIS PROGRAM PERFORMS A TIME-DOMAIN SPECTRAL
C     ANALYSIS OF MICROBAROGRAPH DATA AND PRODUCES A
C     5 X 8 INCH PLOT ON PLAIN PAPER OF THE AMPLITUDE
C     SPECTRUM OF THE TREATED INPUT DATA.
C
C     IT DOES A 2048-POINT TRANSFORM ON UP TO 1024 DATA
C     POINTS AND REQUIRES PRESSURE READINGS (IN MICRO-
C     BARS) SPACED 0.5 MINUTES APART.
C           MAXIMUM LENGTH OF RECORD = 512 MINUTES.
C
C     PSPEC1 PRODUCES A TABLE, ON THE LINE PRINTER, OF
C     FREQUENCY, PERIOD, AMPLITUDE, AND PHASE FOR EACH
C     OF THE FREQUENCY INTERVALS IN THE TRANSFORM.
C
C     THE SPECTRAL PLOT OBTAINED REPRESENTS A FAST
C     FOURIER TRANSFORM OF THE INPUT ARRAY AFTER IT HAS
C     BEEN OPERATED UPON BY SUBROUTINES LEASQR, APODIZ,
C     AND AVRGE.
C
C     DATA INPUT FORMAT    16F5.0
C     SIGNAL END OF DATA BY INSERTING +999 AS LAST
C     INPUT POINT.
C
C     CONTROL INPUT REQUIRED: NUMBER OF DATA CARDS
C     (LT OR EQ 64).       CONTROL INPUT FORMAT:   I3
C
C     CONTROL INPUT CARD IS FIRST DATA CARD.
C
C     SECOND DATA CARD CONTAINS THE NUMBER OF THE
C     MICROBAROGRAPH FROM WHICH THE RECORD IS TAKEN,
C     THE TIME (IN GMT) OF THE START OF THE RECORD, THE
C     TIME (IN GMT) OF THE END OF THE RECORD, AND THE
C     DATE.     (FORMAT  I2,1X,6A5)
C     EG:  1 0000 - 0100 GMT, 01 JAN. 1971
C
C     SUBROUTINES REQUIRED: APODIZ,AVRGE,LEASQR,TFRAP1
C
C
      DIMENSION A(2048),B(2048),C(1024),D(1024),DATE(6)
      PI=ACOS(-1.0)
C
C     READ IN THE IDENTIFIERS.
C
      READ (5,10) NCARD
   10 FORMAT (I3)
      WRITE (6,20) NCARD
   20 FORMAT (1H1,5X,15HNO. OF CARDS = ,I3)
      READ (5,11) INSTR, (DATE(N), N=1,6)
   11 FORMAT (I2,1X,6A5)
      WRITE (6,21) INSTR
```

```
     21 FORMAT (1H ,5X,32HDATA FROM MICROBAROGRAPH
    1 NUMBER,I2)
        BARGPH=FLOAT(INSTR)
        WRITE (6,22) (DATE(N), N=1,6)
     22 FORMAT (1H ,5X,11HRECORD OF  ,6A5/)
        WRITE (6,23)
     23 FORMAT (1H-,5X,17HINPUT DATA ARRAY:,///)
C
C       READ IN THE DATA ARRAY AND PRINT IT OUT.
C
        DO 100 I=1,NCARD
        J=16*(I-1)+1
        K=J+15
        READ (5,12) (D(L), L=J,K)
     12 FORMAT (16F5.0)
        WRITE (6,24) (D(L), L=J,K)
     24 FORMAT (10X,16F6.0)
    100 CONTINUE
C
C       COUNT THE NO. OF DATA POINTS IN THE INPUT
C       ARRAY AND SELECT THE LARGEST EVEN NUMBER.
C
        W=0.0
        DO 101 I=1,1024
        IF (D(I).GT.900.) GO TO 1
        W=W+1.0
    101 CONTINUE
      1 W1=W/2.0
        M=IFIX(W1)
        N=2*M
        WRITE (6,25) W,N
     25 FORMAT (1H ,5X,27HNO. OF INPUT DATA POINTS = ,
    1F6.0,/,6X,28HNO. OF USABLE DATA POINTS = ,I5///)
        W=FLOAT(M)
C
C       REMOVE ANY CONSTANT SLOPE FROM THE DATA ARRAY.
C
        CALL LEASQR(D,N)
C
C       SMOOTH THE DATA BY APODIZING.
C
        CALL APODIZ(D,N)
C
C       REMOVE ANY RESIDUAL ZERO-FREQUENCY COMPONENTS.
C
        CALL AVRGE(D,N)
C
C       INITIALIZE TFRAP1'S ENTRY ARRAYS TO ZERO.
C
        DO 102 I=1,2048
```

```
101         A(I)=0.0
102         B(I)=0.0
103       102 CONTINUE
104   C
105   C     SPLIT THE DATA ARRAY, INVERT THE TWO HALVES,
106   C     AND PLACE AT THE ENDS OF TR1.
107   C
108         K=2049-M
109         DO 103 I=K,2048
110         J=I-K+1
111         A(I)=D(J)
112       103 CONTINUE
113         DO 104 I=1,M
114         J=I+M
115         A(I)=D(J)
116       104 CONTINUE
117   C
118   C     CALL THE FAST FOURIER TRANSFORM ROUTINE.
119   C
120         CALL TFRAP1(A,B,C,D,2048,1024,1)
121   C
122   C     OBTAIN THE AMPLITUDE AND PHASE INFORMATION FROM
123   C     THE COMPLEX FOURIER COEFFICIENTS.
124   C     TRANSLATE THE SPECTRAL SPACING TO
125   C     FREQUENCY INTERVALS.
126   C
127         WRITE (6,26)
128        26 FORMAT(1H1,12X,9HFREQUENCY,6X,6HPERIOD,7X,
129          19HAMPLITUDE,6X,5HPHASE,7X,5HPHASE)
130         WRITE (6,27)
131        27 FORMAT(12X,12H(PER MINUTE),3X,9H(MINUTES),4X,
132          111H(MICROBARS),3X,9H(RADIANS),3X,9H(DEGREES)///)
133         FREQ=0.0
134         DO 105 I=1,513
135         C(I)=(SQRT(A(I)**2+B(I)**2))/W
136         IF (I-1) 2,2,3
137        2 PER=9999.9999
138         PHASE=0.0
139         GO TO 4
140        3 PER=1.0/FREQ
141         PHASE=PI/2.0-ATAN2(B(I),A(I))
142         FNPER=(W/2.0)/PER
143         DIFF=FNPER-AINT(FNPER)
144         PHASE=PHASE-(2.0*PI*DIFF)
145         IF (PHASE.GT.PI) PHASE=PHASE-2.0*PI
146         IF (PHASE.LT.(-PI)) PHASE=PHASE+2.0*PI
147        4 A(I)=PER
148         B(I)=PHASE
149         PHASE=(180.0/PI)*B(I)
150         WRITE (6,28) FREQ,A(I),C(I),B(I),PHASE
```

```
151      28 FORMAT(12X,F8.5,5X,F10.4,F13.3,F13.4,F12.3)
152         FREQ=FREQ+1.0/1024.0
153     105 CONTINUE
154   C     CALL THE PLOTTING ROUTINES TO GRAPH THE
155   C     AMPLITUDE SPECTRUM.
156   C
157         CALL PLOTS (30,30.0,10.75,2)
158         CALL PLOT (5.0,2.25,-3)
159         DO 106 I=1,511
160         J=I+2
161         A(I)=A(J)
162         C(I)=C(J)
163     106 CONTINUE
164         CALL SCALE3(C,5.0,511,1,0)
165         CALL SCALE3(A,8.0,511,1,1)
166         CALL AXIS3(0.,0.,21HAMPLITUDE (MICROBARS),21,5.,
167        190.,C(512),C(513),-1,1.0,1)
168         CALL AXIS3(0.,0.,16HPERIOD (MINUTES),-16,8.,0.,
169        1A(512),A(513),-2,0.,0)
170         CALL SYMBOL(5.,4.9,0.1,35HU.W.O. MICROBAROGRAPH
171        1 SPECTRAL PLOT,0.,35)
172         CALL SYMBOL(5.25,4.7,0.1,DATE,0.0,30)
173         CALL SYMBOL(5.45,4.5,0.1,23HMICROBAROGRAPH
174        1 NUMBER  ,0.0,23)
175         CALL NUMBER(7.35,4.5,0.1,BARGPH,0.0,-1)
176         CALL LINE3(A,C,511,1,0,0,2)
177         CALL ENDPLT
178         STOP
179         END
```

PSPEC1 is a FORTRAN main program designed to call the FFT subroutine TFRAP1. It accepts pressure readings (in microbars) which have been derived by sampling the microbarograph output chart at intervals of 0.5 minute. It performs a 2048-point transform on up to 1024 data points and produces both a graph of the amplitude spectrum and a line-printer listing of frequency, period, amplitude, and phase. PSPEC1 requires, in addition to TFRAP1, the FORTRAN subroutines APODIZ, AVRGE, and LEASQR.

A.2 Apodisation:

The Fourier transform of an infinite length of record comprised of a single cosine component $\cos(\omega_o t)$ is the impulse function (Hsu, 1970)

$$\pi\delta(\omega - \omega_o) + \pi\delta(\omega + \omega_o) \quad . \qquad - (A7)$$

The selection of a finite length of such a record is tantamount to modulating the infinite cosine record by the symmetrical boxcar function $\Pi(t)$ defined by

$$\Pi(t) = \begin{cases} 0 & |t| > \frac{T}{2} \\ 1 & |t| < \frac{T}{2} \end{cases} \qquad - (A8)$$

where T is the total length of the record. Then, by the modulation theorem (Bracewell, 1965), the Fourier transform of this finite length of record will be

$$\pi F \left[\delta(\omega - \omega_o) + \delta(\omega + \omega_o)\right] \qquad - (A9)$$

where F is the Fourier transform of $\Pi(t)$ and is given by

$$F = \frac{T \sin(\omega T/2)}{\omega T/2} \quad . \qquad \text{- (A10)}$$

In other words, the Fourier transform of a finite length of record of the function

$$f(t) = \cos(\omega_o t) \qquad \text{- (A11)}$$

is the diffraction function (A10) centered upon frequency ω_o.

The spectrum produced by the Fourier analysis of a data sample of finite length will, therefore, contain secondary maxima, or side-lobes, which may make interpretation of the spectrum difficult. These side-lobes, being a direct result of the use of the boxcar data window, can be reduced considerably through the use of a data window whose Fourier transform is a diffraction pattern which has a greater fraction of the transmitted energy concentrated in the central maximum. This technique is termed "apodisation" (from the Greek "apodi", meaning "without feet").

The data window used in the present work was suggested by Connes (1961) for use in Fourier transform spectroscopy and is described in some detail by Jacquinot and Roizen-Dossier (1964). It consists of multiplying the data record by the function

$$\xi(t) = \begin{cases} \left[1 - \left(\frac{t}{T/2}\right)^2\right]^2 & |t| < \frac{T}{2} \\ 0 & |t| > \frac{T}{2} \end{cases} \quad . \qquad \text{- (A12)}$$

The shape of the Connes data window for a record of unit length is

shown in Figure A-1.

The effect of apodisation is clearly seen in Figures A-2 and A-3 which represent PSPEC1 analyses of test data consisting of approximately 10 periods of a sinusoidal signal having a period of 15 minutes and an amplitude of 100 microbars. Figure A-2 represents a FFT of the test data without apodisation while Figure A-3 shows the amplitude spectrum in the case where the test data have been modified by the subroutine APODIZ. It is evident that the effect of apodisation is to reduce considerably the heights of the side-lobes at the expense of a slight broadening of the spectral line.

A.3 Removal of Low-Frequency Components:

Frequency components having very long periods are of no interest in the present work but may yet appear in the data. For instance, a steadily increasing ambient pressure appears on the microbarograph chart as a shift in the zero-frequency component of Δp. Such components may manifest themselves as large-amplitude spectral lines at very long periods and may interfere with the interpretation of the spectrum.

Subroutine AVRGE simply removes the zero-frequency component from the amplitude spectrum by subtracting the mean of the input data array from each element in that array before entry into TFRAP1.

Subroutine LEASQR fits the microbarograph data to a straight line by the method of least squares estimators (Mood and Graybill, 1963). The data array is modelled by

$$\Delta p(t)_i = \eta + \zeta t_i + \varepsilon_i \qquad - (A13)$$

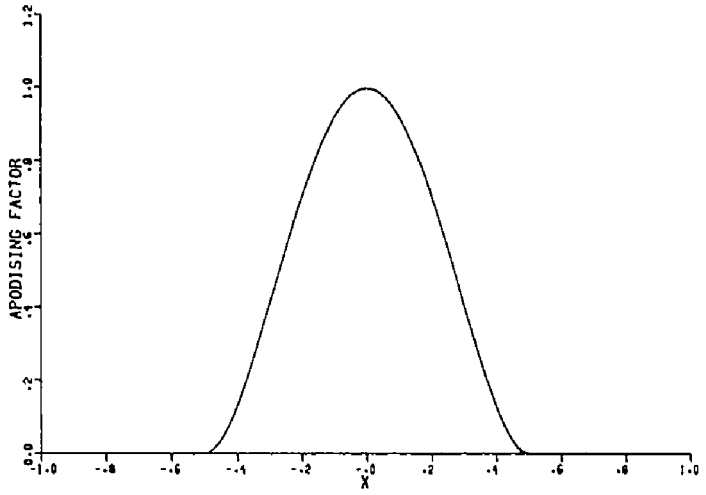

Figure A-1. The Connes apodising data window

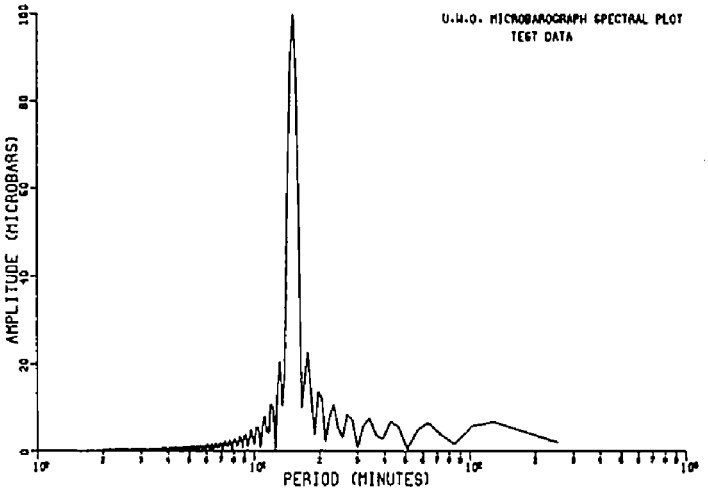

Figure A-2. The spectrum of the unapodised test data.

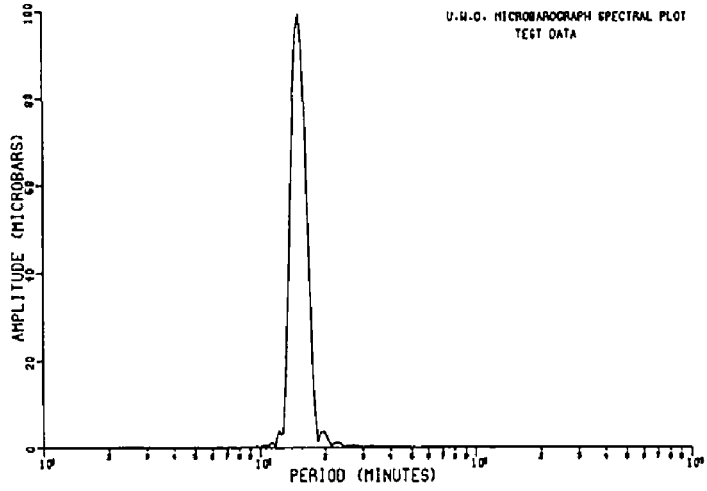

Figure A-3. The spectrum of the apodised test data.

FORTRAN PROGRAM APODIZ

```
 1  C  SUBROUTINE APODIZ APPLIES THE CONNES APODIZING
 2  C  FUNCTION   T(X) = (1-(4*X/N)**2)**2
 3  C             X = RUNNING POINT NUMBER
 4  C             N = NUMBER OF POINTS
 5  C  TO THE DATA ARRAY BEFORE ENTRY INTO TFRAP1.
 6  C
 7  C  IT INCREASES THE SPECTRAL LINE WIDTH BY A FACTOR OF
 8  C  1.53 (AT HALF-AMPLITUDE) AND DECREASES THE HEIGHT
 9  C  OF THE HIGHEST SIDE-LOBE BY A FACTOR OF ABOUT 5.5.
10  C    I.E.  THE HEIGHT OF THE HIGHEST (PRINCIPAL)
11  C  SIDE-LOBE IS ABOUT 0.04 TIMES THE HEIGHT OF THE
12  C  CENTRAL PEAK.
13  C
14  C
15          SUBROUTINE APODIZ (DATA,N)
16          DIMENSION DATA (1)
17          M=N/2
18          W=M
19          DO 100 I=1,N
20          J=I-M-1
21          X=J
22          X=X/W
23          X=(1.0-X**2)**2
24          X=X/0.534
25          DATA(I)=DATA(I)*X
26  100     CONTINUE
27          RETURN
28          END
```

FORTRAN PROGRAM AVRGE

```
 1  C  SUBROUTINE AVRGE CALCULATES THE MEAN OF THE ELEMENTS
 2  C  OF THE INPUT ARRAY AND SUBTRACTS THAT MEAN FROM EACH
 3  C  ARRAY ELEMENT.
 4  C
 5  C
 6        SUBROUTINE AVRGE (DATA,N)
 7        DIMENSION DATA(1)
 8        RN=N
 9        SUM=0.0
10        DO 100 I=1,N
11    100 SUM=SUM+DATA(I)
12        AVG=SUM/RN
13        DO 101 I=1,N
14    101 DATA(I)=DATA(I)-AVG
15        RETURN
16        END
```

FORTRAN PROGRAM LEASQR

```
1   C  SUBROUTINE LEASQR PERFORMS A LEAST SQUARES FIT OF
2   C  THE INPUT ARRAY TO A STRAIGHT LINE AND SUBTRACTS
3   C  THAT LINEAR COMPONENT FROM THE ARRAY.
4   C
5   C
6         SUBROUTINE LEASQR (DATA,N)
7         DIMENSION DATA(1)
8         RN=N
9         SIGX=0.0
10        SIGY=0.0
11        SIGX2=0.0
12        SIGXY=0.0
13        X=1.0
14        DO 100 I=1,N
15        SIGX=SIGX+X
16        SIGY=SIGY+DATA(I)
17        X=X+0.5
18    100 CONTINUE
19        XBAR=SIGX/RN
20        YBAR=SIGY/RN
21        X=1.0
22        DO 101 I=1,N
23        SIGXY=SIGXY+(DATA(I)-YBAR)*(X-XBAR)
24        SIGX2=SIGX2+(X-XBAR)**2
25        X=X+0.5
26    101 CONTINUE
27        B=SIGXY/SIGX2
28        A=YBAR-B*XBAR
29        X=1.0
30        DO 102 I=1,N
31        YLESQR=A+B*X
32        DATA(I)=DATA(I)-YLESQR
33        X=X+0.5
34    102 CONTINUE
35        RETURN
36        END
```

where the ε_i are error factors. The least squares estimators η_ℓ and ζ_ℓ are found by minimizing the sum of the squares of the ε_i -- i.e. by minimizing

$$\sum_{i=1}^{N} \varepsilon_i^2 = \sum_{i=1}^{N} \left(\Delta p(t)_i - \eta - \zeta t_i \right)^2 \qquad \text{- (A14)}$$

The values of the least squares estimators are then

$$\eta_\ell = \overline{\Delta p(t)} - \zeta_\ell \bar{t} \qquad \text{- (A15)}$$

$$\zeta_\ell = \frac{\sum_{i=1}^{N} \left(\Delta p(t)_i - \overline{\Delta p(t)} \right) \left(t_i - \bar{t} \right)}{\sum_{i=1}^{N} \left(t_i - \bar{t} \right)^2} \qquad \text{- (A16)}$$

where

$$\overline{\Delta p(t)} = \frac{1}{N} \sum_{i=1}^{N} \Delta p(t)_i \qquad \text{- (A17)}$$

and

$$\bar{t} = \frac{1}{N} \sum_{i=1}^{N} t_i \qquad \text{- (A18)}$$

The effect of LEASQR on the data is depicted in Figures A-4 and A-5 which represent PSPEC1 analyses of 150 minutes of a test function given by

$$\Delta p(t) = 100 \sin(2\pi t/15) + 75 \sin(2\pi t/7.6) + (-1.5 + 2t) \qquad \text{- (A19)}$$

$$t = 0, 0.5, 1.0, 1.5, 2.0, \ldots. \text{ minutes.}$$

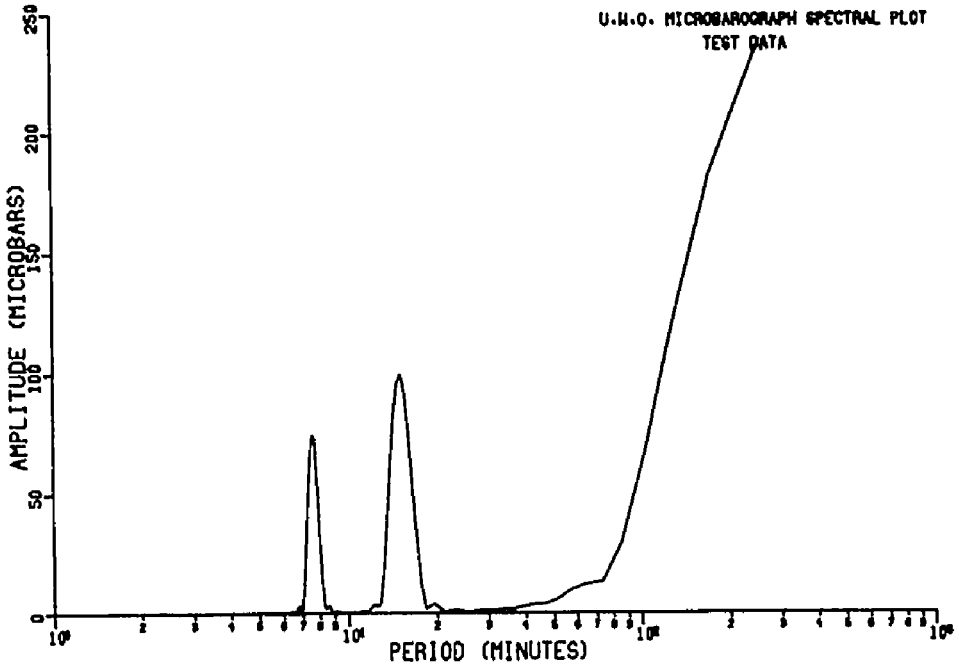

Figure A-4. The spectrum of test data without the LEASQR correction.

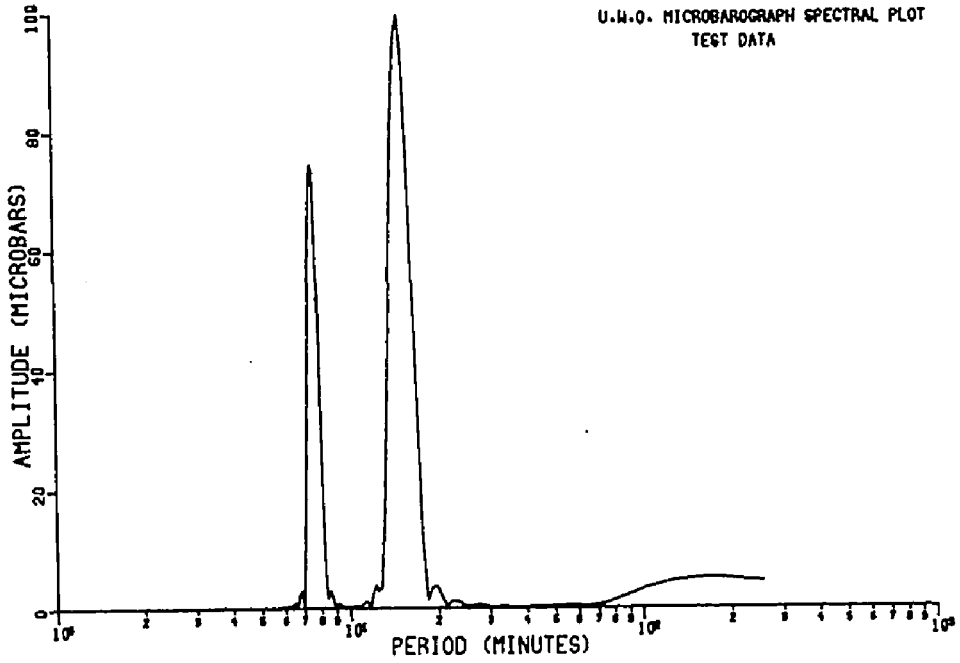

Figure A-5. The spectrum of test data with the LEASQR correction.

In Figure A-4, the LEASQR correction has not been applied and the linear component of (A19) manifests itself as a large signal at long periods. The use of LEASQR results in much diminished amplitude at low frequencies (Figure A-5).

A.4 Cross-correlation:

The cross-correlation coefficient $\sigma_{ij}(\tau)$ for two data vectors i and j is given by (Jenkins and Watts, 1969)

$$\sigma_{ij}(\tau) = \frac{\gamma_{ij}(\tau)}{\sqrt{\upsilon_i \upsilon_j}} \qquad - (A20)$$

$$\tau = 0, \Delta t, 2\Delta t, 3\Delta t, \ldots, N\Delta t$$

where $\gamma_{ij}(\tau)$ is the cross-correlation function defined by (Lange, 1967)

$$\gamma_{ij}(\tau) = \sum_{t=0}^{N\Delta t} \Delta p_i(t)\ \Delta p_j(t + \tau) \qquad - (A21)$$

and the quantities υ_i are defined by

$$\upsilon_i \equiv \gamma_{ii}(0) = \sum_{t=0}^{N\Delta t} \left[\Delta p_i(t)\right]^2 \qquad - (A22)$$

For records which are identical functions of time but which are displaced in time by an amount τ_o such that

$$\Delta p_j(t) = \Delta p_i(t - \tau_o) \qquad \begin{matrix} i = 1,2,3 \\ i \neq j \end{matrix} \qquad - (A23)$$

the function $\sigma_{ij}(\tau)$ will range between +1 and -1 and will have the value +1 at a lag given by

$$\tau = \tau_o = t_{ij} \quad . \qquad \text{- (A24)}$$

If the records are similar but not identical, the maximum value of $\sigma_{ij}(\tau)$ will be less than unity but will still occur at $\tau=\tau_o$.

Since the records of Δp are discrete series with spacing Δt = 0.5 minute, the cross-correlation coefficients $\sigma_{ij}(\tau)$ are also discrete series with spacing $\Delta\tau$ = 0.5 minute. For this reason, after the maximum value of the $\sigma_{ij}(\tau)$ array is determined, a least squares quadratic fit is performed to the five points around the maximum. The derivative of this quadratic function is evaluated to locate the value τ_o.

The cross-correlation computations are performed by the ALGOL main program CORREL, designed for use with a DEC PDP-10 time-sharing system. CORREL creates, on output, a disk file which contains:

(a) N, the number of points in each array

(b) the quantities $\sqrt{v_3 v_2}$, $\sqrt{v_3 v_1}$, $\sqrt{v_2 v_1}$

(c) three arrays containing the function series $\sigma_{32}(\tau)$, $\sigma_{31}(\tau)$, $\sigma_{21}(\tau)$

(d) three arrays containing the auto-correlation function series

$$\sigma_{ii}(\tau) = \frac{\gamma_{ii}(\tau)}{v_i} \qquad i = 1,2,3 \quad . \qquad \text{- (A25)}$$

These quantities are thus available for printing, plotting, or further analysis.

The least squares quadratic fit required by CORREL is performed by the ALGOL procedure CURVEFIT which is a transliteration into ALGOL of a FORTRAN program described in detail by McCracken and

```
ALGOL PROGRAM CORREL                                    PAGE  1

 1  !    THIS PROGRAM PERFORMS AUTO- AND CROSS-CORRELATIONS
 2  ON THE DATA TAKEN FROM THE ARRAY OF THREE MICROBARO-
 3  GRAPHS. IT ACCEPTS PRESSURE READINGS (IN MICROBARS)
 4  SPACED 0.5 MINUTES APART AND WRITTEN IN THE 16F5.0
 5  FORMAT WHICH IS REQUIRED BY PROGRAMS PSPEC AND PSPEC1.
 6
 7       THE DATA FROM MICROBAROGRAPHS 1, 2, AND 3 ARE READ
 8  IN THAT ORDER AND THE AVERAGE PRESSURE VALUE IS REMOVED
 9  FROM EACH DATA ARRAY. THE CROSS-CORRELATION COEFFICIENT
10  ARRAY IS COMPUTED FOR EACH PAIR OF MICROBAROGRAPHS AND
11  THE MAXIMUM VALUE OF EACH CROSS-CORRELATION COEFFICIENT
12  IS SELECTED. THE CURVE-FITTING PROGRAM CURVEFIT IS USED
13  TO FIND THE VALUE OF THE LAG TIME FOR WHICH THE
14  COEFFICIENT IS MAXIMUM.
15
16       WHEN THE THREE TIME LAGS ARE KNOWN (CORRESPONDING
17  TO THE TIME DIFFERENCES BETWEEN PAIRS OF RECORDS FOR
18  MAXIMUM CROSS-CORRELATION), PROGRAM DIRECT IS CALLED TO
19  SOLVE FOR THE ANGLE OF ARRIVAL AND VELOCITY OF THE
20  PRESSURE EVENT.
21
22       AUTO-CORRELATION COEFFICIENTS ARE ALSO COMPUTED
23  FOR EACH OF THE DATA ARRAYS.
24
25       CORREL EXPECTS THE DATA TO BE IN A DISK FILE NAMED
26  ALG05.DAT AND CREATES ON OUTPUT A DISK FILE NAMED
27  ALG08.DAT WITH PROTECTION CODE 155. THIS OUTPUT FILE
28  CONTAINS:
29    1.   N       THE NUMBER OF POINTS IN EACH ARRAY
30    2.   SUMI    THE SUM OF THE SQUARES OF THE DATA POINTS
31               IN THE RECORD FROM MICROBAROGRAPH NUMBER I
32               (I = 1,2,3)
33    3.   THE CROSS-CORRELATION ARRAYS FROM INSTRUMENT
34               PAIRS 3-2, 3-1, AND 2-1
35    4.   THE AUTO-CORRELATION ARRAYS FROM INSTRUMENTS
36               1, 2, AND 3
37
38       EXTERNAL PROCEDURES REQUIRED: CURVEFIT, DIRECT
39
40
41  ;
42    BEGIN
43    INTEGER NCARD,INST1;
44    STRING DATE1;
45    EXTERNAL REAL PROCEDURE CURVEFIT, DIRECT;
46     INPUT (5,"DSK");
47     OUTPUT (8,"DSK");
48     SELECTINPUT (5);
49     OPENFILE (5,"ALG05.DAT");
50    READ (NCARD,INST1,DATE1);
```

```
51      BEGIN
52      ARRAY ATSUM1,ATSUM2,ATSUM3,D1,D2,D3,CRSUM1,CRSUM2,
53          CRSUM3[1:16*(NCARD+1) ],C,CRV,TME[1:7];
54      REAL AS1,AS2,AS3,AVG1,AVG2,AVG3,SUM1,SUM2,SUM3,SUM,
55          CROSS.SUM,MAX,T,T32,T31,T21,V,BETA;
56      INTEGER I,J,K,L,N,N1,N2,N3,I1,I2,
57          INST2,INST3;
58      STRING DATE2,DATE3;
59      SWITCH SW:=SW1,SW2,SW3;
60      SWITCH TW:=TW1,TW2,TW3;
61      N1:=N2:=N3:=0;
62      SUM1:=SUM2:=SUM3:=0;
63      FOR I:=1 UNTIL 16*NCARD DO
64          BEGIN
65          READ (D1[I]);
66          IF D1[I]>900 THEN GOTO L1;
67          SUM1:=SUM1+D1[I];
68          N1:=N1+1;
69          END;
70  L1:READ (NCARD,INST2,DATE2);
71      FOR I:=1 UNTIL 16*NCARD DO
72          BEGIN
73          READ (D2[I]);
74          IF D2[I]>900 THEN GOTO L2;
75          SUM2:=SUM2+D2[I];
76           N2:=N2+1;
77          END;
78  L2:READ (NCARD,INST3,DATE3);
79      FOR I:=1 UNTIL 16*NCARD DO
80          BEGIN
81          READ (D3[I]);
82          IF D3[I]>900 THEN GOTO L3;
83          SUM3:=SUM3+D3[I];
84          N3:=N3+1;
85          END;
86  L3:N:=IMIN(N1,N2,N3);
87      CLOSEFILE (5);
88      AVG1:=SUM1/N1;
89      AVG2:=SUM2/N2;
90      AVG3:=SUM3/N3;
91      SUM1:=SUM2:=SUM3:=0;
92      FOR I:=1 UNTIL N DO
93          BEGIN
94          D1[I]:=D1[I]-AVG1;
95          D2[I]:=D2[I]-AVG2;
96          D3[I]:=D3[I]-AVG3;
97          SUM1:=SUM1+D1[I]↑2;
98          SUM2:=SUM2+D2[I]↑2;
99          SUM3:=SUM3+D3[I]↑2;
100         END;
```

```
101      WRITE ("[2C5S]PROGRAM CORREL[C5S]RECORD OF ");
102      WRITE (DATE1);
103      WRITE ("[C]");
104      FOR L:=1 UNTIL 3 DO
105          BEGIN
106          GOTO SW[L];
107      SW1:SUM:=SQRT(SUM2*SUM3);
108          FOR I:=1 UNTIL N DO
109              BEGIN
110              ATSUM1[I]:=D2[I];
111              ATSUM2[I]:=D3[I];
112              END;
113          I1:=INST2;
114          I2:=INST3;
115          GOTO L4;
116      SW2:SUM:=SQRT(SUM1*SUM3);
117          FOR I:=1 UNTIL N DO
118            ATSUM1[I]:=D1[I];
119          I1:=INST1;
120          GOTO L4;
121      SW3:SUM:=SQRT(SUM1*SUM2);
122          FOR I:=1 UNTIL N DO
123            ATSUM2[I]:=D2[I];
124          I2:=INST2;
125       L4:WRITE ("[C5S]DATA FROM MICROBAROGRAPHS ");
126          PRINT (I1,2,0);
127          WRITE ("  AND  ");
128          PRINT (I2,2,0);
129          FOR I:=1 UNTIL N DO
130              BEGIN
131              CROSS.SUM:=0;
132              FOR J:=1 UNTIL N DO
133                BEGIN
134                K:=J+I-1;
135                IF K>N THEN K:=K-N;
136                CROSS.SUM:=CROSS.SUM+ATSUM1[J]*ATSUM2[K];
137                END;
138              CRSUM3[I]:=CROSS.SUM/SUM;
139              END;
140          MAX:=0;
141          FOR I:=1 UNTIL N DO
142            IF CRSUM3[I]>MAX THEN
143              BEGIN
144              MAX:=CRSUM3[I];
145              J:=I;
146              END;
147          FOR I:=1 UNTIL 5 DO
148            BEGIN
149            K:=J-3+I;
150            IF K<1 THEN K:=K+N;
```

```
151             IF K>N THEN K:=K-N;
152             CRV[I]:=CRSUM3[K];
153             END;
154           TME[1]:=0.5*(J-3);
155           FOR I:=2 UNTIL 5 DO
156             TME[I]:=TME[I-1]+0.5;
157           CURVEFIT (TME,CRV,5,2,C);
158           T:=-C[2]/(2*C[3]);
159           IF T>20 THEN T:=T-0.5*N;
160           IF T<(-20) THEN T:=T+0.5*N;
161           WRITE ("[C5S]MAXIMUM CORRELATION");
162           WRITE (" COEFFICIENT = ");
163           PRINT (MAX,2,3);
164           WRITE ("  AT T = ");
165           PRINT (T,3,3);
166           GOTO TW[L];
167           TW1:T32:=T;      GOTO L5;
168           TW2:T31:=T;      GOTO L5;
169           TW3:T21:=T;
170        L5:WRITE ("[C]");
171           FOR I:=1 UNTIL N DO
172               BEGIN
173               IF L=1 THEN CRSUM1[I]:=CRSUM3[I];
174               IF L=2 THEN CRSUM2[I]:=CRSUM3[I];
175               END;
176           END;
177        DIRECT (T32,T31,T21,V,BETA);
178        WRITE ("[2C5S]RESULTS OF CROSS-CORRELATIONS:");
179        WRITE ("[2C5S]VELOCITY = ");
180        PRINT (V,4,2);
181        WRITE ("  METERS/SECOND[5S]BEARING = ");
182        PRINT (BETA,4,1);
183        WRITE ("  DEGREES[C14S]= ");
184        V:=V*2.237;
185        PRINT (V,4,2);
186        WRITE ("  MILES/HOUR[2C]");
187        WRITE ("[3P]");
188        FOR I:=1 UNTIL N DO
189            BEGIN
190            AS1:=AS2:=AS3:=0;
191            FOR J:=1 UNTIL N DO
192                BEGIN
193                K:=J+I-1;
194                IF K>N THEN K:=K-N;
195                AS1:=AS1+D1[J]*D1[K];
196                AS2:=AS2+D2[J]*D2[K];
197                AS3:=AS3+D3[J]*D3[K];
198                END;
199            ATSUM1[I]:=AS1/SUM1;
200            ATSUM2[I]:=AS2/SUM2;
```

```
201          ATSUM3[I]:=AS3/SUM3;
202          END;
203       SELECTOUTPUT (8);
204       OPENFILE (8,"ALG08.DAT",%155);
205       NCARD:=2*NCARD;
206       IF (NCARD*8-N)>8 THEN NCARD:=NCARD-1;
207       I1:=2;
208       I2:=3;
209       PRINT (N,5,0);     WRITE ("[C]");
210       PRINT (SUM1);      WRITE ("[C]");
211       PRINT (SUM2);      WRITE ("[C]");
212       PRINT (SUM3);      WRITE ("[C]");
213       FOR L:=1 UNTIL 6 DO
214           BEGIN
215           PRINT (NCARD,3,0);
216           WRITE ("[C]");
217           IF L<4 THEN
218               BEGIN
219               IF L=2 THEN I1:=1;
220               IF L=3 THEN I2:=2;
221               PRINT (I1,1,0);
222               PRINT (I2,1,0);
223               END
224               ELSE
225               BEGIN
226               K:=L-3;
227               PRINT (K,1,0);
228               END;
229           WRITE ("[S]");
230           WRITE (DATE1);
231           IF L=2 THEN FOR I:=1 UNTIL N DO
232             CRSUM1[I]:=CRSUM2[I];
233           IF L=3 THEN FOR I:=1 UNTIL N DO
234             CRSUM1[I]:=CRSUM3[I];
235           IF L=4 THEN FOR I:=1 UNTIL N DO
236             CRSUM1[I]:=ATSUM1[I];
237           IF L=5 THEN FOR I:=1 UNTIL N DO
238             CRSUM1[I]:=ATSUM2[I];
239           IF L=6 THEN FOR I:=1 UNTIL N DO
240             CRSUM1[I]:=ATSUM3[I];
241           N1:=NCARD-1;
242           FOR I:=1 UNTIL N1 DO
243               BEGIN
244               J:= 8*(I-1) + 1;
245               WRITE ("[C]");
246               FOR K:=J UNTIL J+7 DO
247                 PRINT (CRSUM1[K],2,4);
248               END;
249           WRITE ("[C]");
250           FOR I:=8*N1+1 UNTIL N DO
```

```
251             PRINT (CRSUM1[I],2,4);
252           CRSUM1[N+1]:=999.0;
253           PRINT (CRSUM1[N+1],5,1);
254           FOR I:=N+2 UNTIL 8*NCARD DO
255               BEGIN
256               CRSUM1[I]:=0.0;
257               PRINT (CRSUM1[I],2,4);
258               END;
259           WRITE ("[C]");
260           END;
261       CLOSEFILE (8);
262       END;
263     END
```

ALGOL PROGRAM CURVEFIT PAGE 1

```
 1  !   THIS IS A GENERALIZED PROGRAM WHICH PERFORMS A
 2  LEAST SQUARES POLYNOMIAL FIT. THE DEGREE OF THE POLY-
 3  NOMIAL IS SPECIFIED AS DATA -- FIRST TO TENTH DEGREE
 4  FITS ARE POSSIBLE.
 5      THE PROGRAM IS AN ADAPTATION OF A FORTRAN IV PROGRA
 6  GIVEN BY DANIEL D. MCCRACKEN AND WILLIAM S. DORN IN
 7  "NUMERICAL METHODS AND FORTRAN PROGRAMMING" (JOHN WILEY
 8  & SONS, 1964).
 9      THE PRINCIPAL VARIABLES ARE:
10   NUMBER   THE ACTUAL NUMBER OF X-Y DATA PAIRS
11   M        THE DEGREE OF THE POLYNOMIAL FIT DESIRED
12            (MAXIMUM 10)
13   N        THE NUMBER OF EQUATIONS (=M+1)
14   X,Y      ARRAYS FOR THE DATA PAIRS
15   A        ARRAY FOR THE SUMS, WHICH BECOME THE COEFF-
16            ICIENTS OF THE UNKNOWNS IN THE SIMULTANEOUS
17            EQUATIONS
18   B        ARRAY FOR THE CONSTANT TERMS IN THE SIMUL-
19            TANEOUS EQUATIONS
20   C        ARRAY FOR THE UNKNOWNS, WHICH BECOME THE
21            COEFFICIENTS IN THE POLYNOMIAL
22   P        ARRAY FOR THE POWERS OF THE X(I), FROM 1 TO 2
23
24  ;
25  REAL PROCEDURE CURVEFIT (X,Y,NUMBER,M,C);
26  VALUE NUMBER,M;  INTEGER NUMBER,M;   REAL ARRAY X,Y,C;
27  BEGIN
28  REAL ARRAY A[1:M+1,1:M+1], B[1:M+1], P[1:2*M];
29  INTEGER I,J,K,L,N,MX2,NM1,IP1,KP1;
30  REAL FACTOR,SUM,TEMP;
31  MX2:=M*2;
32  FOR I:=1 UNTIL MX2 DO
33    BEGIN
34    P[I]:=0;
35    FOR J:=1 UNTIL NUMBER DO
36     P[I]:=P[I]+X[J]↑I;
37    END;
38  N:=M+1;
39  FOR I:=1 UNTIL N DO
40    FOR J:=1 UNTIL N DO
41      BEGIN
42      K:=I+J-2;
43      IF K>0 THEN A[I,J]:=P[K] ELSE A[1,1]:=NUMBER;
44      END;
45  B[1]:=0;
46  FOR J:=1 UNTIL NUMBER DO
47    B[1]:=B[1]+Y[J];
48  FOR I:=2 UNTIL N DO
49    BEGIN
50    B[I]:=0;
```

```
51    FOR J:=1 UNTIL NUMBER DO
52      B[I]:=B[I]+Y[J]*X[J]↑(I-1);
53    END;
54  NM1:=N-1;
55  FOR K:=1 UNTIL NM1 DO
56    BEGIN
57    KP1:=K+1;
58    L:=K;
59    FOR I:=KP1 UNTIL N DO
60      IF (ABS(A[I,K])-ABS(A[L,K]))>0 THEN L:=I;
61    IF (L-K)<=0 THEN GOTO L2;
62    FOR J:=K UNTIL N DO
63      BEGIN
64      TEMP:=A[K,J];
65      A[K,J]:=A[L,J];
66      A[L,J]:=TEMP;
67      END;
68    TEMP:=B[K];
69    B[K]:=B[L];
70    B[L]:=TEMP;
71  L2:FOR I:=KP1 UNTIL N DO
72       BEGIN
73       FACTOR:=A[I,K]/A[K,K];
74       A[I,K]:=0;
75       FOR J:=KP1 UNTIL N DO
76         A[I,J]:=A[I,J]-FACTOR*A[K,J];
77       B[I]:=B[I]-FACTOR*B[K];
78       END;
79     END;
80  C[N]:=B[N]/A[N,N];
81  I:=NM1;
82  L3:IP1:=I+1;
83  SUM:=0;
84  FOR J:=IP1 UNTIL N DO
85    SUM:=SUM+A[I,J]*C[J];
86  C[I]:=(B[I]-SUM)/A[I,I];
87  I:=I-1;
88  IF I>0 THEN GOTO L3;
89  END
```

Dorn (1964), who discuss at length the algorithm used and give examples of the accuracies obtainable with the program.

The maximum cross-correlation coefficients, as determined by CORREL and CURVEFIT, are simply the quantities t_{ij}, the time displacements corresponding to maximum correlation, as discussed in Chapter III. These numbers can therefore be used to evaluate the velocity v and angle of arrival β of the pressure wave. The necessary computations, as discussed in Chapter III, are performed by the ALGOL procedure DIRECT.

A.5 Simultaneous Triple Cross-correlation:

The values of the t_{ij} computed by CORREL are, in practice, approximate since the three Δp records are considered only in pairs. Thus, the determinations of t_{32} and t_{31} imply a value for t_{21} which may be different from that produced by the final cross-correlation. This effect occurs because the maximum value of $\sigma_{ij}(\tau)$ is, in practice, always less than unity. Hence, the values of the t_{ij} produced by CORREL invariably fail to satisfy the condition

$$t_{31} = t_{32} + t_{21} \qquad \text{- (A26)}$$

$$t_{ij} \equiv t_i - t_j$$

and the resulting values of v and β are incorrect.

The ALGOL program TRICRS deals with this difficulty through a simultaneous cross-correlation of all three Δp records. The definition of the cross-correlation coefficient (A20) is extended to

```
ALGOL PROGRAM DIRECT                                    PAGE  1

 1  !   THIS PROGRAM COMPUTES THE BEARING AND VELOCITY OF
 2  PRESSURE WAVES INCIDENT UPON AN ARRAY OF THREE MICRO-
 3  BAROGRAPHS.
 4      THE DEFINITIONS OF QUANTITIES ARE:   (I,J = 1,2,3)
 5   TI      THE TIME OF ARRIVAL OF THE WAVE AT STATION
 6           NUMBER I
 7   TIJ     THE TIME DIFFERENCE  TI - TJ
 8   DI      THE LENGTH OF THE SIDE OPPOSITE STATION NUMBER
 9           I OF THE TRIANGLE FORMED BY THE ARRAY OF THREE
10           MICROBAROGRAPHS
11   PHII    THE ANGLE BETWEEN TRUE NORTH AND SIDE NUMBER I
12   V       THE HORIZONTAL COMPONENT OF VELOCITY OF THE
13           INCIDENT WAVE
14   BETA    THE ANGLE OF ARRIVAL (IN DEGREES WITH RESPECT
15           TO TRUE NORTH) OF THE INCIDENT WAVE
16
17      THE EQUATIONS TO BE SOLVED ARE:
18           COS(BETA-PHI1) = (V/D1)*T32
19           COS(BETA-PHI2) = (V/D2)*T31
20           COS(BETA+PHI3) = (V/D3)*T21
21
22      FOR THE U.W.O. ARRAY:
23           D1 = 4.10 KM          PHI1 = 82.8 DEGREES
24           D2 = 4.57 KM          PHI2 = 26.5 DEGREES
25           D3 = 4.11 KM          PHI3 = 29.0 DEGREES
26
27
28 ;
29    REAL PROCEDURE DIRECT (T32,T31,T21,V,BETA);
30    VALUE T32,T31,T21;  REAL T32,T31,T21,V,BETA;
31    BEGIN
32    REAL C1,C2,C3,D1,D2,D3,DR,PHI1,PHI2,PHI3,PI,S1,S2,S3,
33      V1,V2,V3,X,X1,X2,X3;
34    INTEGER N;
35    PI:=2*ARCCOS(0);
36    DR:=PI/180;
37    D1:=4.10&3;
38    D2:=4.57&3;
39    D3:=4.11&3;
40    PHI1:=82.8*DR;
41    PHI2:=26.5*DR;
42    PHI3:=29*DR;
43    C1:=COS(PHI1);
44    C2:=COS(PHI2);
45    C3:=COS(PHI3);
46    S1:=SIN(PHI1);
47    S2:=SIN(PHI2);
48    S3:=SIN(PHI3);
49    T32:=T32*60;
50    T31:=T31*60;
```

```
51    T21:=T21*60;
52    X1:=-(T32*C2/D1-T31*C1/D2)/(T32*S2/D1-T31*S1/D2);
53    X2:= (T32*C3/D1-T21*C1/D3)/(T32*S3/D1+T21*S1/D3);
54    X3:= (T31*C3/D2-T21*C2/D3)/(T31*S3/D2+T21*S2/D3);
55    X:=(X1+X2+X3)/3;
56    BETA:=ARCTAN(X);
57    N:=0;
58  L1: N:=N+1;
59    V1:=D1*COS(BETA-PHI1)/T32;
60    V2:=D2*COS(BETA-PHI2)/T31;
61    V3:=D3*COS(BETA+PHI3)/T21;
62    IF (V1<0 OR V2<0 OR V3<0) THEN
63        BEGIN
64        IF N=1 THEN GOTO L2 ELSE GOTO L3;
65        END
66        ELSE
67        GOTO L4;
68  L2: BETA:=BETA+PI;
69      GOTO L1;
70  L3: WRITE ("[2C5S]***  NO SOLUTION  ***[2C]");
71  L4: V:=(V1+V2+V3)/3;
72    BETA:=BETA/DR;
73    IF BETA<0 THEN BETA:=BETA+360;
74  END
```

```
1  !    THIS PROGRAM PERFORMS A SIMULTANEOUS TRIPLE CROSS-
2  CORRELATION OF THE DATA TAKEN FROM THE ARRAY OF THREE
3  MICROBAROGRAPHS. IT ACCEPTS PRESSURE READINGS (IN
4  MICROBARS) SPACED Ø.5 MINUTES APART AND WRITTEN IN THE
5  16F5.Ø FORMAT WHICH IS REQUIRED BY PROGRAMS PSPEC AND
6  PSPEC1.
7
8       THE DATA FROM MICROBAROGRAPHS 1, 2, AND 3 ARE READ
9  IN THAT ORDER. THE AVERAGE PRESSURE VALUE IS REMOVED
10 FROM EACH DATA ARRAY AND A ZERO-FREQUENCY COMPONENT OF
11 3ØØ MICROBARS IS ADDED TO EACH DATA POINT. THE TRIPLE
12 CROSS CORRELATION COEFFICIENT ARRAY IS COMPUTED AND
13 PROGRAM CURVEFIT IS CALLED TO PERFORM A ROW-WISE AND A
14 COLUMN-WISE FIT ABOUT THE POINT OF MAXIMUM CORRELATION.
15
16      THE POLYNOMIAL COEFFICIENTS PRODUCED BY CURVEFIT
17 ARE USED TO COMPUTE THE VALUES OF THE TIME LAGS T31 AND
18 T21 WHICH CORRESPOND TO THE POINT OF MAXIMUM CORRE-
19 LATION. T32 IS DERIVED AND PROGRAM DIRECT IS CALLED TO
20 CALCULATE THE ANGLE OF ARRIVAL AND VELOCITY OF THE
21 PRESSURE EVENT.
22
23      TRICRS EXPECTS THE DATA TO BE IN A DISK FILE NAMED
24 ALGØ5.DAT.
25
26
27
28      EXTERNAL PROCEDURES REQUIRED: CURVEFIT,DIRECT
29
30
31
32 ;
33   BEGIN
34   INTEGER NCARD,INST1;
35   STRING DATE1;
36   EXTERNAL REAL PROCEDURE CURVEFIT, DIRECT;
37    INPUT (5,"DSK");
38    SELECTINPUT (5);
39    OPENFILE (5,"ALGØ5.DAT");
40   READ (NCARD,INST1,DATE1);
41     BEGIN
42     ARRAY D1,D2,D3[1:16*NCARD],C,CRV,TME[1:7],
43         CRSUM[1:16*NCARD,1:16*NCARD];
44     REAL AVG1,AVG2,AVG3,SUM1,SUM2,SUM3,SUM,
45         CROSS.SUM,MAX,T,T32,T31,T21,V,BETA;
46     INTEGER I,J,K,L,M,N,N1,N2,N3,NCOL,NROW,INST2,INST3;
47     STRING DATE2,DATE3;
48     N1:=N2:=N3:=Ø;
49     SUM1:=SUM2:=SUM3:=Ø;
50     FOR I:=1 UNTIL 16*NCARD DO
```

```
51          BEGIN
52          READ (D1[I]);
53          IF D1[I]>900 THEN GOTO L1;
54          SUM1:=SUM1+D1[I];
55          N1:=N1+1;
56          END;
57   L1:READ (NCARD,INST2,DATE2);
58      FOR I:=1 UNTIL 16*NCARD DO
59          BEGIN
60          READ (D2[I]);
61          IF D2[I]>900 THEN GOTO L2;
62          SUM2:=SUM2+D2[I];
63          N2:=N2+1;
64          END;
65   L2:READ (NCARD,INST3,DATE3);
66      FOR I:=1 UNTIL 16*NCARD DO
67          BEGIN
68          READ (D3[I]);
69          IF D3[I]>900 THEN GOTO L3;
70          SUM3:=SUM3+D3[I];
71          N3:=N3+1;
72          END;
73   L3:N:=IMIN(N1,N2,N3);
74      CLOSEFILE (5);
75      AVG1:=SUM1/N1;
76      AVG2:=SUM2/N2;
77      AVG3:=SUM3/N3;
78      SUM1:=SUM2:=SUM3:=0;
79      FOR I:=1 UNTIL N DO
80        BEGIN
81        D1[I]:=D1[I]-AVG1+300;
82        D2[I]:=D2[I]-AVG2+300;
83        D3[I]:=D3[I]-AVG3+300;
84        SUM1:=SUM1+D1[I]↑3;
85        SUM2:=SUM2+D2[I]↑3;
86        SUM3:=SUM3+D3[I]↑3;
87        END;
88      SUM:=(SUM1*SUM2*SUM3)↑(1/3);
89      FOR I:=1 UNTIL N DO
90        FOR J:=1 UNTIL N DO
91            BEGIN
92            CROSS.SUM:=0;
93            FOR K:=1 UNTIL N DO
94              BEGIN
95              L:=J+K-1;
96              IF L>N THEN L:=L-N;
97              M:=I+K-1;
98              IF M>N THEN M:=M-N;
99              CROSS.SUM:=CROSS.SUM+D1[K]*D2[L]*D3[M];
100             END;
```

```
101             CRSUM[I,J]:=CROSS.SUM/SUM;
102             END;
103         MAX:=0;
104         FOR I:=1 UNTIL N DO
105           FOR J:=1 UNTIL N DO
106             IF CRSUM[I,J]>MAX THEN
107               BEGIN
108               MAX:=CRSUM[I,J];
109               NROW:=I;
110               NCOL:=J;
111               END;
112         WRITE ("[P5S]PROGRAM TRICRS[C5S]RECORD OF ");
113         WRITE (DATE1);
114         WRITE ("[2C5S]TRIPLE CROSS CORRELATION:[C]");
115         FOR L:=1 UNTIL 2 DO
116           BEGIN
117           FOR I:=1 UNTIL 5 DO
118             BEGIN
119             IF L=1 THEN J:=NROW-3+I ELSE J:=NCOL-3+I;
120             IF J<1 THEN J:=J+N;
121             IF J>N THEN J:=J-N;
122             IF L=1 THEN CRV[I]:=CRSUM[J,NCOL]
123                    ELSE CRV[I]:=CRSUM[NROW,J];
124             END;
125           IF L=1 THEN TME[1]:=0.5*(NROW-3)
126                  ELSE TME[1]:=0.5*(NCOL-3);
127           FOR I:=1 UNTIL 4 DO
128             TME[I+1]:=TME[I]+0.5;
129           CURVEFIT (TME,CRV,5,2,C);
130           T:= -C[2]/(2*C[3]);
131           IF T>20 THEN T:=T-0.5*N;
132           IF T<(-20) THEN T:=T+0.5*N;
133           IF L=1 THEN T31:=T ELSE T21:=T;
134           END;
135         WRITE ("[2C5S]MAXIMUM CORRELATION COEFFICIENT = ");
136         PRINT (MAX,2,3);
137         T32:=T31-T21;
138         WRITE ("[2C5S]T32 = ");
139         PRINT (T32,2,3);
140         WRITE ("[C5S]T31 = ");
141         PRINT (T31,2,3);
142         WRITE ("[C5S]T21 = ");
143         PRINT (T21,2,3);
144         DIRECT (T32,T31,T21,V,BETA);
145         WRITE ("[2C5S]VELOCITY = ");
146         PRINT (V,4,2);
147         WRITE ("  METERS/SECOND[5S]BEARING = ");
148         PRINT (BETA,4,1);
149         WRITE ("  DEGREES[C14S]= ");
150         V:=V*2.237;
```

```
151       PRINT (V,4,2);
152       WRITE ("  MILES/HOUR[2C]");
153       END;
154     WRITE ("[3P]");
155     END
```

$$\sigma_{123}(\tau_1,\tau_2) = \frac{\gamma_{123}(\tau_1,\tau_2)}{\sqrt[3]{v_{31}v_{32}v_{33}}} \qquad \text{- (A27)}$$

$$\tau_1 = 0, \Delta t, 2\Delta t, 3\Delta t, \ldots., N\Delta t$$

$$\tau_2 = 0, \Delta t, 2\Delta t, 3\Delta t, \ldots., N\Delta t$$

where

$$\gamma_{123}(\tau_1,\tau_2) = \sum_{t=0}^{N\Delta t} \Delta p_1(t)\ \Delta p_2(t+\tau_1)\ \Delta p_3(t+\tau_2) \qquad \text{- (A28)}$$

and

$$v_{3i} \equiv \gamma_{iii}(0,0) = \sum_{t=0}^{N\Delta t} \left[\Delta p_i(t)\right]^3 \quad . \qquad \text{- (A29)}$$

Whereas the quantities $\sigma_{ij}(\tau)$ are 1 x N arrays, the quantity $\sigma_{123}(\tau_1,\tau_2)$ is an N x N array. Hence, the required computing time increases approximately as N^3 and the number of storage locations required increases approximately as N^2, making TRICRS an expensive program to run.

The definitions (A27) to (A29) have one important failing. Whereas the conventional cross-correlation coefficient remains positive when both records go negative, indicating correctly the similarity between the records, the triple cross-correlation coefficient (A27) does not have this useful property. It is therefore necessary to replace the data vectors Δp_i in equations (A27) to (A29) by the quantities $(\Delta p_i)_+$ which may be defined by

(a) $$(\Delta p_i)_+ = |\Delta p_i| \qquad \text{- (A30)}$$

or

(b) $$(\Delta p_i)_+ = (\Delta p_i)^2 \qquad \text{- (A31)}$$

or

(c) $$(\Delta p_i)_+ = \Delta p_i - \overline{\Delta p_i} + p_c \qquad \text{- (A32)}$$

where

$$\overline{\Delta p_i} = \frac{1}{N} \sum_{t=0}^{N\Delta t} \Delta p_i(t) \qquad \text{- (A33)}$$

and p_c is an arbitrary constant, large with respect to the variations in Δp and the same for all three records.

For the present application, tests showed that option (c) provided the best results, with the arbitrary constant assuming the value p_c = +300 microbars.

After the N-square array of the coefficients $\sigma_{123}(\tau_1,\tau_2)$ has been obtained and the maximum element of that array has been found, procedure CURVEFIT is called twice to do a two-dimensional least squares quadratic fit by which the values of τ_1 and τ_2 are determined for the point where σ_{123} is maximum. This determines t_{31} and t_{21}; t_{32} is then found from equation (A26) and the procedure DIRECT is called to solve the direction-finding equations.

The accuracies obtainable with TRICRS in the present work are discussed in Chapter IV.

APPENDIX B

TABULATED DATA CONCERNING THE OBSERVED WAVES

This Appendix contains, in tabular form, the data upon which the analysis of the waves is based. The significance of each column heading in the tables is explained below:

1. EVENT NO.: Each wave is given an identifying number, the last two digits of which indicate the year in which the wave was recorded.

2. DATE and TIME (GMT): These columns contain the date and time (to the nearest five minutes) of the arrival of the initial part of the wave at the microbarograph array. The time given here is an approximate average of the arrival times at the three stations.

3. V (MPH): The velocity given here is, by virtue of the methods used to obtain the quantities t_{ij} (Chapter III), the horizontal component of the group velocity of the wave. It is expressed here in miles/hour in order to facilitate the plotting of possible source regions on standard maps.

4. BETA (DEG): Beta (β) is the horizontal angle of arrival of the wave, referred to true north and expressed in degrees. Thus, for example, a wave coming from the east would have $\beta = 90$ degrees.

5. FRONTAL TYPE, WAVE?, and MOTION: These columns refer to conditions at the region of origin of the wave. They indicate whether the source region was occupied by a frontal system at the time of origin of the wave, which type of front it was, whether the source was near a

cyclonic wave, and whether the front was approaching the receiving array or receding from it. The phrase "NO APPARENT SOURCE" in these columns indicates that no plausible source was located by the methods discussed in Chapter V.

6. AT SOURCE PRESS and PRECIP: The first of these columns indicates the static pressure system prevalent at the source of the wave. The second tells whether there was precipitation reported in the source region at or near the time of generation of the wave and which type it was. R signifies rain, S snow, T thunderstorm, and W showers.

7. XU + SOURCE IN SAME AIR MASS?: A "YES" in this column indicates that the wave was observed to remain within the same air mass throughout its journey from source to receiver -- i.e. that it did not pass through a frontal zone.

8. XU RADAR ECHO?: The information contained in this column is whether any echoes whatsoever were observed on the radar screen at the London Weather Office (station code XU) at the time of observation of the wave or during the several hours immediately preceding the observation. The radar wavelength is 3.5 cm, so that the echoes indicate regions of concentrations of hydrometeors. The maximum range of the radar unit is about 150 miles.

9. MEAN DIST. (MILES) and MEAN TIME (HOURS): These columns contain the approximate distance between the source and the receiving array and the approximate time required for the wave to traverse this distance.

10. MEAN PERIOD (MIN): The average period of the wave was estimated in each case by measuring the times between peaks on the recording charts and taking the average of these values. The resulting period is approximate, since the method ignores the fact that several frequency

components may be present. However, in the case of the waves for which a computer analysis was performed, this method provided values which were in good agreement with the periods of dominant spectral lines.

11. SURFACE CONDITIONS, XU: The last four columns show the surface weather conditions observed at the London Weather Office (station code XU) at the time when the wave was recorded. The pressure given here is the corrected sea level pressure in millibars, and the wind speed is given in miles/hour. The standard code is used for visible weather and cloud types, viz:

F	Fog	H	Haze	K	Smoke
L	Drizzle	R	Rain	S	Snow
SG	Snow Grains	T	Thunderstorm	W	Showers

The symbols "-" and "--" are used to indicate light and very light precipitation, respectively.

AC	Altocumulus	CU	Cumulus
AS	Altostratus	SC	Stratocumulus
CB	Cumulonimbus	SF	Stratus Fractus
CI	Cirrus	ST	Stratus
CS	Cirrostratus		

The numbers indicate the amount of cloud cover in tenths.

EVENT NO.	DATE	TIME (GMT)	V (MPH)	BETA (DEG)	FRONTAL TYPE	WAVE?	MOTION
10-69	14 NOV	0505	75.6	236	COLD	YES	REC
11-69	14 NOV	0950	77.4	204	COLD	YES	REC
12-69	17 NOV	0640	69.3	273	WARM	YES	APP
13-69	17 NOV	0815	46.5	313	WARM	YES	APP
14-69	22 NOV	0255	29.6	41	WARM	NO	APP
15-69	22 NOV	0345	34.2	43	WARM	NO	APP
16-69	30 NOV	1235	74.5	317	WARM	YES	APP
17-69	6 DEC	1655	65.4	230	WARM	YES	APP
18-69	6 DEC	1740	122.8	163			
19-69	6 DEC	1400	53.3	196	WARM	NO	
20-69	6 DEC	1515	61.5	168	WARM	NO	
21-69	6 DEC	1555	59.4	131	WARM	NO	
22-69	8 DEC	1650	135.5	203	NO APPARENT SOURCE		
23-69	8 DEC	1730	136.4	190	NO APPARENT SOURCE		
24-69	8 DEC	1825	66.6	183	NO APPARENT SOURCE		
25-69	9 DEC	0340	64.6	204	NO APPARENT SOURCE		
26-69	9 DEC	1530	72.3	159	COLD	NO	
27-69	17 DEC	1735	79.8	330	WARM	NO	APP
28-69	24 DEC	2220	48.4	254	NO APPARENT SOURCE		
29-69	25 DEC	0040	53.0	247	NO APPARENT SOURCE		
30-69	25 DEC	0120	49.1	245	NO APPARENT SOURCE		
31-69	29 DEC	0805	66.4	323			
1-70	1 JAN	0625	92.4	246	WARM	NO	APP
2-70	4 JAN	1645	57.3	224			
6-70	12 JAN	0550	43.2	276	COLD	NO	APP
7-70	17 JAN	0540	25.3	340	COLD	NO	APP
10-70	19 JAN	0930	123.0	259	WARM	NO	APP
12-70	24 JAN	1045	44.3	263	WARM	NO	APP
13-70	25 JAN	0655	38.5	313	WARM	YES	APP
14-70	29 JAN	1920	283.9	273			
15-70	29 JAN	1715	155.0	274			
16-70	15 FEB	0350	67.9	268	WARM	YES	APP
18-70	15 FEB	0605	55.4	226	WARM	YES	APP
19-70	15 FEB	2100	111.4	229	WARM	YES	APP
21-70	1 MAR	2025	37.4	312			
22-70	3 MAR	1000	63.8	262	COLD	YES	
23-70	17 MAR	1440	116.9	222	WARM	YES	APP
24-70	19 MAR	2115	76.9	292	NO APPARENT SOURCE		
26-70	22 MAR	0545	103.0	287	WARM	YES	APP
27-70	25 MAR	0640	97.3	254	WARM	YES	APP

EVENT NO.	DATE	TIME (GMT)	V (KMPS)	BETA (DEG)	FRONTAL TYPE	WAVE?	MOTION
28-70	26 MAR	0630	94.4	269	COLD	NO	REC
29-70	29 MAR	0945	105.0	263	WARM	NO	
30-70	30 MAR	0630	112.5	231	COLD	NO	REC
31-70	16 APR	0630	50.5	216	COLD	YES	REC
33-70	18 APR	2005	76.7	241	WARM	YES	APP
34-70	18 APR	2330	130.6	251	WARM	YES	APP
37-70	19 APR	0715	76.0	335	NO APPARENT SOURCE		
38-70	19 APR	0820	33.0	335	NO APPARENT SOURCE		
39-70	23 APR	2015	102.0	282	NO APPARENT SOURCE		
40-70	26 APR	1250	25.1	210	WARM	YES	APP
77-70	30 APR	1500	40.5	247	COLD	YES	APP
78-70	30 APR	1700	79.6	241	COLD	YES	APP
42-70	27 MAY	1530	95.0	275	WARM	YES	APP
43-70	19 JUN	1340	92.5	224	WARM	YES	APP
44-70	21 JUN	0045	66.0	234	WARM	YES	APP
45-70	21 JUN	0215	57.0	228	WARM	YES	APP
46-70	1 JUL	1445	66.2	349	WARM	YES	APP
48-70	6 JUL	2250	63.2	321	COLD	YES	APP
49-70	16 JUL	0645	45.3	149	COLD	NO	REC
50-70	16 JUL	0345	29.5	317	COLD	NO	APP
51-70	27 JUL	1100	33.1	246			
52-70	27 JUL	1330	44.1	261	NO APPARENT SOURCE		
53-70	2 AUG	2355	171.0	245	WARM	YES	APP
54-70	3 AUG	0210	175.0	236	COLD	NO	APP
55-70	16 AUG	0630	79.4	305	COLD	YES	APP
56-70	22 AUG	1230	96.9	235	WARM	YES	APP
57-70	3 SEP	1230	42.3	222	WARM	NO	APP
58-70	6 SEP	1605	116.0	277	COLD	NO	APP
60-70	24 SEP	2040	52.3	275	COLD	YES	APP
61-70	26 SEP	0705	90.2	246	COLD	NO	
62-70	26 SEP	1635	67.3	216	COLD	NO	
63-70	27 SEP	0300	66.7	264	COLD	NO	REC
64-70	27 SEP	0400	53.0	253	COLD	NO	REC
67-70	3 OCT	0130	57.0	253	NO APPARENT SOURCE		
68-70	30 OCT	0450	74.7	215	COLD	NO	APP
69-70	30 OCT	1355	49.4	232	WARM	YES	APP
70-70	11 DEC	0615	62.9	266	WARM	YES	APP
71-70	11 DEC	1355	58.6	239	WARM	YES	APP
72-70	21 DEC	0710	53.5	253	WARM	NO	APP
73-70	21 DEC	1056	68.6	244	WARM	NO	APP

EVENT NO.	DATE	TIME (GMT)	V (MPH)	BETA (DEG)	FRONTAL TYPE	WAVE?	MOTION
74-70	21 DEC	1325	43.6	225	WARM	YES	APP
75-70	31 DEC	0030	50.1	190			
76-70	31 DEC	2130	37.6	200			
68-71	9 JAN	1020	61.6	250	WARM	NO	APP
69-71	16 FEB	0535	64.3	261	WARM	YES	APP
1-71	2 MAR	1740	103.0	281			
2-71	2 MAR	2030	106.6	259			
4-71	3 MAR	0645	122.0	221	WARM	YES	APP
5-71	3 MAR	1050	96.9	229	WARM	YES	APP
6-71	5 MAR	1500	73.3	270	WARM	YES	APP
7-71	6 MAR	0355	66.7	247	WARM	YES	APP
8-71	6 MAR	0600	63.4	249	WARM	YES	APP
9-71	6 MAR	1105	75.0	249	WARM	YES	APP
11-71	6 MAR	2050	65.2	231	WARM	YES	APP
12-71	10 MAR	1120	54.6	274	COLD	YES	
13-71	10 MAR	1345	59.6	279	COLD	YES	
15-71	10 MAR	1445	54.2	274	COLD	YES	
16-71	13 MAR	2020	81.0	247	WARM	YES	APP
17-71	27 MAR	1430	55.3	262	WARM	NO	APP
18-71	26 MAR	0600	61.6	291	WARM	YES	APP
19-71	5 APR	0550	44.5	322			
20-71	10 APR	1005	53.4	313	NO APPARENT SOURCE		
21-71	10 APR	1530	61.7	312	NO APPARENT SOURCE		
22-71	20 APR	0650	69.5	326			
23-71	27 APR	1310	50.6	233	WARM	YES	APP
24-71	5 MAY	1930	94.2	270	COLD	YES	
25-71	6 MAY	0530	90.3	246	WARM	YES	
26-71	7 MAY	0220	133.2	241	WARM	YES	APP
28-71	15 MAY	0055	77.3	181	COLD	NO	REC
29-71	16 MAY	0550	73.8	235	NO APPARENT SOURCE		
30-71	18 MAY	0200	40.0	294	COLD	YES	APP
31-71	29 MAY	1110	37.6	173	COLD	YES	REC
33-71	4 JUN	2300	47.4	260	WARM	YES	APP
35-71	9 JUN	1015	34.0	197	WARM	NO	APP
36-71	12 JUN	1240	72.3	262			
37-71	12 JUN	2255	72.6	269	COLD	YES	APP
38-71	13 JUN	2105	40.3	280			
39-71	17 JUN	0320	64.8	266	COLD	NO	APP
40-71	9 JUL	0320	56.6	280	COLD	YES	APP
41-71	22 JUL	0955	27.2	323	COLD	NO	APP

EVENT NO.	DATE	TIME (GMT)	V (MPH)	BETA (DEG)	FRONTAL TYPE	WAVE?	MOTION
43-71	30 AUG	0125	43.3	332	COLD	YES	APP
44-71	12 SEP	0550	34.2	264	COLD	NO	REC
45-71	12 SEP	0640	32.8	261	COLD	NO	REC
46-71	12 SEP	0730	30.9	195	COLD	NO	REC
47-71	17 SEP	1040	39.0	275			
48-71	17 SEP	2240	93.2	253			
49-71	19 SEP	0645	54.1	267			
50-71	23 SEP	1035	103.3	232	COLD	NO	
51-71	25 SEP	0150	65.8	284	WARM	NO	APP
52-71	25 SEP	0245	119.9	252			
53-71	25 SEP	0445	64.2	245			
54-71	25 SEP	2025	63.6	266	WARM	NO	APP
55-71	25 SEP	2310	44.2	285	WARM	NO	APP
56-71	10 OCT	0815	47.6	206	COLD	YES	REC
57-71	12 OCT	2000	66.7	297	WARM	YES	APP
58-71	13 OCT	0520	50.5	284			
59-71	14 OCT	1555	43.2	284	WARM	NO	APP
60-71	22 OCT	0700	34.3	200			
61-71	22 OCT	0935	35.7	206			
62-71	26 OCT	1735	60.0	258	COLD	YES	APP
63-71	27 OCT	0105	77.5	206	WARM	YES	REC
64-71	27 OCT	0320	73.6	276	WARM	YES	REC
65-71	27 OCT	0600	57.0	273	WARM	YES	REC
66-71	5 NOV	0910	46.6	259	NO APPARENT SOURCE		
67-71	6 NOV	1025	62.8	256	COLD	YES	APP

EVENT NO.	AT SOURCE PRESS	SOURCE PRECIP	XU+SOURCE IN SAME AIR MASS?	XU RADAR ECHO?	MEAN DIST. (MILES)	MEAN TIME (HOURS)
10-69	LOW	R	YES	YES	1300	17.20
11-69	LOW	R	YES	YES	1100	14.21
12-69	LOW	RW	YES	NO	850	12.27
13-69	LOW		YES	NO	175	3.76
14-69	LOW	SW	YES	NO	900	30.41
15-69	LOW	S	YES	NO	750	21.93
16-69	LOW	S	YES	NO	375	5.03
17-69	LOW	R	YES	NO	1300	19.88
18-69	MID	R	YES	NO	700	5.70
19-69	LOW		YES	NO	400	6.86
20-69	LOW		YES	NO	500	8.13
21-69	LOW		YES	NO	500	8.42
22-69				NO		
23-69				NO		
24-69				NO		
25-69				NO		
26-69	HIGH			NO	1075	14.87
27-69	LOW	S	YES	NO	1150	14.41
28-69				NO		
29-69				NO		
30-69				NO		
31-69	MID	S		NO	800	9.26
1-70	LOW	S	YES	NO	500	5.41
2-70	MID	S	YES	YES	325	5.67
6-70	LOW	S	YES	YES	140	3.18
7-70	LOW	S	YES	NO	425	16.80
10-70	MID	S	YES	NO	1200	9.76
12-70	HIGH		YES	NO	925	20.88
13-70	LOW	S	YES	NO	275	7.14
14-70	MID	S	YES	NO	575	2.00
15-70	MID	S	YES	NO	575	3.71
16-70	LOW	S	YES	NO	1000	14.73
18-70	LOW	TW	YES	NO	675	12.18
19-70	LOW	TW	YES	NO	325	7.41
21-70	HIGH	S	YES	YES	135	3.61
22-70	MID	R		NO	275	4.31
23-70	LOW	RS	YES	NO	650	5.60
24-70				NO		
26-70	LOW	R		NO	900	8.74
27-70	LOW	R	YES	NO	775	7.97

EVENT NO.	AT SOURCE PRESS	PRECIP	XU+SOURCE IN SAME AIR MASS?	XU RADAR ECHOT	MEAN DIST. (MILES)	MEAN TIME (HOURS)
28-70	LOW	S	YES	NO	1250	13.24
29-70	LOW	R	YES	NO	600	5.71
30-70	MID		YES	NO	1350	12.00
31-70	LOW	TW		NO	600	11.58
33-70	LOW	TW	YES	NO	650	11.06
34-70	LOW	TW	YES	NO	350	6.54
37-70				NO		
38-70				NO		
39-70				NO		
40-70	MID	TW	YES	NO	625	24.90
77-70	MID	TW	YES	YES	300	7.41
78-70	LOW	TW	YES	YES	1075	13.51
42-70	LOW	TW	YES	NO	875	9.21
43-70	HIGH	TW	YES	NO	600	6.49
44-70	LOW	TW	YES	NO	550	8.09
45-70	LOW	TW	YES	NO	550	9.65
46-70	LOW	TW	YES	NO	240	3.95
48-70	LOW		YES		775	9.31
49-70	MID	TW	YES	YES	125	2.76
50-70	HIGH	TW	YES	YES	75	2.54
51-70	HIGH	RW	YES	YES	450	13.60
52-70				YES		
53-70	HIGH		YES	NO	600	4.68
54-70	HIGH		YES	NO	325	1.66
55-70	MID	TW	YES	YES	350	4.41
56-70	LOW	TW	YES	NO	600	6.19
57-70	MID	TW	YES	YES	400	9.46
58-70	MID	TW	YES	NO	1075	9.27
60-70	LOW	TW	YES	YES	70	1.29
61-70	MID	TW	YES	NO	1025	11.36
62-70	MID	TW	YES	YES	325	4.83
63-70	MID	TW	YES	YES	175	2.55
64-70	MID	TW	YES	YES	175	2.11
67-70				YES		
68-70	HIGH	RW	YES	NO	150	2.01
69-70	LOW	R	YES	NO	150	3.04
70-70	LOW	S		NO	800	12.72
71-70	LOW	RS	YES	NO	250	4.75
72-70	LOW	RW	YES	NO	775	14.49
73-70	MID	R	YES	NO	750	8.47

EVENT NO.	AT SOURCE PRESS	AT SOURCE PRECIP	XU+SOURCE IN SAME AIR MASS?	XU RADAR ECHO?	MEAN DIST. (MILES)	MEAN TIME (HOURS)
74-70	LOW	R	YES	NO	550	6.58
75-70	MID	R	YES	NO	800	15.97
76-70	LOW	RS	YES	NO	575	15.29
68-71	MID		YES	NO	1250	20.29
69-71	MID			NO	1200	16.66
1-71	MID	SR	YES	NO	1500	14.56
2-71	MID	SW	YES	NO	1050	9.72
4-71	LOW	S	YES	NO	725	5.94
5-71	LOW	S	YES	NO	950	9.90
6-71	LOW	S	YES	YES	1100	15.01
7-71	LOW	S	YES	NO	850	12.74
8-71	LOW	S	YES	NO	850	13.41
9-71	LOW		YES	YES	800	10.67
11-71	LOW		YES	YES	100	1.53
12-71	LOW	S	YES	NO	1200	14.15
13-71	LOW	S	YES	NO	1100	12.28
15-71	LOW	S	YES	NO	1100	13.06
16-71	LOW		YES	NO	890	10.96
17-71	LOW		YES	NO	625	9.67
18-71	LOW		YES	YES	375	4.58
19-71	MID	SW	YES	NO	240	5.39
20-71				NO		
21-71				NO		
22-71	LOW	RW	YES	NO	900	12.95
23-71	LOW		YES		650	12.80
24-71	LOW	TW	YES	NO	1000	10.62
25-71	LOW	RW	YES	YES	500	5.54
26-71	LOW	TW	YES	NO	600	4.50
28-71	HIGH		YES	NO	1250	16.07
29-71				NO		
30-71	LOW	TW	YES	NO	550	13.75
31-71	LOW	R	YES	NO	650	17.57
33-71	LOW	TW	YES		1275	26.90
35-71	MID		YES	NO	400	11.76
36-71	MID	TW	YES	YES	140	1.94
37-71	MID		YES	YES	700	9.64
38-71	MID	TW	YES	YES	775	19.23
39-71	LOW		YES	NO	1050	12.38
40-71	HIGH	TW	YES	NO	250	4.42
41-71	MID	RW	YES	YES	475	17.46

EVENT NO.	AT SOURCE PRESS	PRECIP	XU+SOURCE IN SAME AIR MASS?	XU RADAR ECHO?	MEAN DIST. (MILES)	MEAN TIME (HOURS)
43-71	MID		YES	NO	575	13.28
44-71	LOW	TW	YES	NO	450	13.16
45-71	LOW	TW	YES	NO	450	13.72
46-71	LOW	TW	YES	NO	450	14.56
47-71	MID	RW	YES	YES	1100	28.21
48-71	LOW	TW	YES	NO	1100	11.80
49-71	HIGH	TW	YES	NO	775	14.33
50-71	HIGH	TW		NO	975	9.44
51-71	MID		YES	NO	625	12.54
52-71	MID	R	YES	NO	1000	8.34
53-71	MID	TW		NO	1250	19.47
54-71	MID		YES	YES	600	9.43
55-71	MID		YES	YES	550	12.44
56-71	MID	RW	YES	YES	550	11.55
57-71	LOW		YES	NO	1125	16.87
58-71	LOW	RW	YES	NO	700	13.66
59-71	HIGH		YES	NO	1200	27.76
60-71	HIGH	RW	YES	NO	550	16.03
61-71	HIGH	RW	YES	NO	550	15.41
62-71	LOW	R	YES	NO	1300	21.67
63-71	LOW	RW	YES	NO	800	10.32
64-71	LOW	RW	YES	NO	1100	14.95
65-71	LOW	RW	YES	NO	1100	19.30
66-71				NO		
67-71	MID	RW	YES	YES	195	3.11

EVENT NO.	MEAN PERIOD (MIN)	SURFACE CONDITIONS, XU PRESS (MB)	WIND (MPH)	VISIBLE WEATHER	CLOUD COVER
10-69	15.8	999.1	8	FS-	S6SF4
11-69	9.2	998.0	7	FS-	SF5SC3SC2
12-69	11.5	1027.3	15		CS5
13-69	20.0	1025.9	10		AC2
14-69	7.2	1027.4	4		CI1
15-69	8.2	1027.3	2		AC2CI
16-69	5.7	1006.4	14		AC10
17-69	14.5	1025.2	5		AC10
18-69	13.5	1024.9	6		SC7AC3
19-69	5.0	1015.3	12	H	SC10
20-69	7.1	1015.7	11	H	SC10
21-69	6.0	1016.2	12	H	SC10
22-69	9.8	1016.2	14	H	SC10
23-69	10.5	1015.9	12	H	SC10
24-69	7.5	1015.4	9	H	SC10
25-69	5.5	1018.7	9		SC10
26-69	15.0	1022.9	8		CI1
27-69	5.9	1026.4	6	H	SC5
28-69	8.0	1026.2	5		AC1CI2
29-69	9.9	1026.9	6		CI1
30-69	9.5	1026.8	7		
31-69	7.9	1023.3	2		AC5
1-70	8.5	1020.9	6		SC2
2-70	13.0	1018.9	10	HS--	SC9
6-70	7.0	1010.8	6	S-	S10
7-70	6.8	1016.5	7		SC10
10-70	8.6	1019.6	0	S--	SC9
12-70	6.2	1021.6	0		
13-70	4.7	1009.4	6	FH	SC10
14-70	3.6	1004.8	14	FSG-	ST10
15-70	3.1	1003.9	14	FL-	ST10
16-70	9.3	1023.4	15		AC5CS3
18-70	6.1	1021.2	13		AC4CI1
19-70	11.0	1016.0	9		AC2CI1
21-70	12.0	1025.6	10	H	AS10
22-70	11.5	1026.2	23		SC10
23-70	9.0	1030.4	4	K	CS2
24-70	7.2	1026.5	15		CU1
26-70	14.8	1013.6	5	H	AC4CI2
27-70	14.1	1011.2	7	H	AC1

EVENT NO.	MEAN PERIOD (MIN)	SURFACE CONDITIONS, XU PRESS (MB)	WIND (MPH)	VISIBLE WEATHER	CLOUD COVER
28-70	12.5	1020.1	15	H	SC3
29-70	5.5	1021.4	7		AS8
30-70	24.5	1023.9	7		CI1
31-70	10.1	1022.4	6		SC1
33-70	11.0	1024.6	10		SC9
34-70	11.5	1023.4	7		AS2CS2
37-70	16.5	1021.7	10		AC2CS2
38-70	8.0	1021.1	13		AC1CS4
39-70	9.9	1015.5	16		AC2CI
40-70	4.9	1015.2	8	H	
77-70	22.0	1015.9	10	HR-	SC8AC2
78-70	14.0	1015.6	16	H	SC1AC3AC4
42-70	7.2	1017.6	11		CU7SC3
43-70	10.0	1009.6	17		CU6SC1SC2
44-70	8.9	1017.2	0		AC2CI1
45-70	11.3	1016.7	6		AC1CI1
46-70	9.1	1016.3	8	H	AC5AC4
48-70	9.5	1015.7	9		CU1 CI1
49-70	14.5	1004.9	13		SC4
50-70	12.8	1013.2	4		AC2CI1
51-70	10.0	1017.9	2	F	
52-70	11.0	1018.6	4	FH	ST10
53-70	9.5	1009.7	6		CI2
54-70	8.0	1009.8	9		CI4
55-70	13.6	1017.0	6	FH	CI1
56-70	9.5	1015.8	9		CU3AC2CI1
57-70	7.0	1011.4	8	FR--	F3ST5SC2
58-70	16.0	1018.2	5		CI2
60-70	9.4	1014.1	17		CU5AC4
61-70	10.0	1018.6	0	F	F10
62-70	8.5	1011.4	13	H	SF10
63-70	13.0	1015.0	13	R--	SF2SC8
64-70	6.8	1015.1	5	R--	SC10
67-70	4.5	1001.4	8	R--	SC7AC2
68-70	10.1	1020.9	12	FR-	ST10
69-70	11.0	1022.8	10	FR-	SF10
70-70	8.5	1022.6	12	S	S10
71-70	9.6	1019.0	16	S	S10
72-70	7.0	1025.3	6		SC10
73-70	8.6	1024.2	2		SC9

EVENT NO.	MEAN PERIOD (MIN)	SURFACE PRESS (Mb)	WIND (MPH)	CONDITIONS, XU VISIBLE WEATHER	CLOUD COVER
74-70	12.0	1024.5	5		SC7AC3
75-70	11.0	1022.5	3	F	F5
76-70	8.0	1021.2	2	F	
68-71	10.0	1019.2	7		SC4CI
69-71	9.1	1021.4	0	FS--	SC10
1-71	5.8	1022.2	6		SC4AS3CS1
2-71	3.6	1021.5	9		SC2AS3CS3
4-71	8.1	1020.7	2		CI1
5-71	8.0	1018.7	6		AS8
6-71	18.0	1014.7	13		AC7CS2
7-71	11.8	1013.9	0		AC6CS
8-71	6.1	1013.7	4	S-	S10
9-71	7.9	1010.0	7	FR-	SF10
11-71	13.2	1003.3	18	S-	S5SF5
12-71	10.3	1026.5	0		SC1
13-71	6.0	1027.3	5	H	AC8
15-71	5.1	1027.0	8	H	AC9
16-71	12.0	1024.4	10		CU3CS6
17-71	5.8	1024.1	5		CI1
18-71	9.0	1016.5	12		SC10
19-71	11.5	1033.8	0		CI1
20-71	11.5	1020.1	5		SC6
21-71	10.5	1023.0	7		
22-71	8.1	1018.2	0		CI1
23-71	11.0	1017.8	4		CI2
24-71	9.0	1006.3	11		CU2AC4
25-71	13.0	1007.5	3	F	AC5CS2
26-71	13.5	1016.3	6		
28-71	18.0	1019.6	0		
29-71	6.8	1011.2	6		CI1
30-71	14.0	1012.7	6		CI3CI
31-71	18.5	1020.4	0		
33-71	11.0	1019.2	8		Cb1
35-71	18.5	1020.9	5		AC1CI
36-71	14.0	1014.1	4	H	H4AC1CI
37-71	8.1	1009.6	7	HT	Cb4AS6
38-71	9.8	1003.7	13		CU1SC3CS3
39-71	11.6	1016.3	0		
40-71	9.8	1016.5	3		SC2CI1
41-71	14.0	1016.9	6	FH	SC1CI2

EVENT NO.	MEAN PERIOD (MIN)	SURFACE CONDITIONS, XU PRESS (MB)	WIND (MPH)	VISIBLE WEATHER	CLOUD COVER
43-71	22.0	1021.5	5		CI 1
44-71	6.9	1010.6	3		AC4CS3
45-71	6.0	1010.6	3		AC3CS3
46-71	8.5	1020.4	5		AC10
47-71	13.7	1021.0	8		SC3AC6
48-71	13.3	1023.0	4		SC3AC1CI2
49-71	8.0	1022.7	12		SC6AC4
50-71	15.5	1021.1	4	F	AC2CI3
51-71	13.0	1026.8	0		
52-71	11.2	1026.6	0		
53-71	11.8	1023.6	0		
54-71	9.1	1025.1	7		CU4AS6
55-71	9.0	1023.8	6		SC4AC4AC2
56-71	12.1	1010.5	2	F	F8AC2
57-71	14.1	1016.5	9		CU4SC2CI1
58-71	13.5	1017.7	5		CI3
59-71	8.8	1014.6	8	FH	ST10
60-71	8.3	1023.2	3	F	AC6CI2
61-71	7.3	1021.9	7	F	AC6
62-71	8.3	1013.1	11	H	SC8SC2
63-71	13.0	1012.6	4	F	AC2CI1
64-71	10.0	1012.5	4	F	F6
65-71	10.0	1012.7	4	F	F7
66-71	5.0	1024.8	5		SC1AC3
67-71	9.1	1015.8	15		AC9

APPENDIX C

SOME REPRESENTATIVE WAVES AND THEIR SPECTRA

In this Appendix (Figures C-1 to C-24) are presented photo-reproductions, approximately actual size, of the chart records of 14 of the waves, including 10 for which a computer analysis was performed (see Appendix A). Also shown in each case are the amplitude spectra produced by the FORTRAN program PSPEC1. The two additional waves which were computer analyzed are discussed in Chapter V.

The amplitude spectra suffer from the fact that each record lasts for only a few periods of the dominant component. This makes resolution poor and produces rather broad spectral lines, an effect which can also be seen in the test data shown in Figures A-2 to A-5, Appendix A. In addition, it must be noted that these spectra have not been corrected for changes in amplitude and phase which take place in the microbarograph. Since most of the waves have dominant periods near the center of the instrument response curve (Chapter III), such changes are not large. They are, in any case, the same for all three microbarographs.

Nonetheless, a slowly varying static pressure component in the atmosphere may generate an output signal from the microbarograph which would appear in the spectrum as a large component of low frequency. Tests have shown that the spectrum of a microbarogram may be incorrect if the record contains components of significant amplitude which have

periods greater than the sample length. In the present work, the shortest microbarogram to be Fourier analyzed was 30 minutes long, and the pass-band of the microbarographs was chosen such that the lower half-power point lies at about 32 minutes.

For the reasons discussed above, the portion of the amplitude spectrum corresponding to periods greater than about 30 minutes is considered to be unreliable.

The values given for the cross-correlation coefficients σ_{ij} in each case are the maximum values as reported by the ALGOL program CORREL (see Appendix A).

1. Event Number 16-70:

$\sigma_{32} = 0.947$ $\sigma_{31} = 0.642$ $\sigma_{21} = 0.675$

The major portion of this wave appears to occur between 0400Z and 0430Z, although there is a suspicion of similar structure before and after this time interval. Records 2 and 3 are nearly identical, but record 1 shows an alteration in the shape of the wave. Spectra 2 and 3 show common peaks at 7.2 and 11 minutes, as well as at longer periods. Spectrum 1 shows a reduced 11 minute component but a rather large peak at about 8 minutes. It is not known whether the apparent shift of the spectral line from 7.2 to 8 minutes is physically significant or merely an effect of the lack of resolution and the breadth of the spectral lines. This emphasizes the fact that the spectra should be interpreted as amplitude density curves rather than as line spectra.

2. Event Number 18-70:

$\sigma_{32} = 0.758$ $\sigma_{31} = 0.648$ $\sigma_{21} = 0.687$

A wave-like structure appeared between 0555Z and 0630Z, approximately two hours after the recording of the initial stages of Event no. 16-70. Again the best correlation is between records 2 and 3. The event appears to be of greater duration on record 1. The amplitude spectra are fairly clean and suggest a significant component at a period of about 6.5 minutes.

3. Event Number 31-70:

$\sigma_{32} = 0.966$ $\sigma_{31} = 0.962$ $\sigma_{21} = 0.964$

This is a large-amplitude wave, with good correlation across the receiving array. It appears to have vanished after 0715Z at station 1, although charts 2 and 3 show continued oscillation until about 0730Z. The spectra show the presence of a prominent component at about 10 minutes having a mean amplitude of about 90 microbars.

4. Event Number 42-70:

$\sigma_{32} = 0.953$ $\sigma_{31} = 0.950$ $\sigma_{21} = 0.966$

This wave is also well correlated over the microbarograph array. A 7 minute component, having a mean amplitude of about 85 microbars, appears most prominent between 1540Z and 1615Z. It is probable that the portion of the amplitude spectrum at longer periods is due to the activity shown on the chart recordings between 1520Z and 1540Z.

5. Event Number 43-70:

$\sigma_{32} = 0.969$ $\sigma_{31} = 0.949$ $\sigma_{21} = 0.963$

What appears to be a prominent component at about 10 minutes period is shown by the spectra to be comprised of two components, one at about nine minutes and one at about 13 minutes, each having a mean amplitude of appriximately 60 microbars. It is not clear what meaning can be assigned to the occurrence of this double peak or to the presence of the somewhat smaller component at about 23 minutes.

6. Event Number 50-70:

$\sigma_{32} = 0.956$ $\sigma_{31} = 0.880$ $\sigma_{21} = 0.900$

Although the wave does not appear to be uniformly sinusoidal, the spectra reveal that the records contain one dominant component having a period of about 13 minutes and a mean amplitude of 70 microbars. Some signals at shorter periods are also shown, having a much smaller amplitude than the 13 minute peak.

7. Event Number 58-70:

$\sigma_{32} = 0.947$ $\sigma_{31} = 0.972$ $\sigma_{21} = 0.974$

Again the wave is extremely well preserved over the extent of the receiving array. The spectra are especially featureless except for a 16 minute component of about 60 microbars amplitude.

8. Event Number 60-70:

$\sigma_{32} = 0.717$ $\sigma_{31} = 0.912$ $\sigma_{21} = 0.780$

This is the shortest event to be machine analyzed, only two periods in duration. The best correlation is between records 1 and 3, although it appears that only the amplitude is changed in record 2. The spectra show two peaks, one of about 60 microbars at 10.5 minutes and one of about 30 microbars at about 30 minutes. Little credence can be assigned to the latter for reasons discussed at the beginning of this Appendix.

9. Event Number 62-70:

$\sigma_{32} = 0.969$ $\sigma_{31} = 0.946$ $\sigma_{21} = 0.926$

These records show what appears to be a wave of about 8.5 minutes period between 1830Z and 1900Z. The correlation between records is good. The spectra show a predominant component of mean amplitude about 90 microbars and period approximately 9 minutes. It is not clear what importance should be attached to the component at about 35 minutes, although its description is suspect for reasons discussed above.

10. Event Number 74-70:

$\sigma_{32} = 0.962$ $\sigma_{31} = 0.915$ $\sigma_{21} = 0.938$

The dominant feature of this event is a large component, having a mean amplitude of about 130 microbars, at a period of about 13 minutes.

11. Events 39-71, 54-71, 55-71, and 62-71:

These events were not machine analyzed and are included here as additional examples of the waves observed in this experiment. With the exception of Event number 55-71, they are representative of some of the lower amplitude oscillations which were recorded.

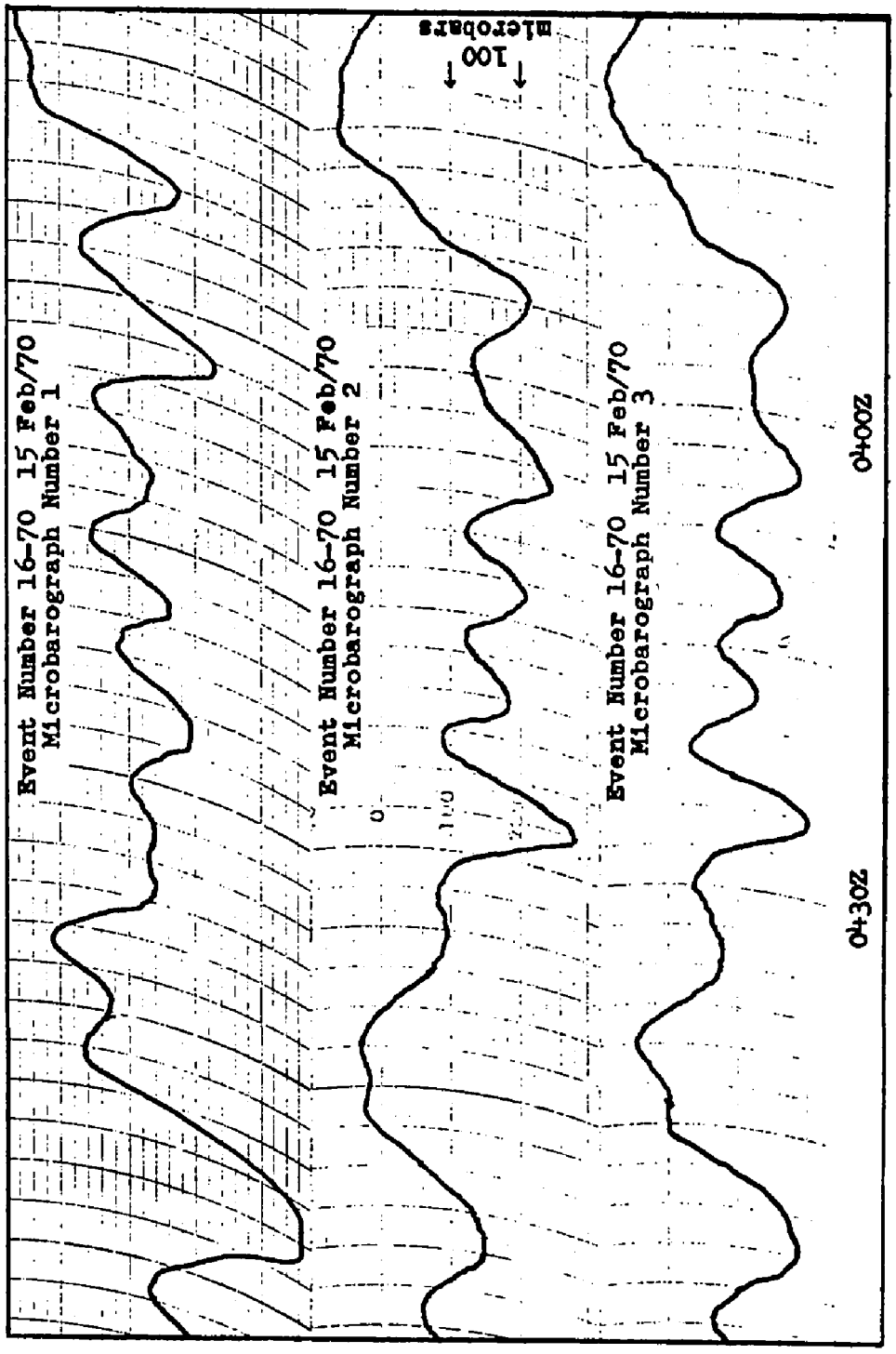

Figure C-1. Microbarograms, Event Number 16-70.

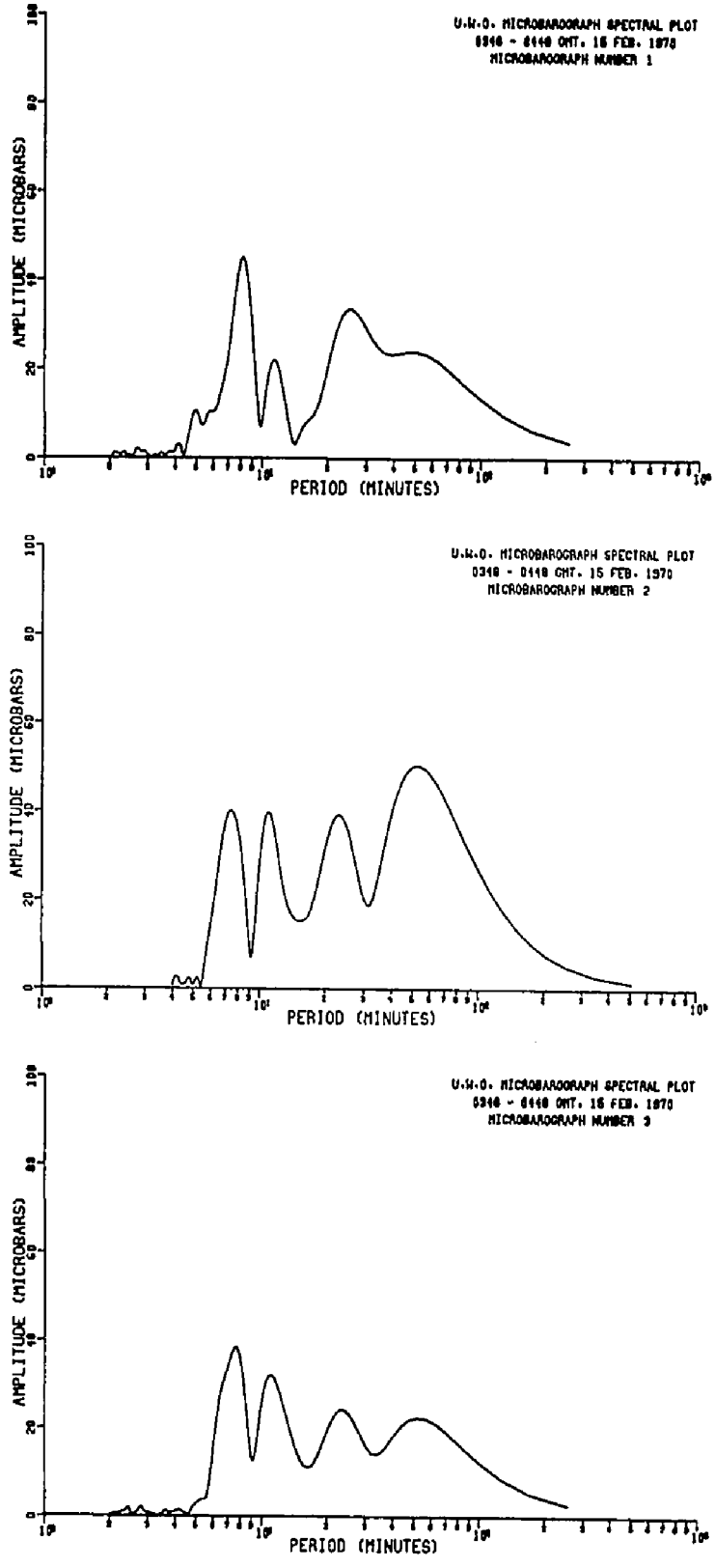

Figure C-2. Amplitude spectra, Event Number 16-70.

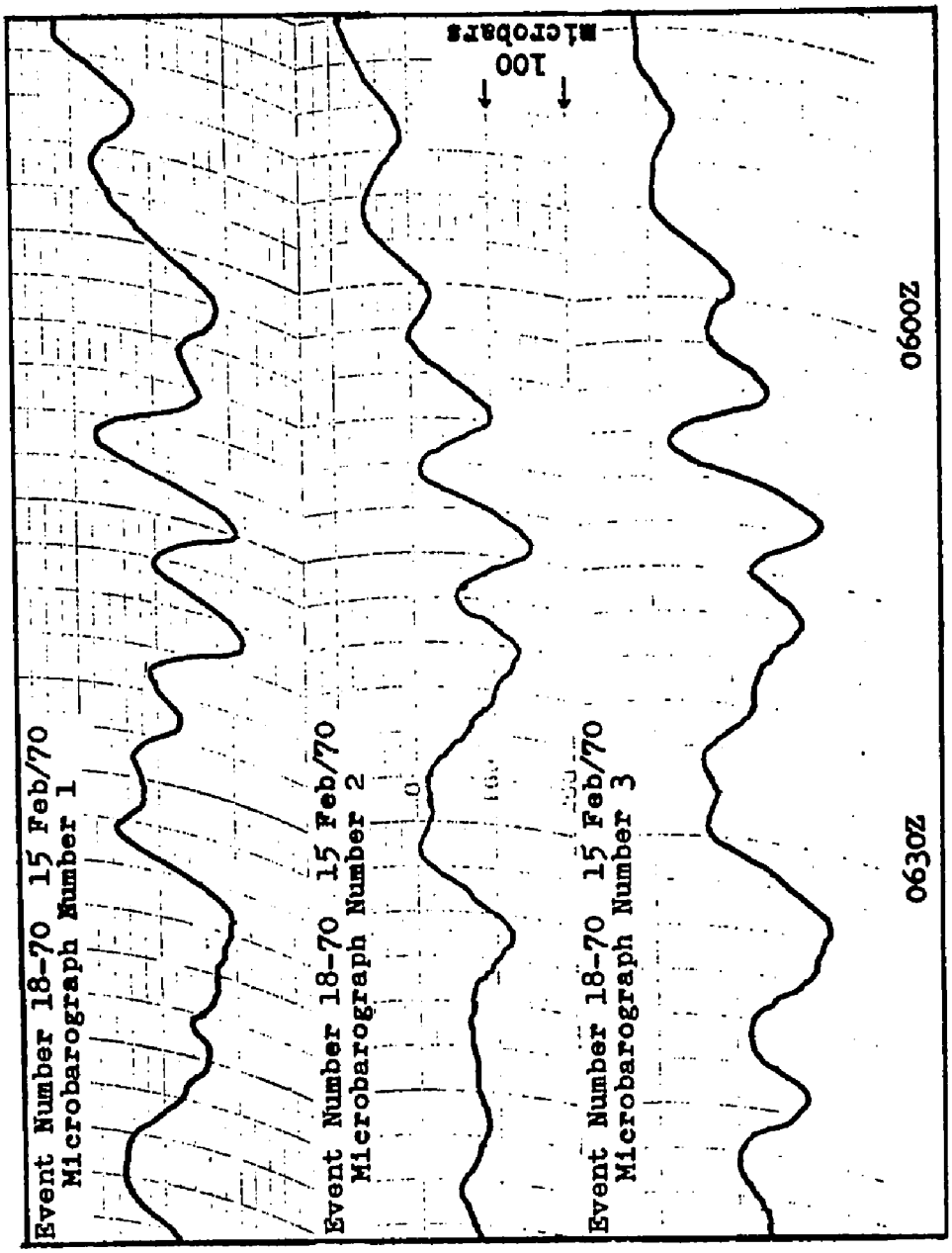

Figure C-3. Microbarograms, Event Number 18-70.

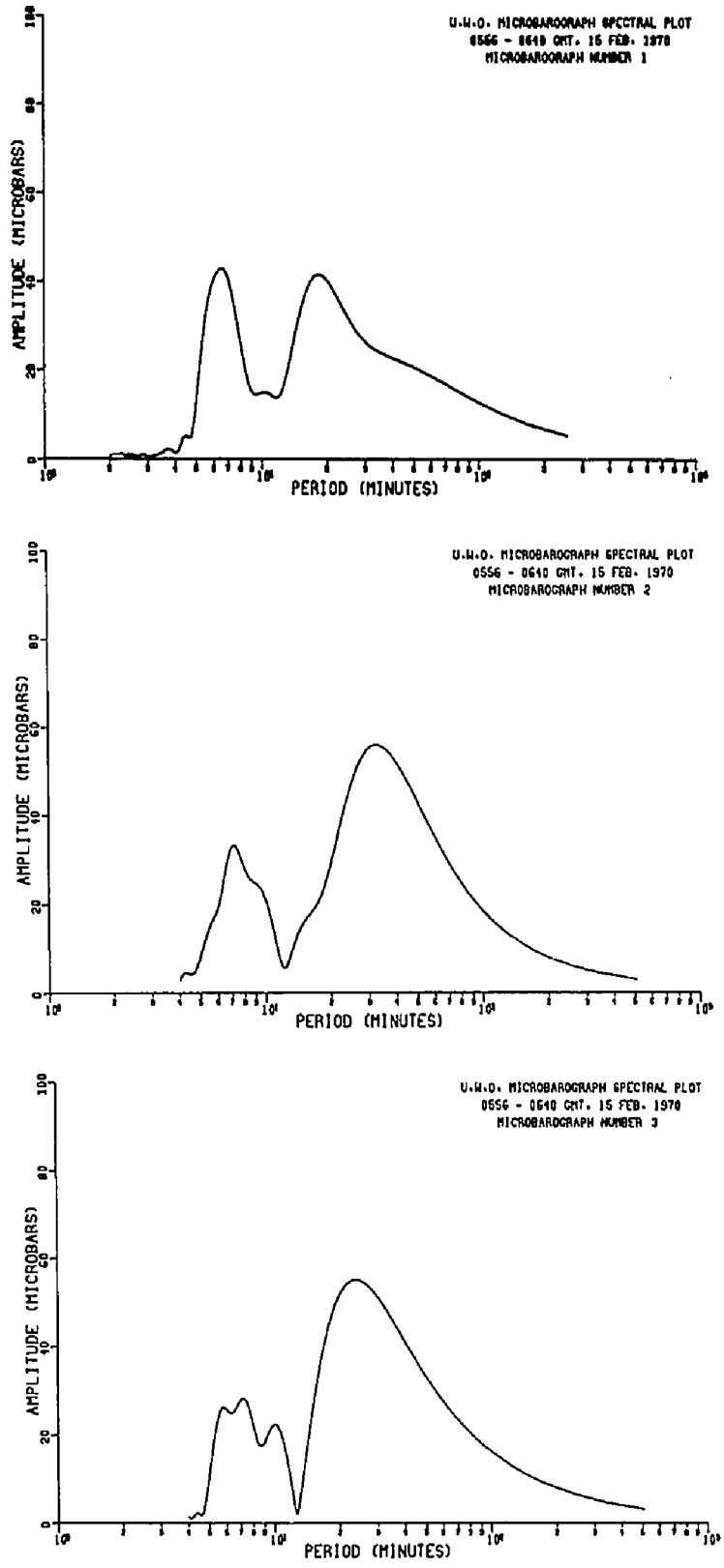

Figure C-4. Amplitude spectra, Event Number 18-70

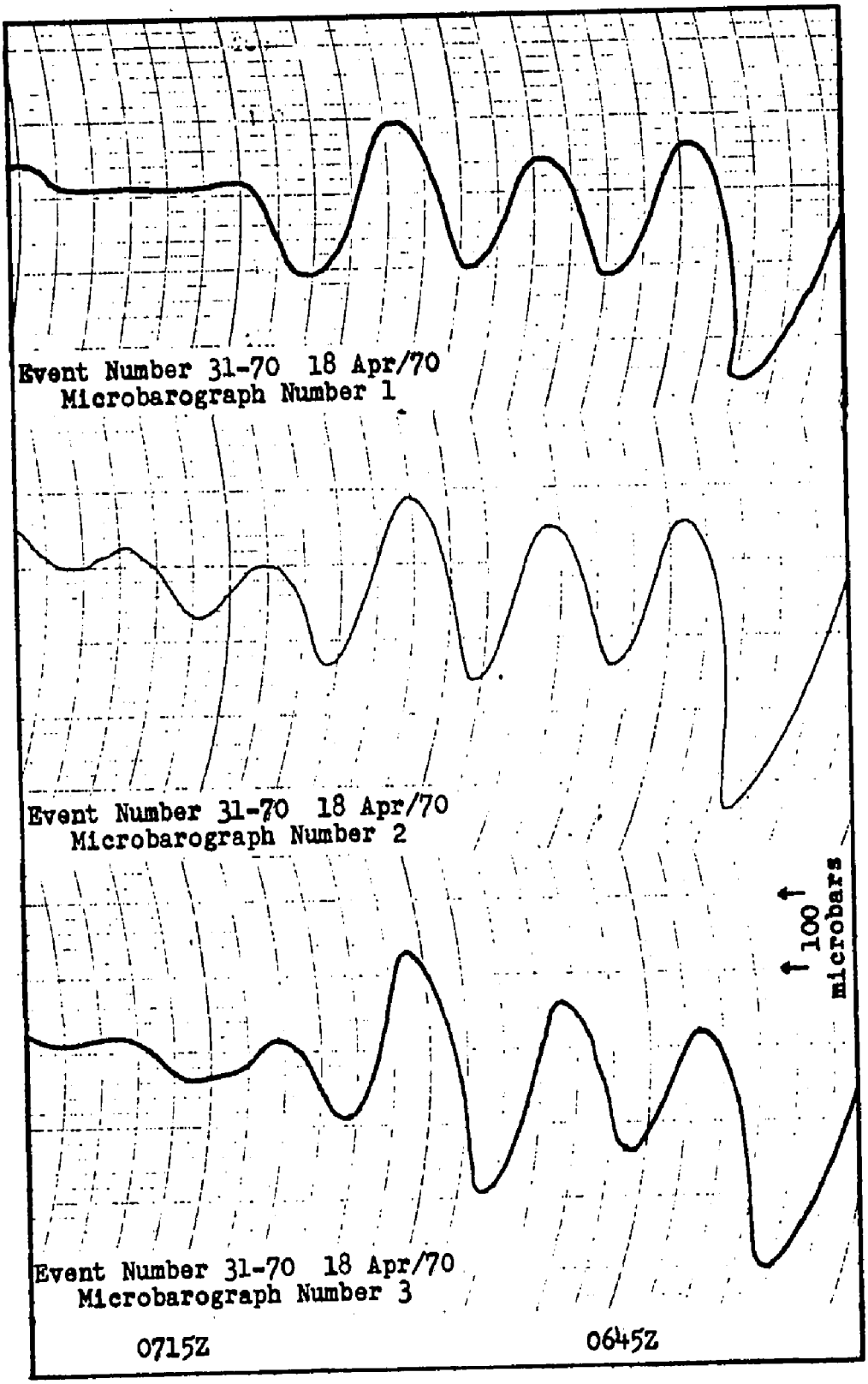

Figure C-5. Microbarograms, Event Number 31-70.

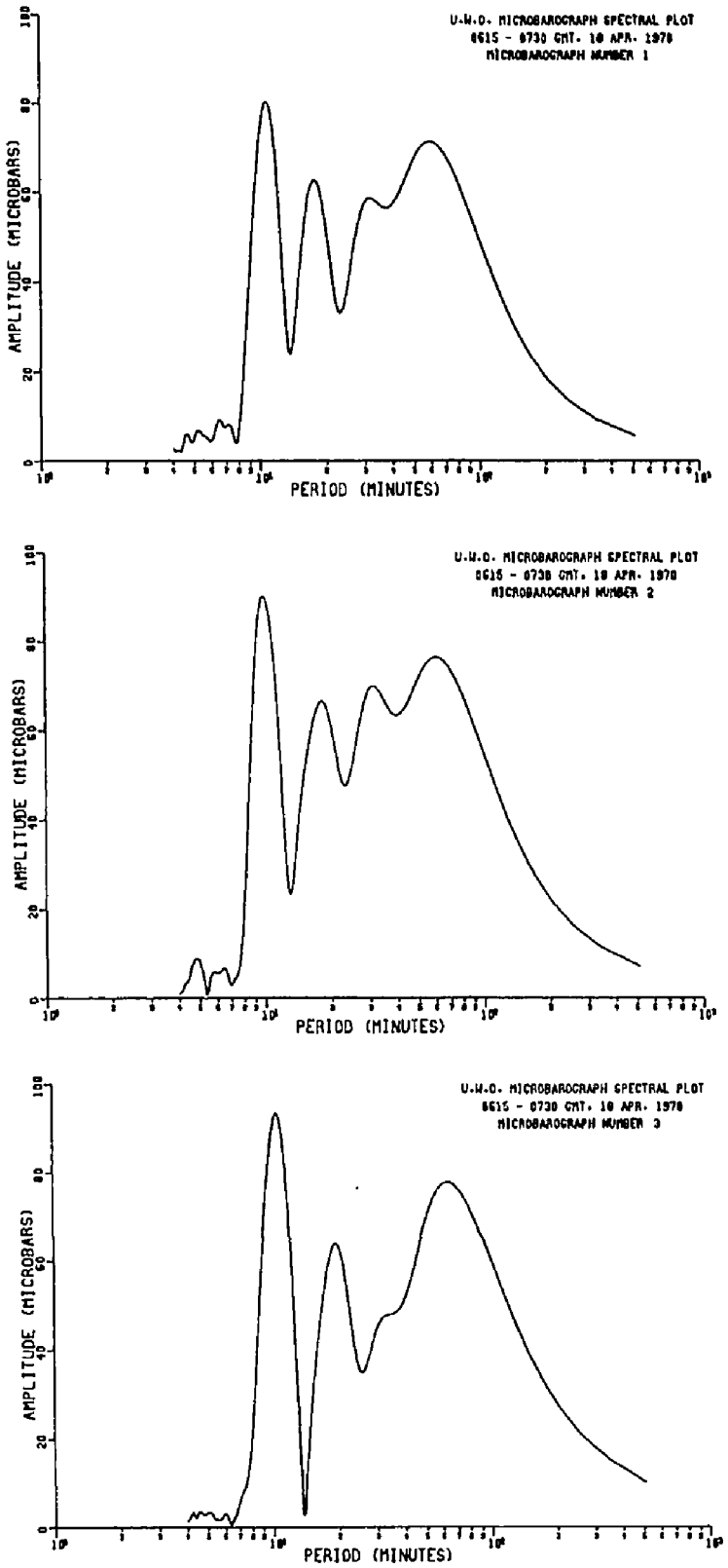

Figure C-6. Amplitude spectra, Event Number 31-70.

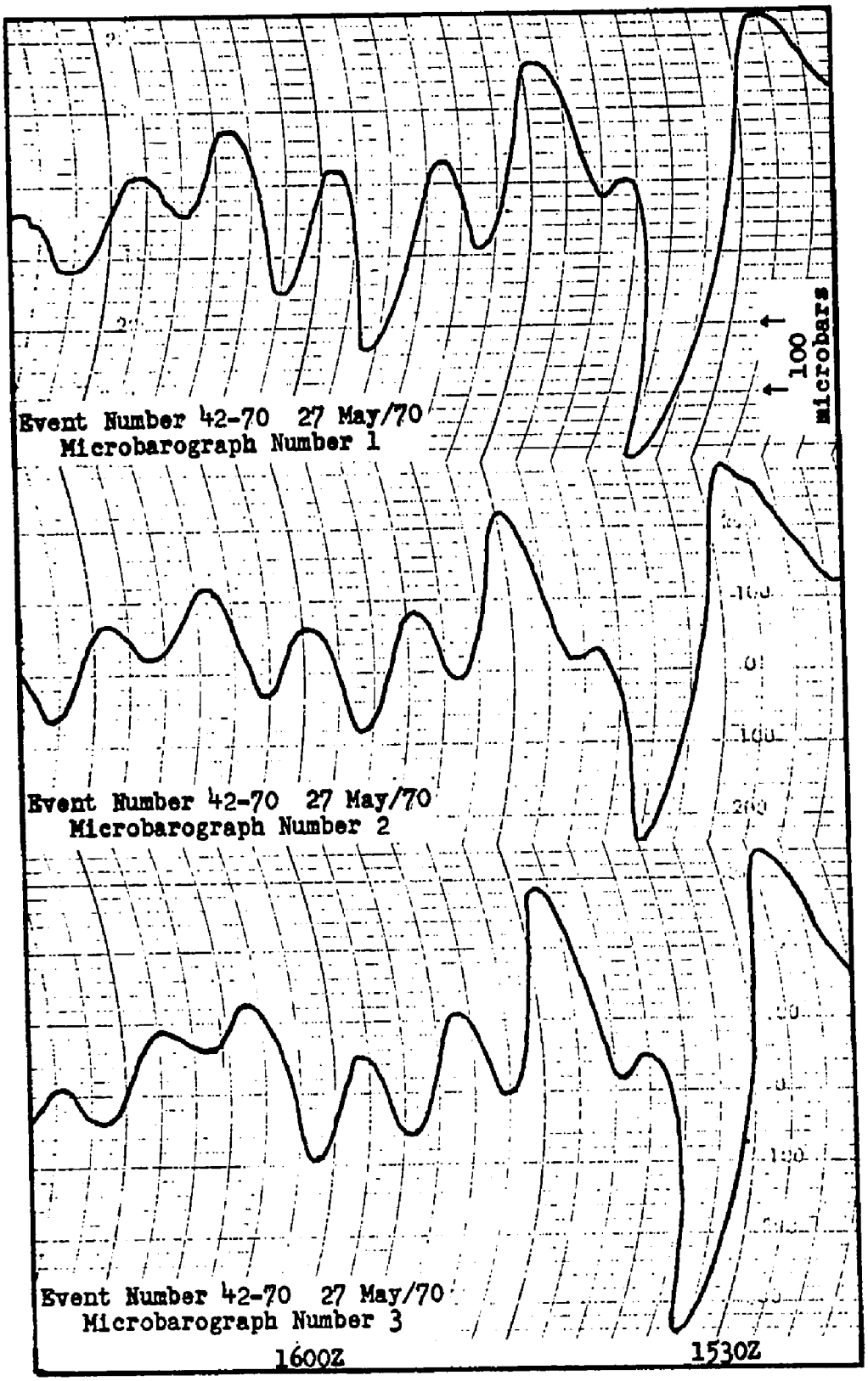

Figure C-7. Microbarograms, Event Number 42-70.

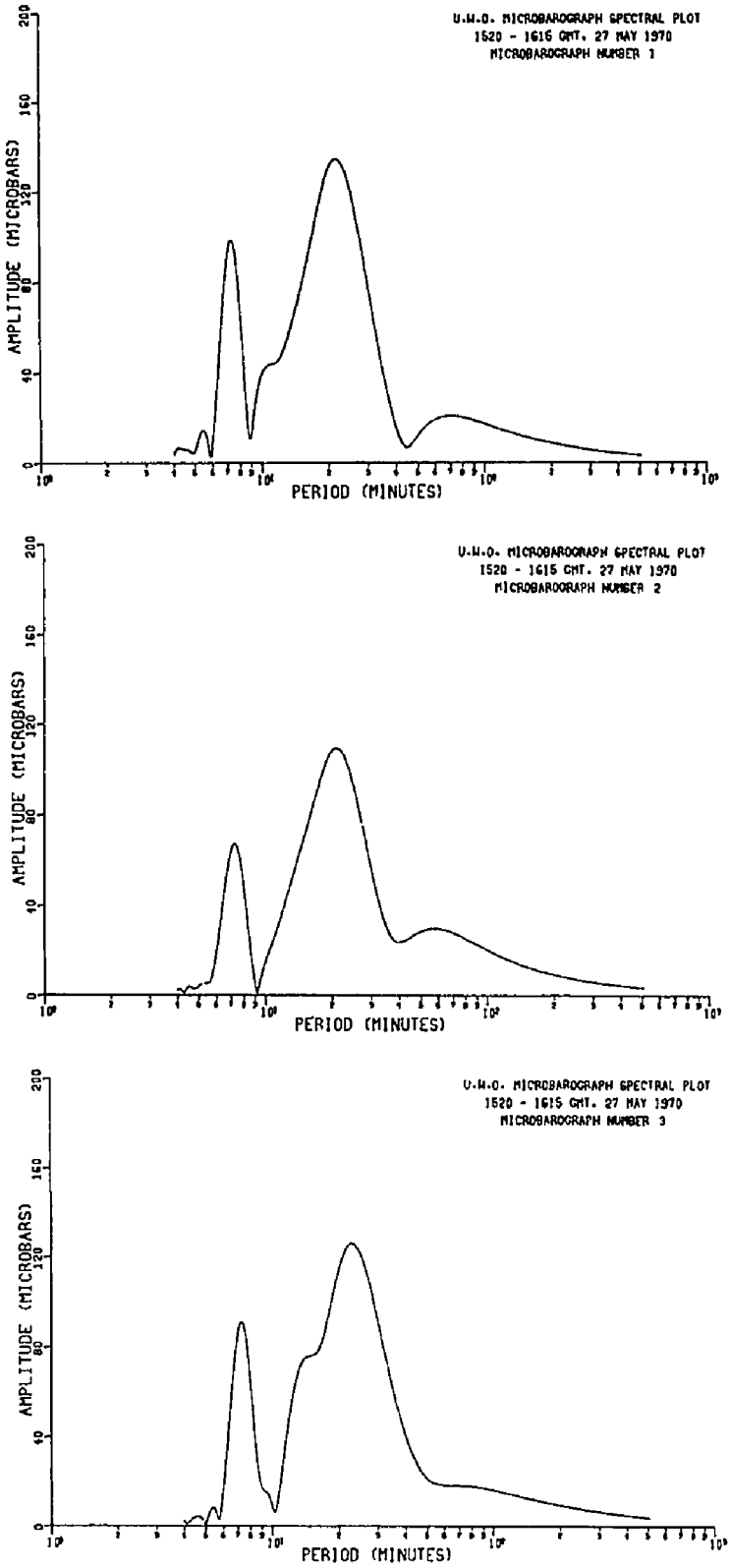

Figure C-8. Amplitude spectra, Event Number 42-70.

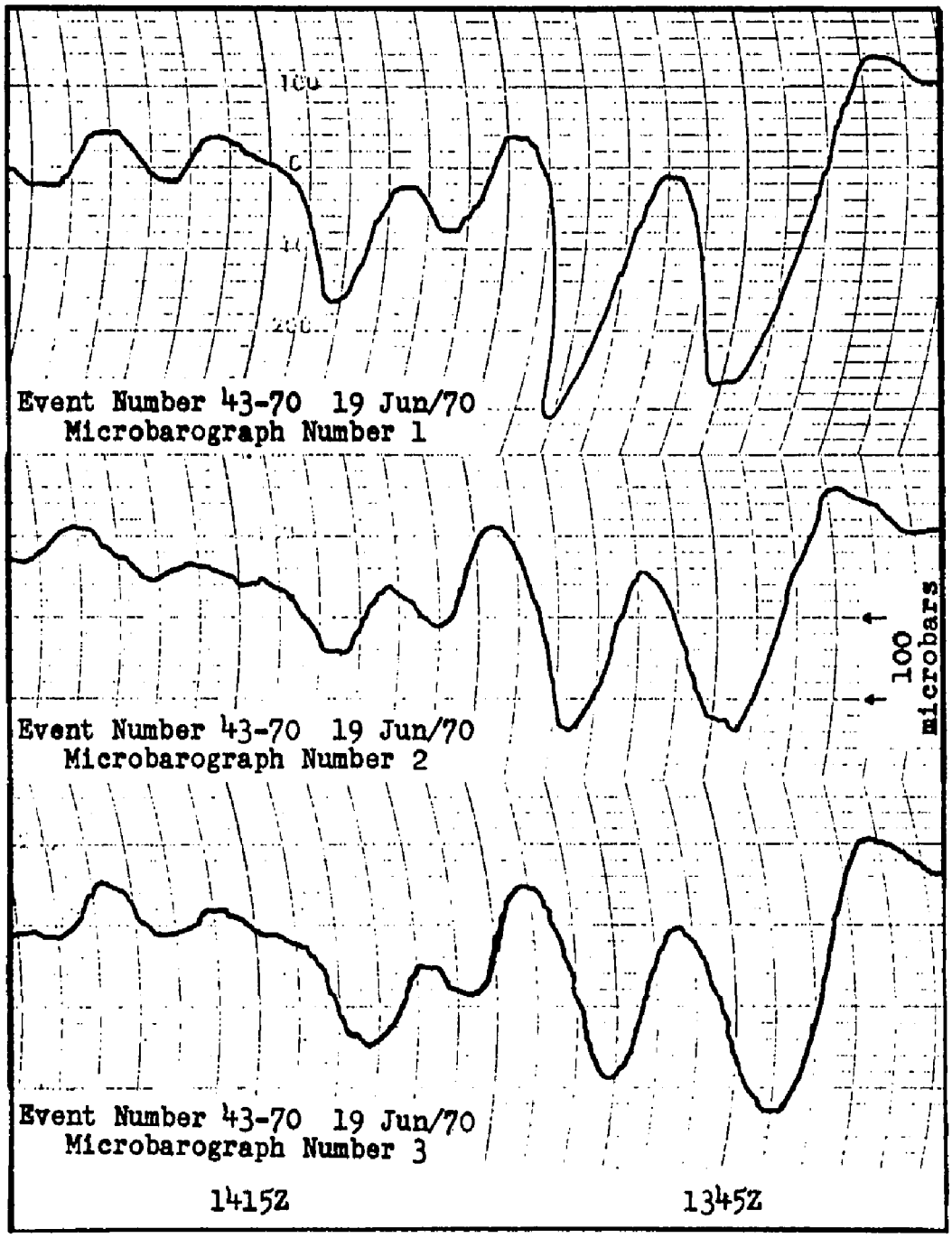

Figure C-9. Microbarograms, Event Number 43-70.

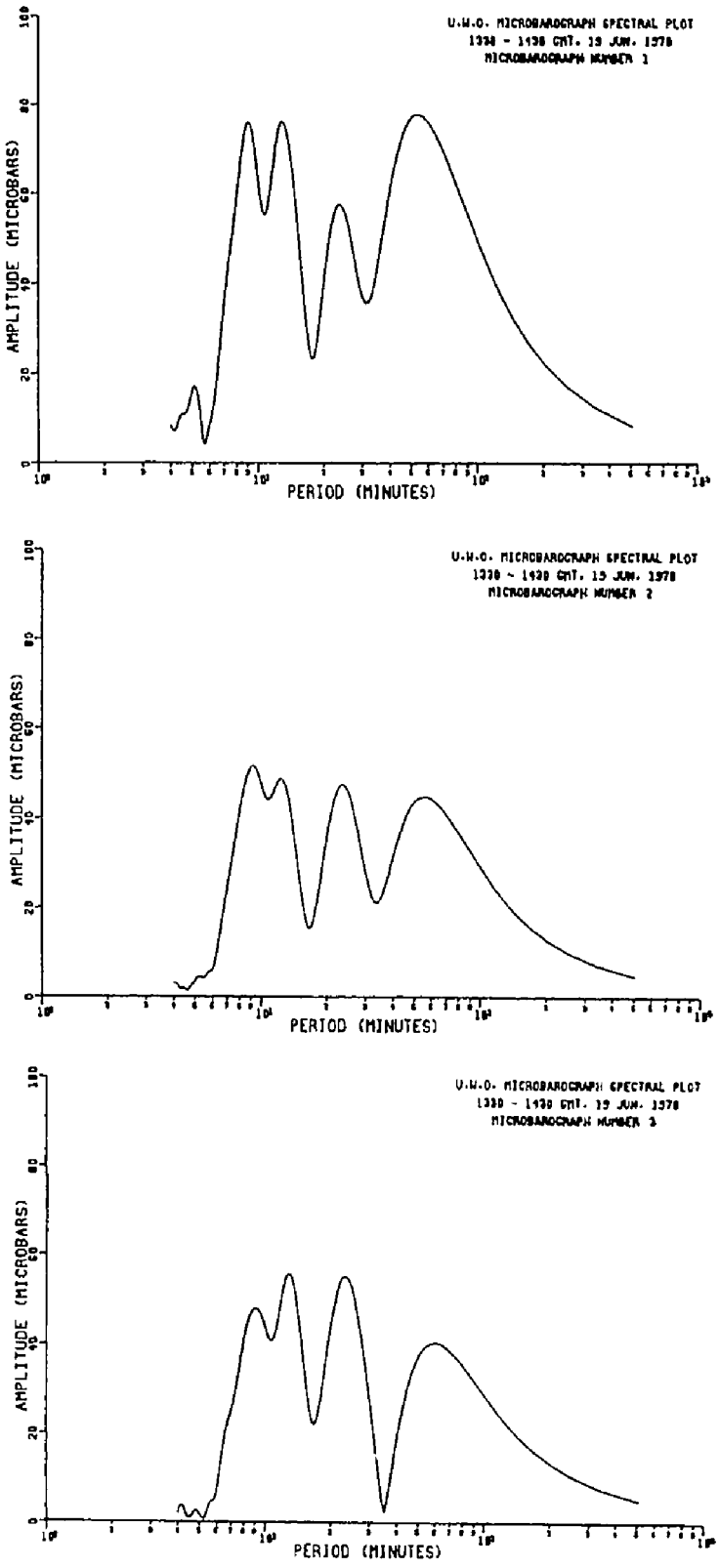

Figure C-10. Amplitude spectra, Event Number 43-70.

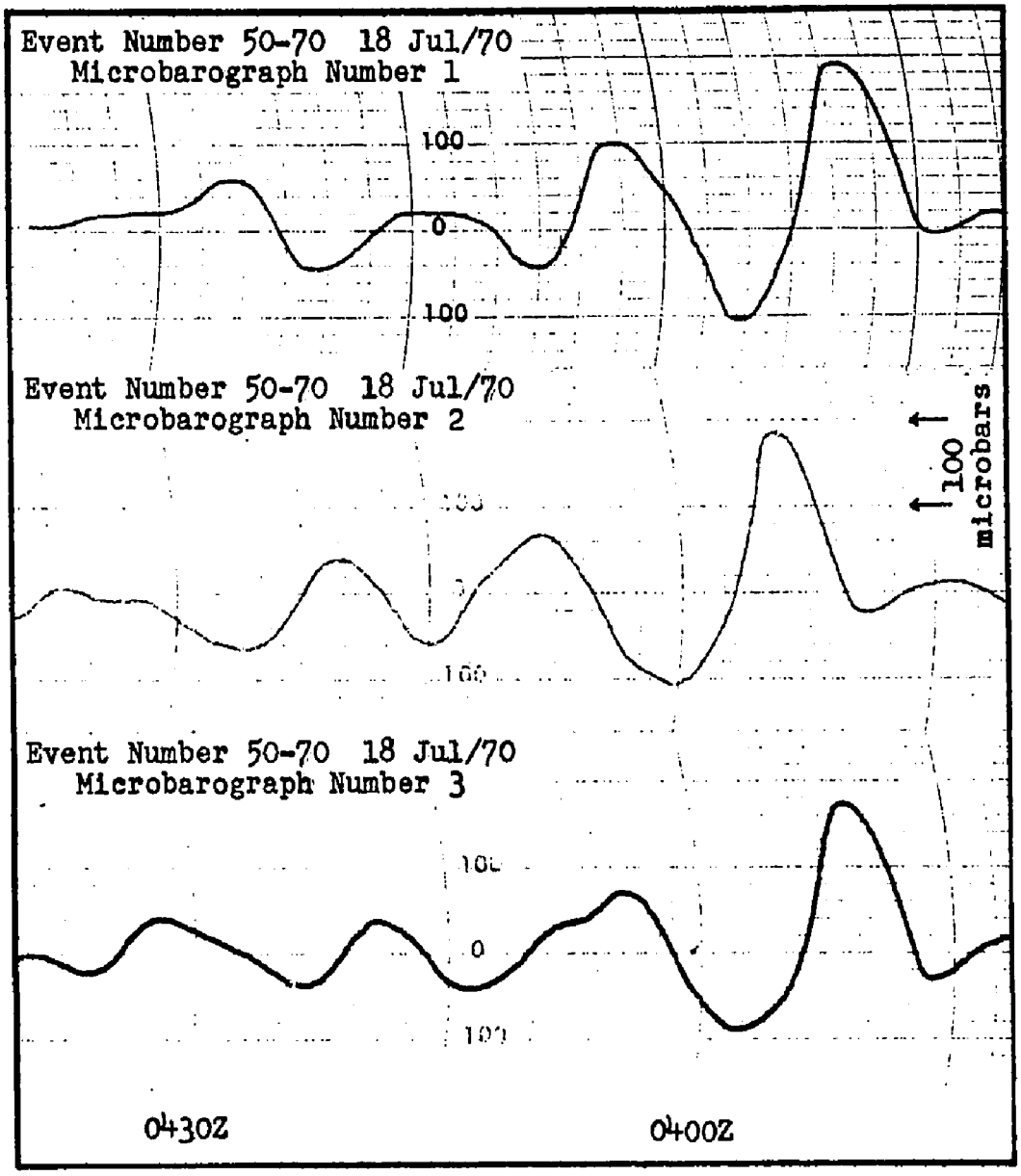

Figure C-11. Microbarograms, Event Number 50-70.

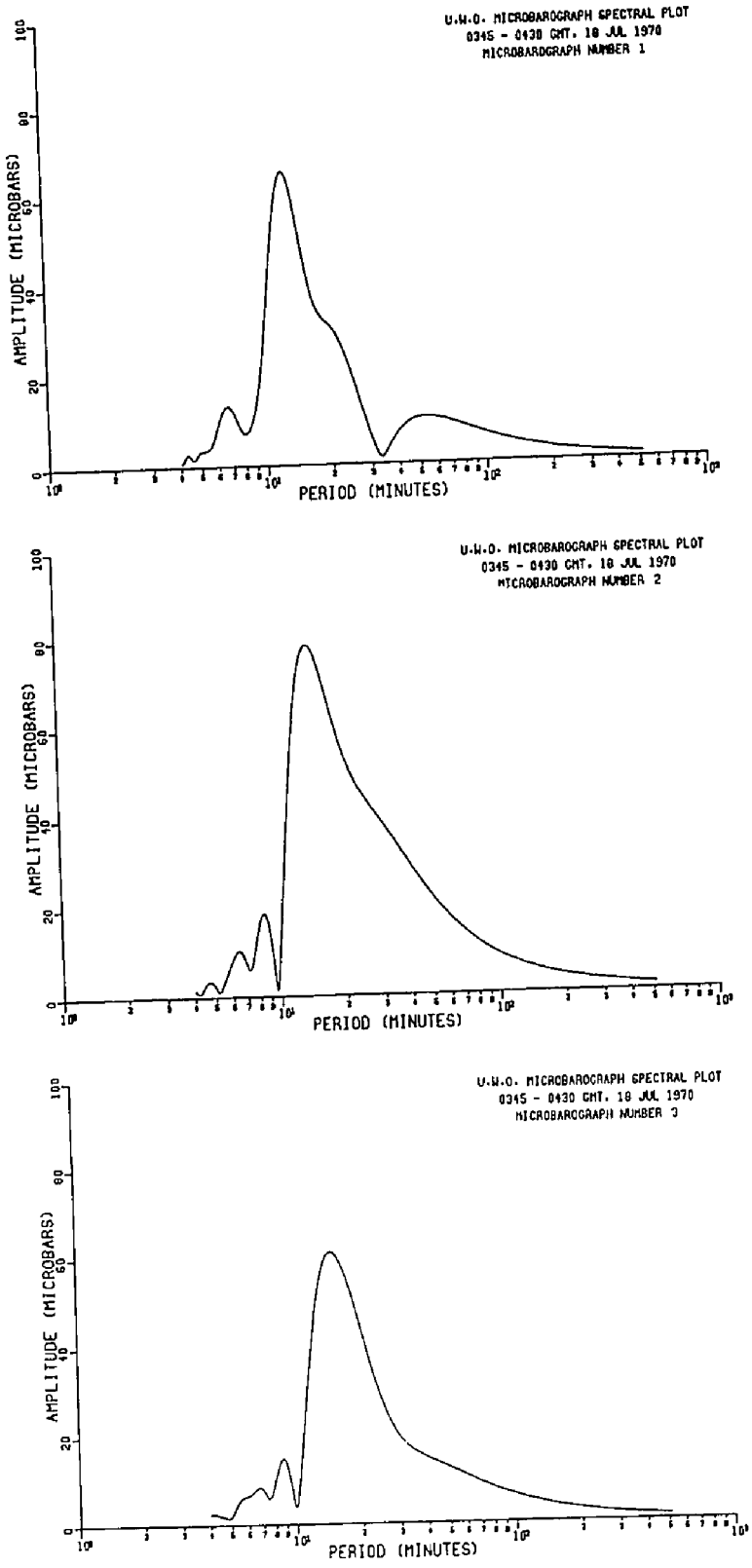

Figure C-12. Amplitude spectra, Event Number 50-70.

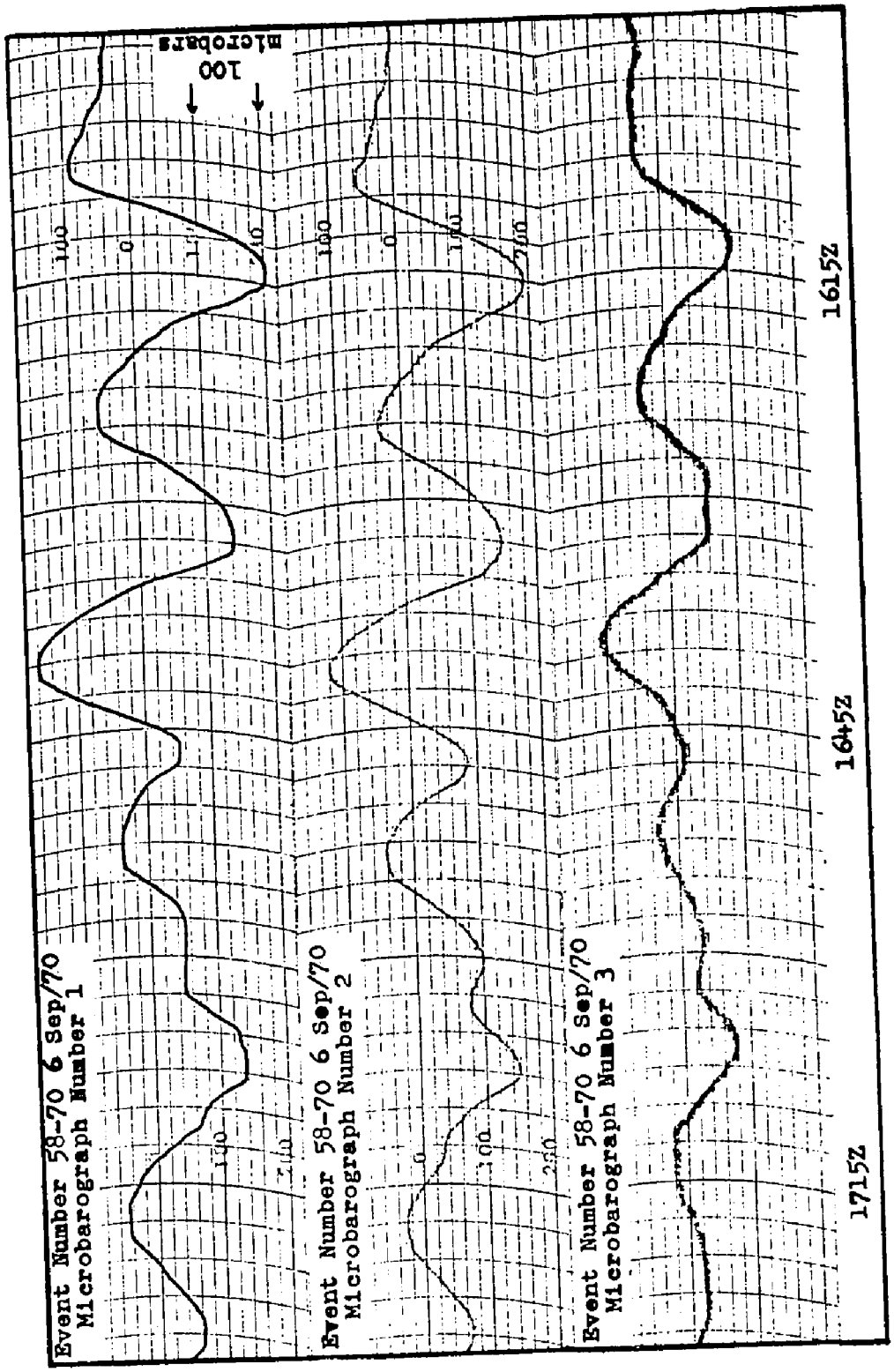

Figure C-13. Microbarograms, Event Number 58-70.

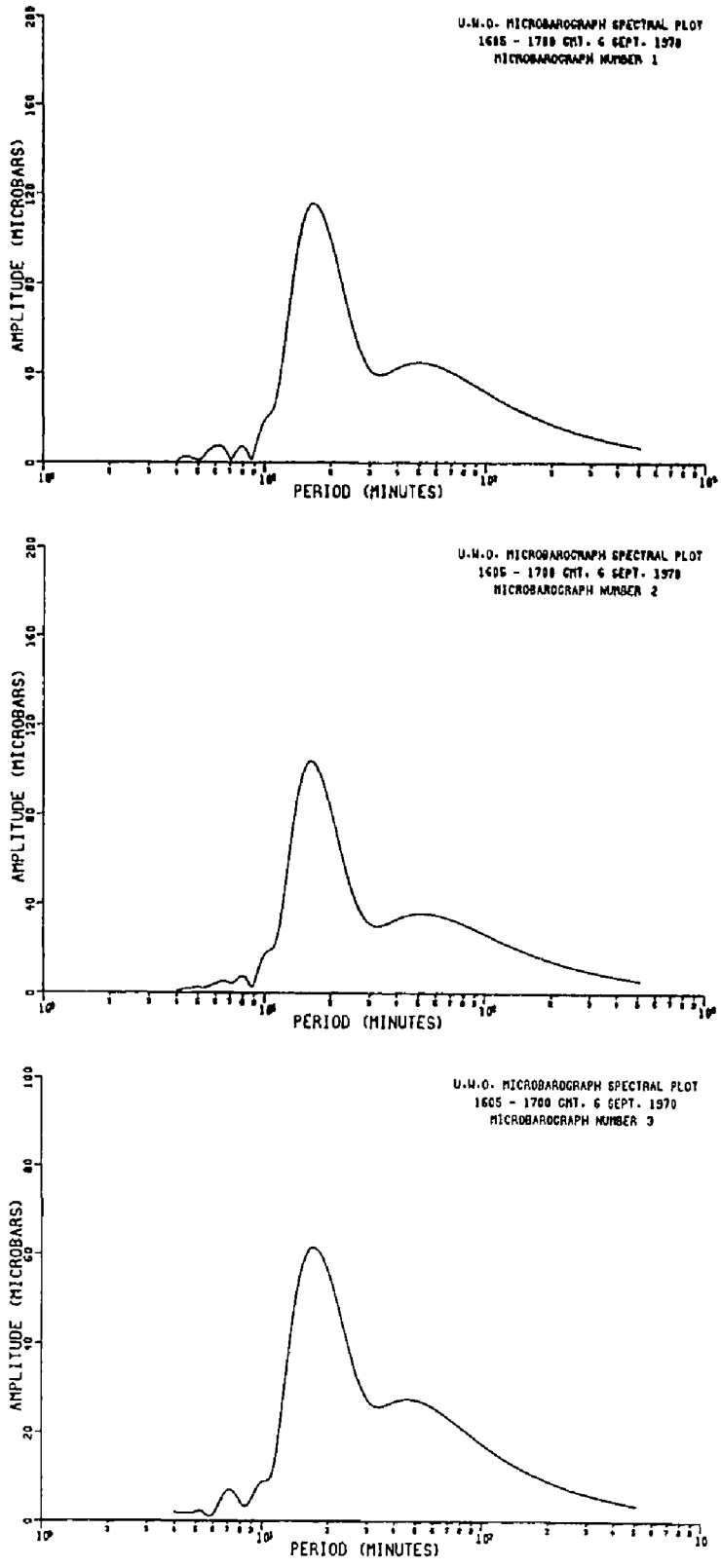

Figure C-14. Amplitude spectra, Event Number 58-70.

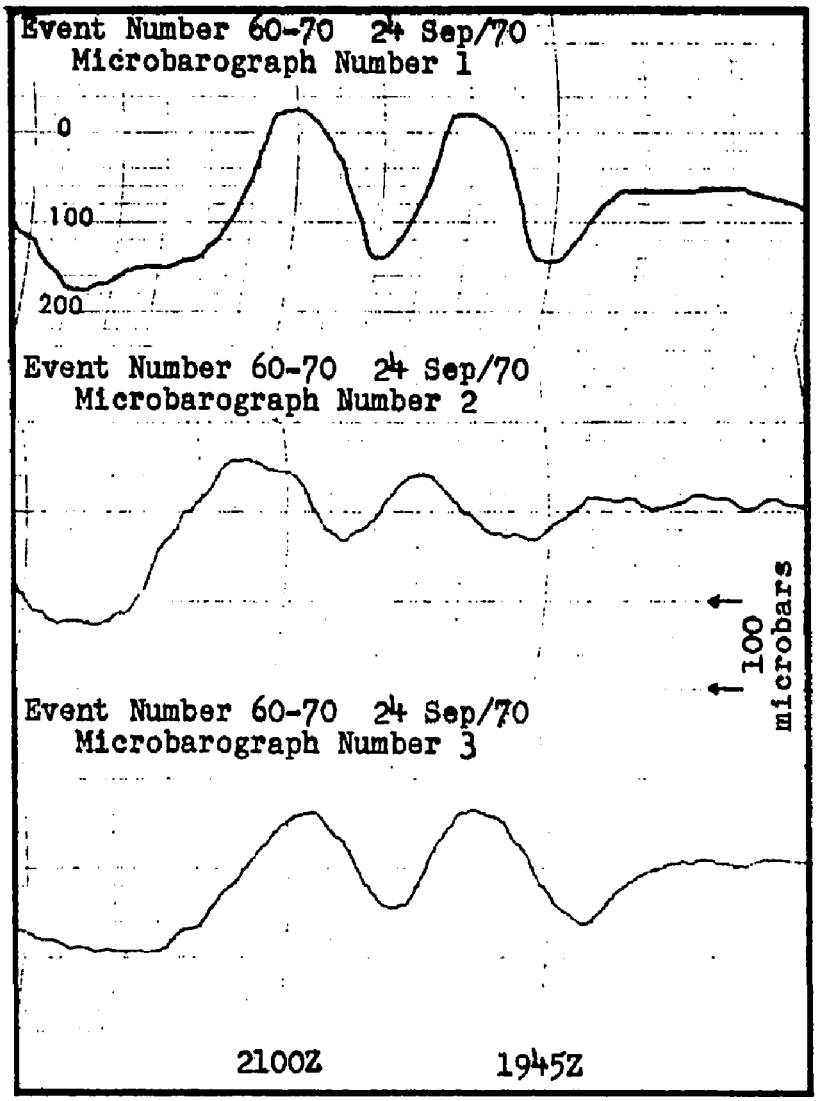

Figure C-15. Microbarograms, Event Number 60-70.

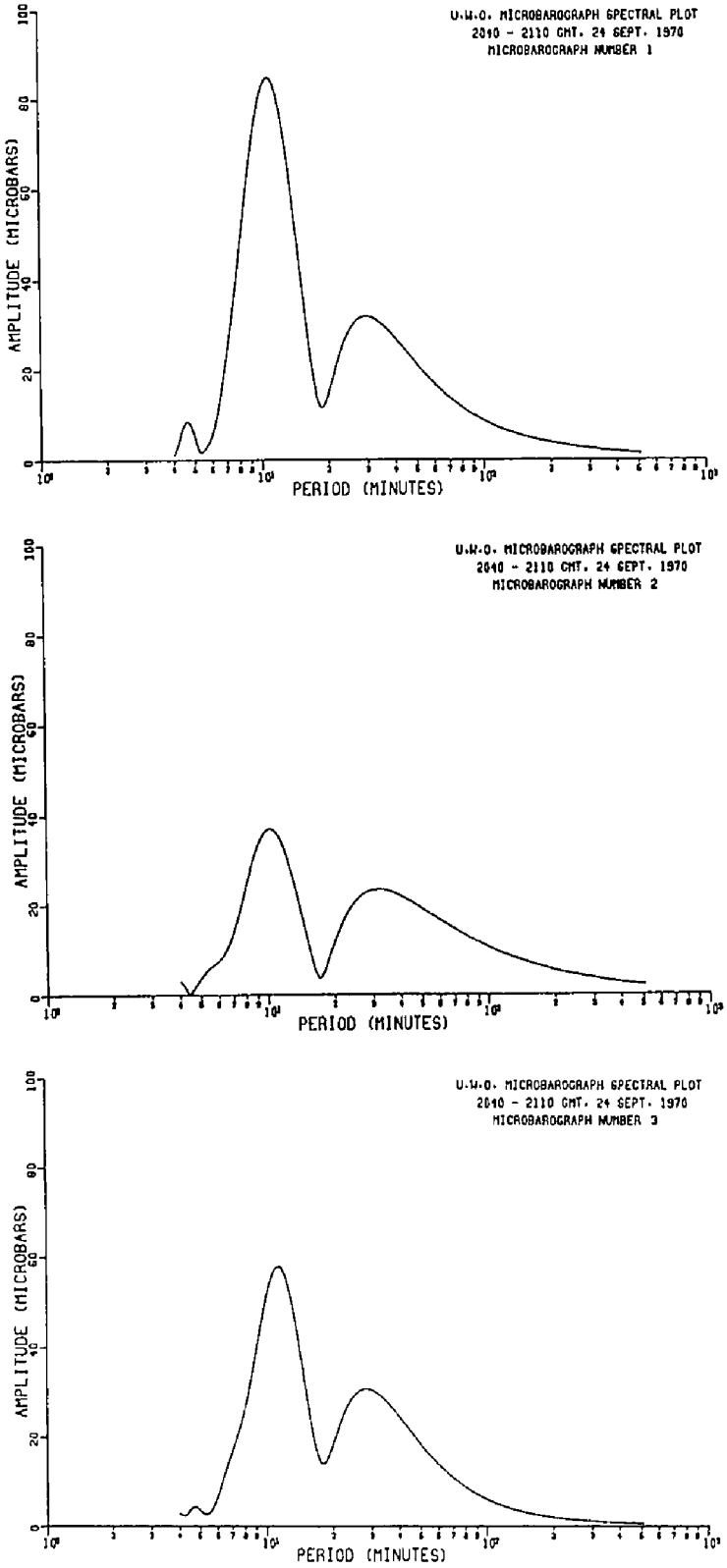

Figure C-16. Amplitude spectra, Event Number 60-70.

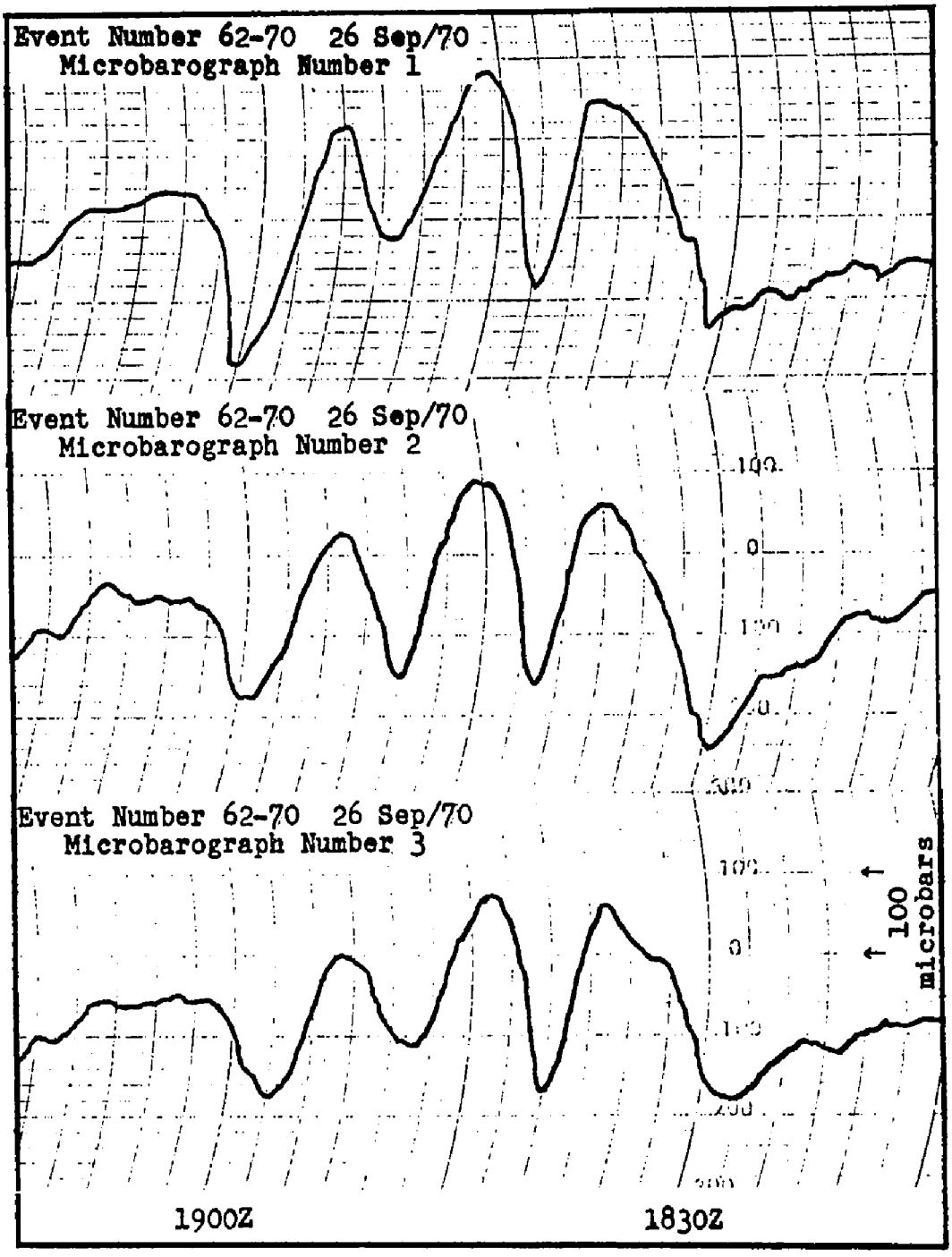

Figure C-17. Microbarograms, Event Number 62-70.

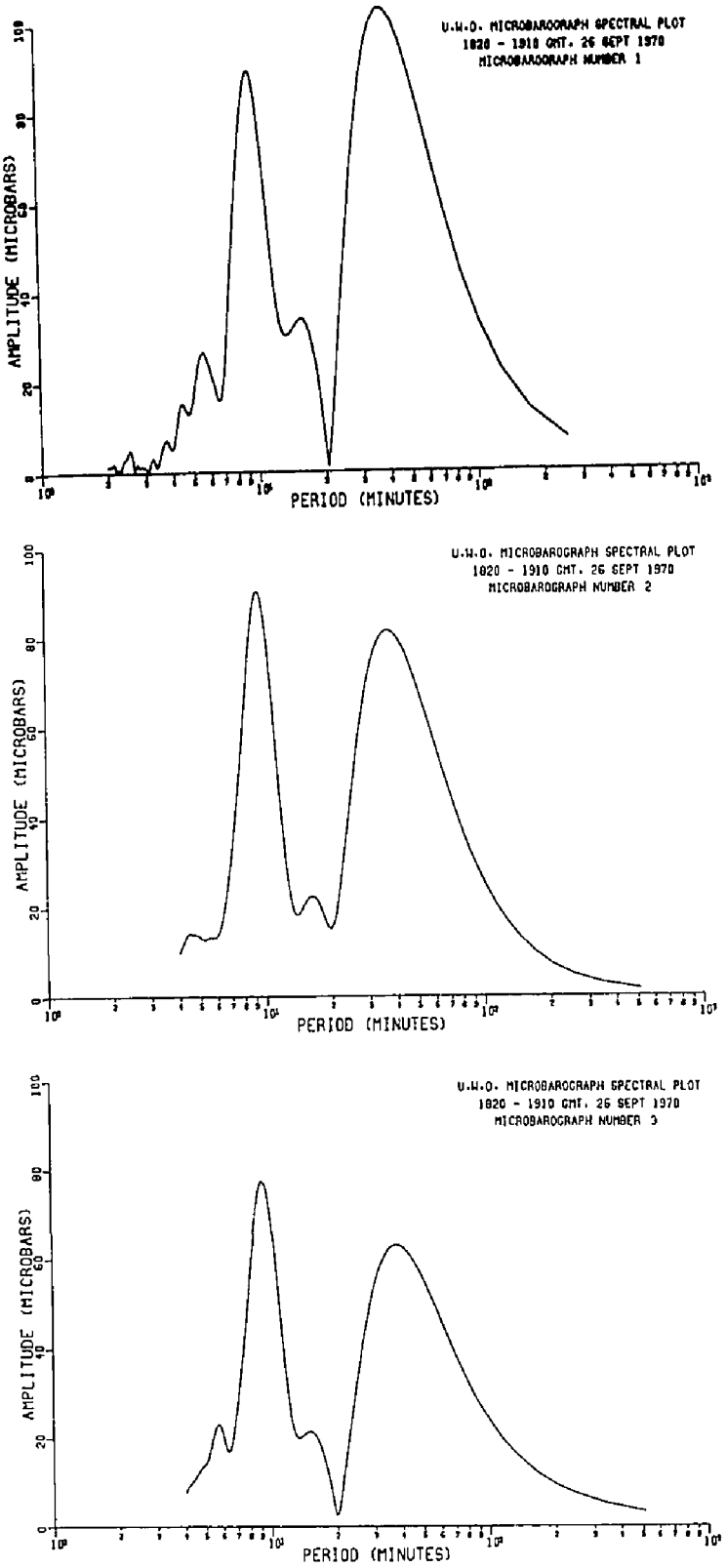

Figure C-18. Amplitude spectra, Event Number 62-70.

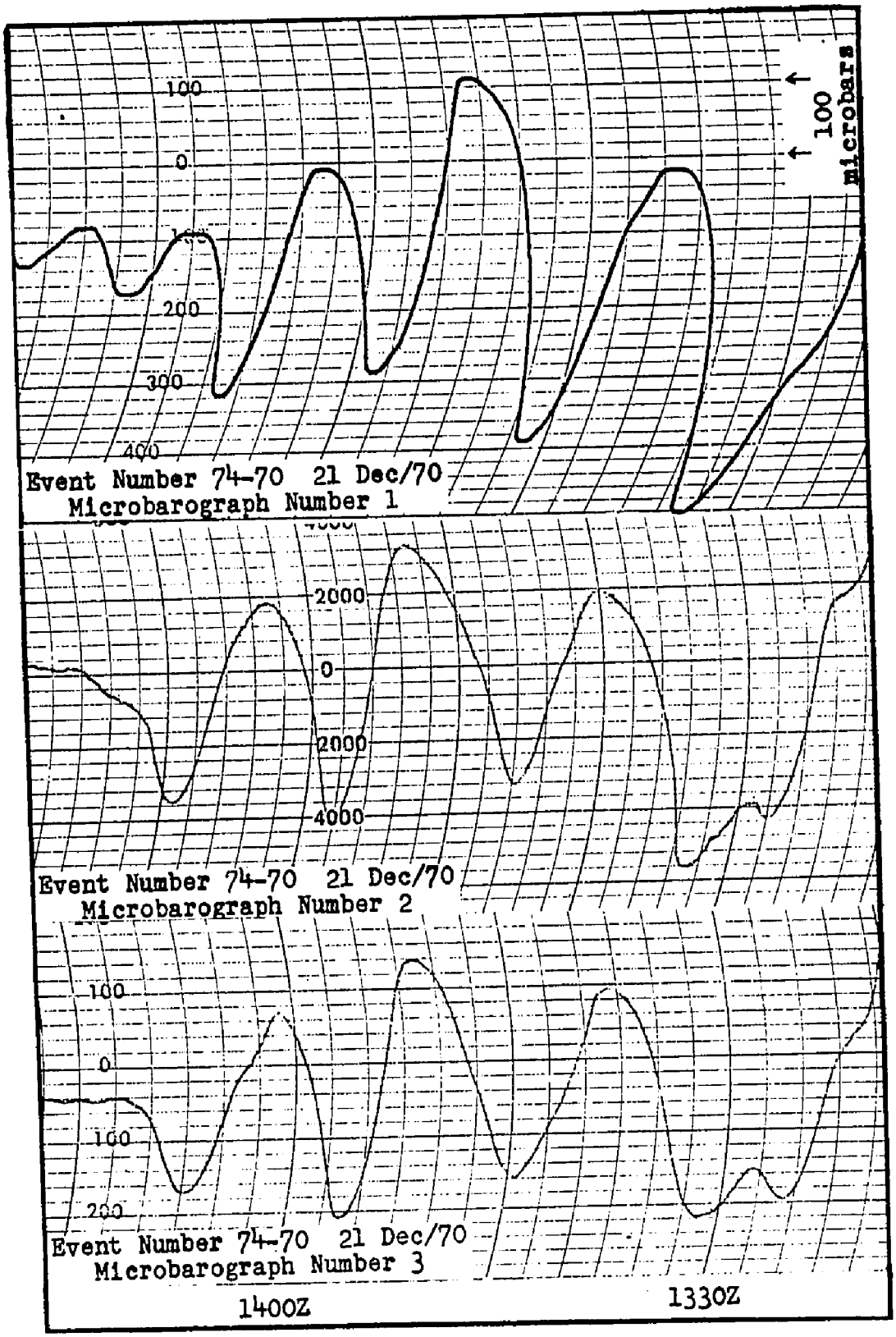

Figure C-19. Microbarograms, Event Number 74-70.

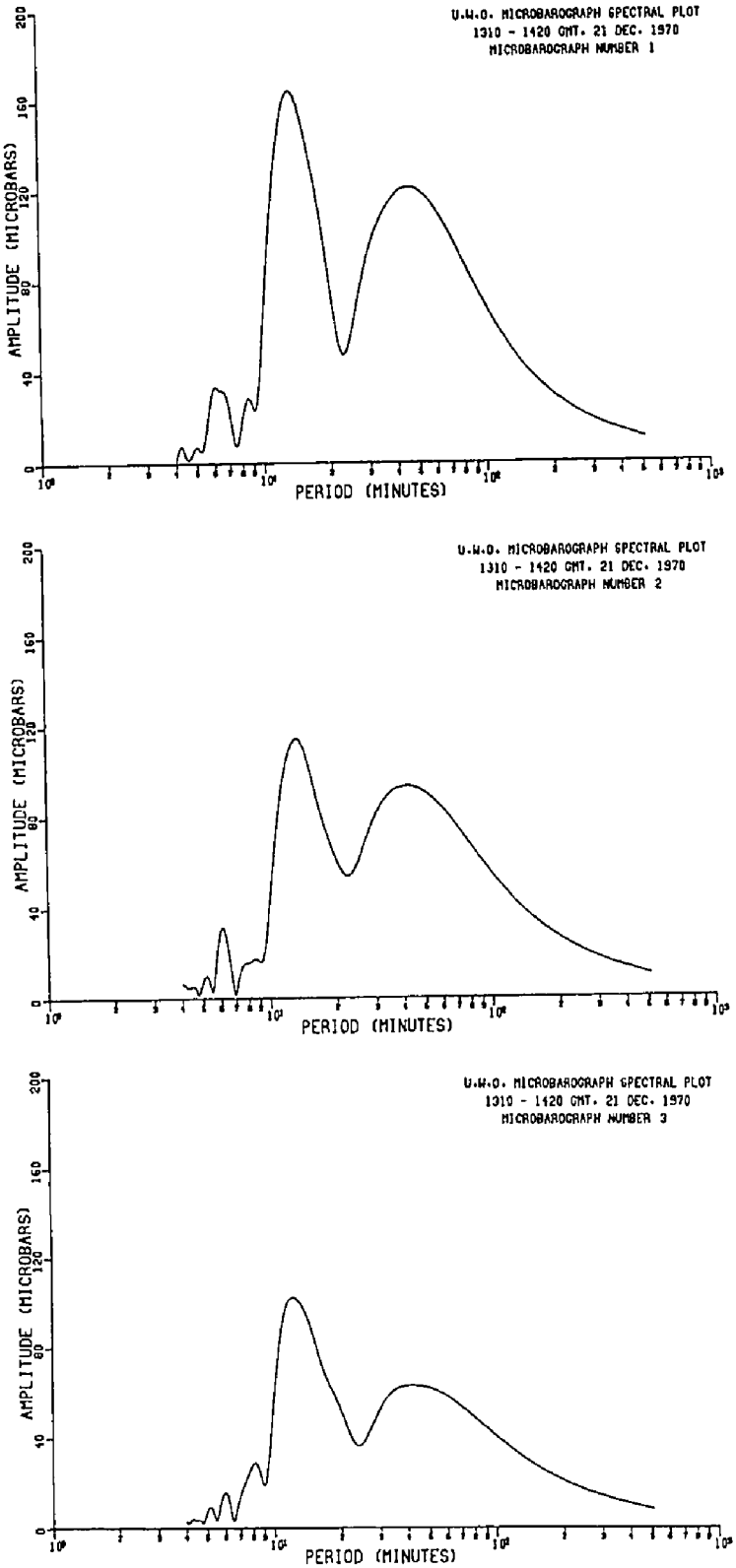

Figure C-20. Amplitude spectra, Event Number 74-70.

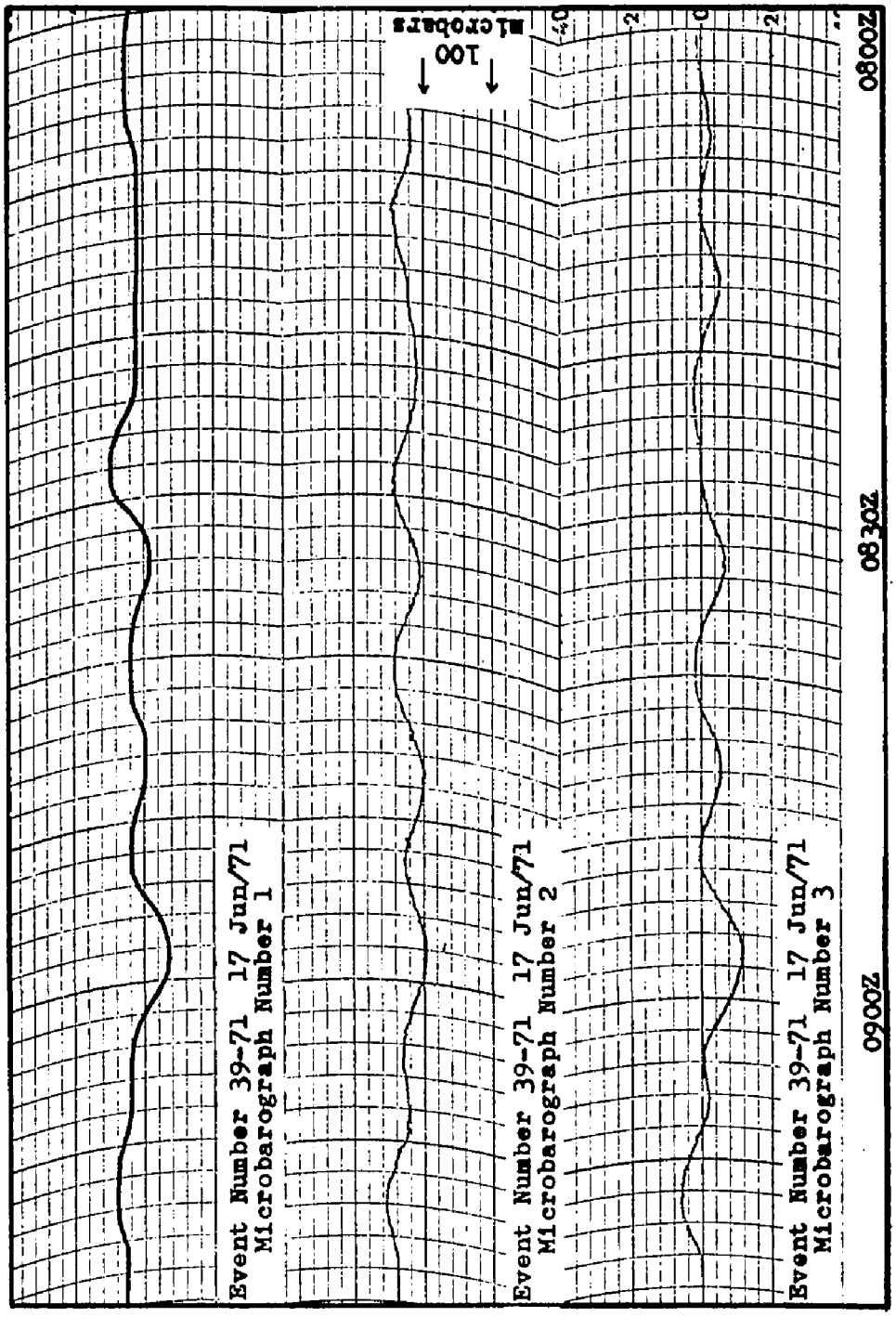

Figure C-21. Microbarograms, Event Number 39-71.

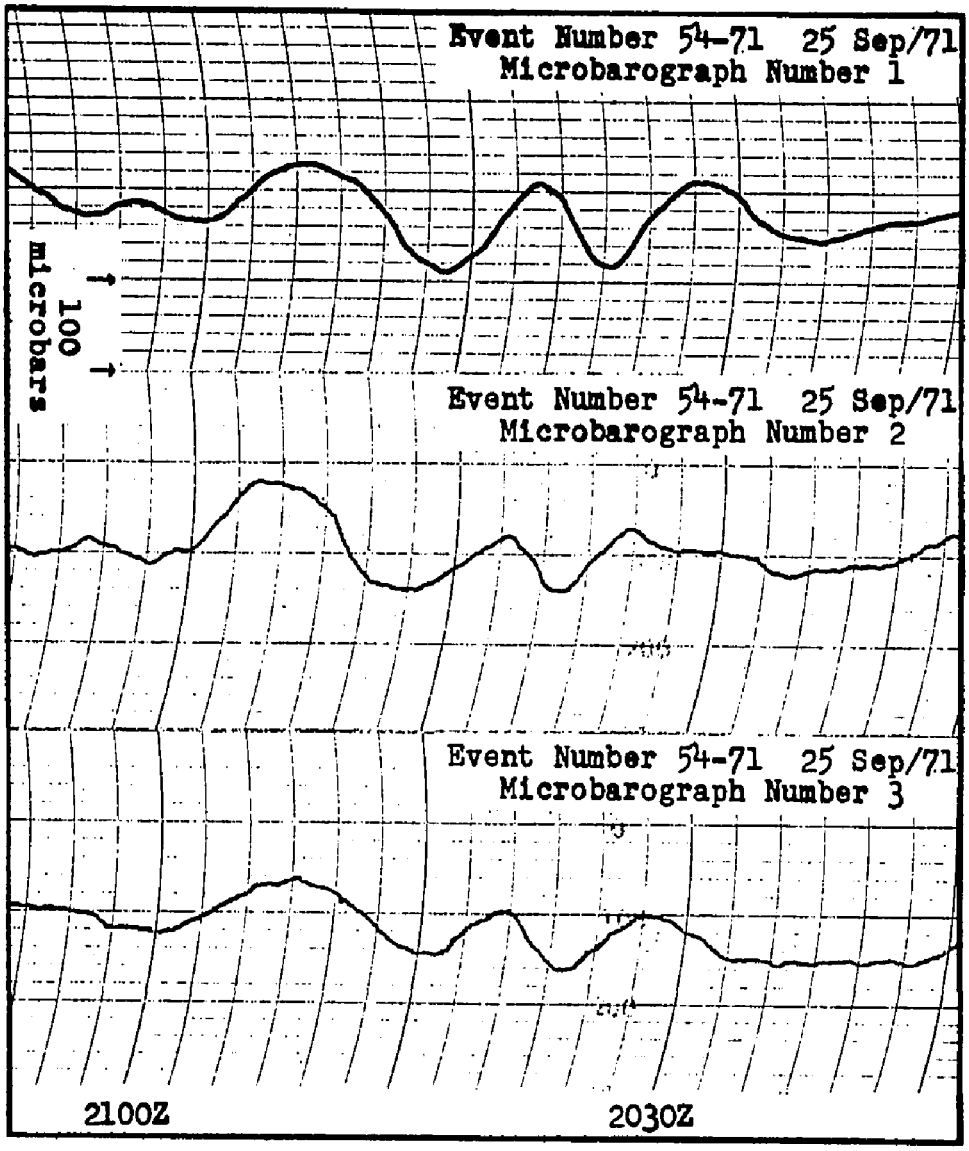

Figure C-22. Microbarograms, Event Number 54-71.

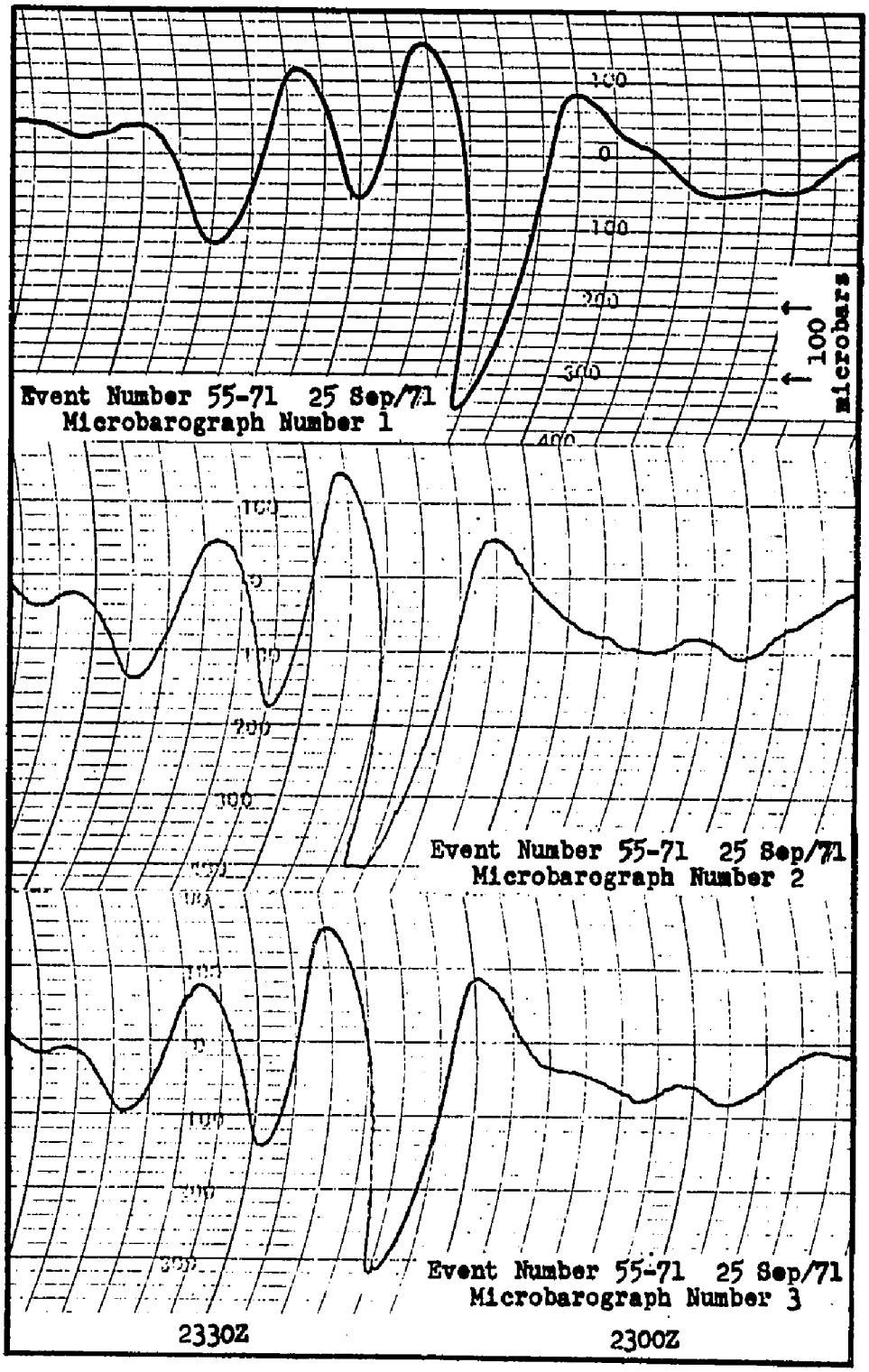

Figure C-23. Microbarograms, Event Number 55-71.

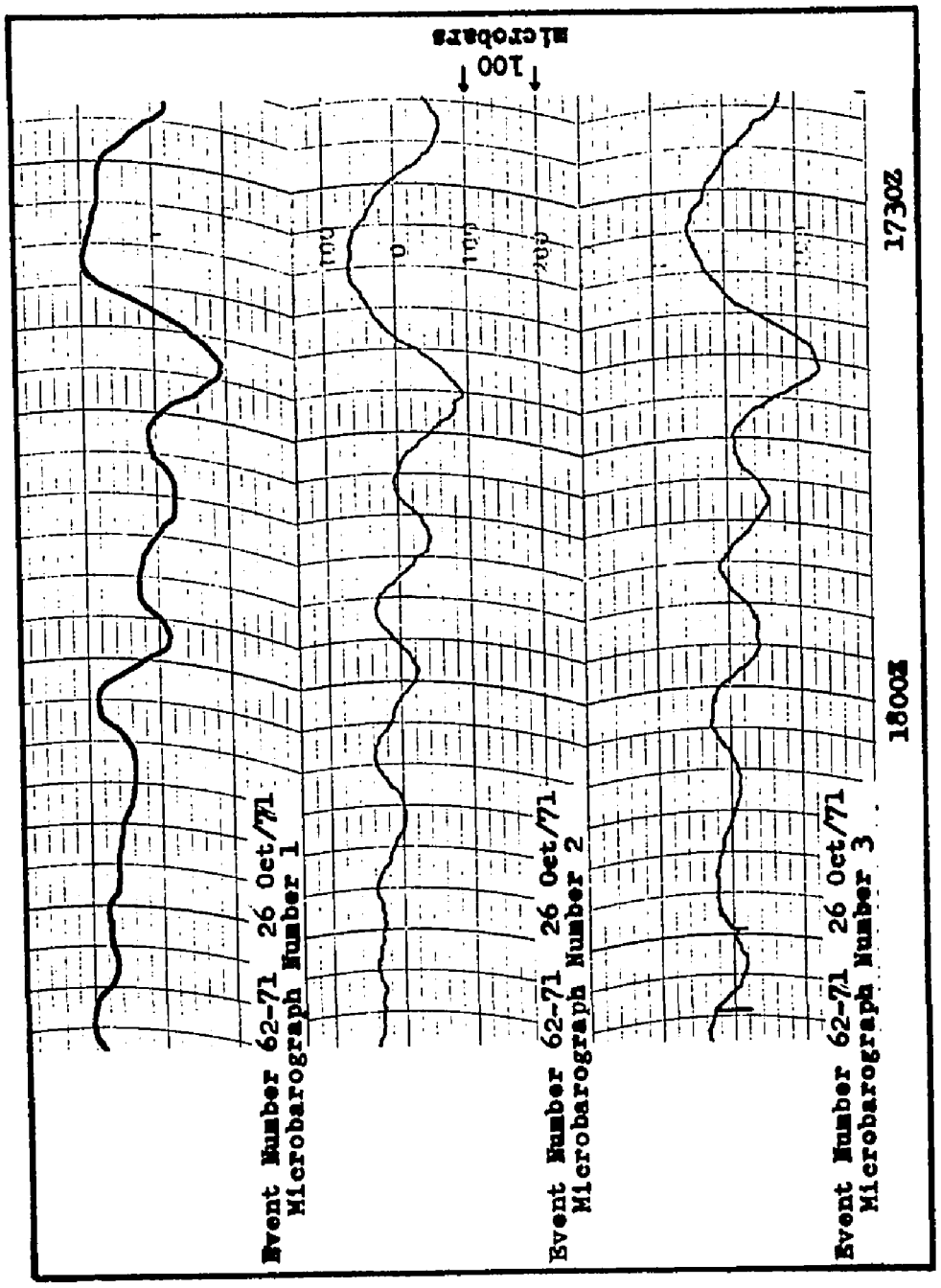

Figure C-24. Microbarograms, Event Number 62-71.

APPENDIX D

THE INVERTED MATRIX OF THE LINEARIZED PERTURBATION EQUATIONS

The matrix of the coefficients of the perturbation parameters in the linearized perturbation equations is (Chapter II)

$$\begin{bmatrix} (-iK_x gH) & (0) & (0) & (i\omega) \\ (-iK_z gH - g) & (g) & (i\omega) & (0) \\ (i\omega) & (-i\omega\gamma) & \left(\frac{\gamma - 1}{H}\right) & (0) \\ (0) & (i\omega) & \left(-\frac{1}{H} - iK_z\right) & (-iK_x) \end{bmatrix} \quad - (D1)$$

Its inverse or reciprocal matrix is then another 4 x 4 matrix

$$\left[G \right] = \begin{bmatrix} G_{11} & G_{12} & G_{13} & G_{14} \\ G_{21} & G_{22} & G_{23} & G_{24} \\ G_{31} & G_{32} & G_{33} & G_{34} \\ G_{41} & G_{42} & G_{43} & G_{44} \end{bmatrix} \quad - (D2)$$

whose elements are as shown in Table D-1.

TABLE D-1

THE ELEMENTS OF THE INVERTED MATRIX (D2)

$$G_{11} = -i(\gamma-1)\frac{g}{H}K_x + i\omega^2\gamma K_x$$

$$G_{21} = g(\gamma-1)K_xK_z - ig\frac{(\gamma-1)}{H}K_x + i\omega^2K_x$$

$$G_{31} = i\omega\gamma gHK_xK_z + (\gamma-1)g\omega K_x$$

$$G_{41} = -\omega\gamma gK_z - i\omega\gamma gHK_z^2 + i\omega^3$$

$$G_{12} = i\omega^2\gamma K_z + \frac{\omega^2}{H}$$

$$G_{22} = \frac{\omega^2}{H} + i\omega^2K_z - (\gamma-1)gK_x^2$$

$$G_{32} = i\omega^3 - i\omega\gamma gHK_x^2$$

$$G_{42} = \omega gK_x + i\omega\gamma gHK_xK_z$$

$$G_{13} = i\omega^3 - \frac{i\omega g}{H} + \omega gK_z$$

$$G_{23} = i\omega gHK_x^2 + 2\omega gK_z - \frac{i\omega g}{H} + i\omega gHK_z^2$$

$$G_{33} = \omega^2g + i\omega^2gHK_z - g^2HK_x^2$$

$$G_{43} = g^2HK_xK_z + i\omega^2gHK_x - ig^2K_x$$

$$G_{14} = i\omega^3\gamma - i(\gamma-1)\frac{\omega g}{H}$$

$$G_{24} = i\omega^3 + \omega(\gamma-1)gK_z - i\omega(\gamma-1)\frac{g}{H}$$

$$G_{34} = i\omega^2\gamma gHK_z + (\gamma-1)g\omega^2$$

$$G_{44} = i\omega^2\gamma gHK_x - i(\gamma-1)g^2K_x$$

APPENDIX E

THE DERIVATIONS OF THE PERTURBATION EQUATIONS

The basic equations which govern wave motions in the atmosphere are the equations of continuity, motion, and adiabatic state (Hines, 1960). In this Appendix, these equations are derived† and are linearized by the application of perturbation methods.

E.1 The Perturbation Parameters:

It is assumed that the perturbations in density, pressure, and fluid velocity are small with respect to the undisturbed quantities, so that terms higher than first order in the perturbation variables can be neglected in the hydrodynamic equations. It is convenient to write the perturbation parameters in the form (Georges, 1967)

$$\left.\begin{aligned} \rho &= \rho_o(1 + \rho') \\ p &= p_o(1 + p') \\ \vec{u} &= \vec{u}' \end{aligned}\right\} \qquad \text{- (E1)}$$

where the subscript o denotes the unperturbed atmosphere and the primes (') refer to the perturbation parameters. The quantities ρ' and p' are thus dimensionless.

The above definition of $\vec{u}'$ assumes that the unperturbed atmosphere is at rest.

---

† The derivations of the hydrodynamic equations presented here are similar to those given by Milne-Thomson (1962).

E.2 The Equation of Continuity:

The equation of continuity for fluid motion can be derived by considering a volume of fluid V_o in which there are no sources or sinks. Then the outward flux of mass through the surface bounding V_o must equal the rate of mass decrease within V_o:

$$\oint \rho \vec{u} \cdot d\vec{s} = -\frac{\partial}{\partial t} \int \rho \, dV \quad . \qquad - (E2)$$

The integral over the surface of V_o can be transformed to a volume integral so that the continuity condition becomes

$$\int_{V_o} \left[\frac{\partial \rho}{\partial t} + \nabla \cdot (\rho \vec{u}) \right] dV = 0 \quad . \qquad - (E3)$$

Since equation (E3) must remain valid for any V_o, the equation of continuity is simply

$$\frac{\partial \rho}{\partial t} + \nabla \cdot (\rho \vec{u}) = 0 \quad . \qquad - (E4)$$

Substitution of the perturbation parameters (E1) into (E4) results in

$$\frac{\partial \rho_o}{\partial t} + \frac{\partial}{\partial t}(\rho_o \rho') + \nabla \cdot \left[\rho_o (1+\rho') \, \vec{u}' \right] = 0 \qquad - (E5)$$

which reduces to

$$\rho_o \frac{\partial \rho'}{\partial t} + \nabla \rho_o \cdot \vec{u}' + \rho_o \nabla \cdot \vec{u}' = 0 \quad . \qquad - (E6)$$

Since ρ_o is a function of z only,

$$\vec{u}' \cdot \nabla \rho_o = u_z' \frac{\partial \rho_o}{\partial z} \qquad \text{- (E7)}$$

and so the perturbation continuity equation is

$$\rho_o \frac{\partial \rho'}{\partial t} + u_z' \frac{\partial \rho_o}{\partial z} + \rho_o \nabla \cdot \vec{u}' = 0 \quad . \qquad \text{- (E8)}$$

E.3 The Equation of Motion:

The Eulerian equation of motion is obtained by writing the net pressure force on a submerged volume of fluid as

$$- \oint p \, d\vec{s} = - \int \nabla p \, dV \quad . \qquad \text{- (E9)}$$

Thus a unit volume of fluid experiences a pressure force $-\nabla p$ and Newton's law becomes (per unit volume)

$$\rho \frac{d\vec{u}}{dt} = -\nabla p - \rho \vec{g} \quad . \qquad \text{- (E10)}$$

The quantity $d\vec{u}/dt$ is not, however, the velocity derivative of the fluid at a fixed observation point but rather the acceleration of an individual fluid particle as it moves about spatially within the fluid. Clearly, then,

$$d\vec{u} = \frac{\partial \vec{u}}{\partial t} dt + \frac{\partial \vec{u}}{\partial x} dx + \frac{\partial \vec{u}}{\partial y} dy + \frac{\partial \vec{u}}{\partial z} dz \qquad \text{- (E11)}$$

so that

$$\frac{d\vec{u}}{dt} = \frac{\partial \vec{u}}{\partial t} + (\vec{u} \cdot \nabla) \vec{u} \quad . \qquad \text{- (E12)}$$

This operation is sometimes referred to as "substantial differentiation" or "differentiation following the fluid" (Milne-Thomson, 1962).

With the inclusion of the definition (E12), the equation of motion for the fluid becomes

$$\rho \frac{\partial \vec{u}}{\partial t} + \rho(\vec{u}\cdot\nabla)\vec{u} = -\nabla p - \rho\vec{g} \quad . \qquad \text{- (E13)}$$

Substituting into (E13) the perturbation parameters as defined by equation (E1) and discarding terms higher than first order in the perturbation variables results in the perturbation equation of motion

$$\rho_o \frac{\partial \vec{u}'}{\partial t} = -p_o \nabla p' - p' \nabla p_o - \rho_o \rho' \vec{g} \quad . \qquad \text{- (E14)}$$

E.4 The Equation of Adiabatic State:

The adiabatic relation

$$\frac{p}{p_o} = \left(\frac{\rho}{\rho_o}\right)^{\gamma} \qquad \text{- (E15)}$$

becomes, with the inclusion of the equation of state

$$p = \rho R_m T \qquad \text{- (E16)}$$

and the definition of the speed of sound

$$c^2 = \gamma R_m T \quad , \qquad \text{- (E17)}$$

the adiabatic equation of state

$$\frac{dp}{dt} = c^2 \frac{d\rho}{dt} \qquad \text{- (E18)}$$

so that the perturbation equation of state can be written, using the operator defined by equation (E12), as

$$p_o \frac{\partial p'}{\partial t} + (\vec{u}' \cdot \nabla)\, p_o = c^2 \left[\rho_o \frac{\partial \rho'}{\partial t} + (\vec{u}' \cdot \nabla)\, \rho_o \right] \quad . \qquad - (E19)$$

Equations (E8), (E14), and (E19) form the set of perturbation equations which describe the wave motion. These linearized equations can be solved in the manner discussed in Chapter II.

APPENDIX F

THE MEASUREMENT OF THE DIAMETER OF THE MICROBAROGRAPH INLET TUBES

It was noted in Chapter III that the accuracy of the determination of the response characteristic of the microbarograph depends upon the accuracy to which the internal diameter of the capillary tubing is known. The measurement of this parameter was done in the following way.

A section of the copper tubing used was clamped in a horizontal position and was connected to a constant-level reservoir positioned some three meters above. Water was allowed to flow through the tubing under the influence of the constant hydrostatic head ρgh, and the rate of flow was measured by weighing the mass of water which passed through the tube in a known interval of time. The rate of flow of mass through the tubing is given by

$$\frac{\Delta M}{\Delta t} = \rho \frac{\pi d^2}{4} \bar{v} \qquad - (F1)$$

where $\bar{v}$, the average flow velocity within the tube, is given by (Milne-Thomson, 1962)

$$\bar{v} = \frac{d^2}{32\mu} \frac{\rho g h}{L} \qquad - (F2)$$

Thus $\overline{d^4}$, the average value of the fourth power of the internal diameter of the section of tubing, can be found directly as

$$\overline{d^4} = \frac{128}{\pi} \frac{\mu}{\rho^2} \frac{L}{gh} \frac{\Delta M}{\Delta t} \qquad - (F3)$$

The length of the tube L and the hydrostatic head h can be easily measured. A careful measurement of the water temperature, with reference to standard tables, provides accurate value of μ and ρ. It is then possible, having measured $\Delta M/\Delta t$, to obtain the value of $\overline{d^4}$ with an uncertainty of less than 1%.

APPENDIX G

THE MICROBAROGRAPH SITES

The instrument sites referred to in Chapter III (Figure 10) were chosen to provide not only appropriate geometry for the direction finding analysis but also sufficient access to the atmosphere so that the records obtained would be accurate representations of the microstructure of atmospheric pressure.

Instrument number 1 was located in a spacious laboratory on the second floor of the Physics Building at the University. This building is one of the oldest on the campus and is neither centrally air-conditioned nor hermetically sealed. Access to the atmosphere is gained primarily through leaks around the windows.

Site number 2 was in a storage area in the basement of a large industrial building. Although most of this plant is centrally air-conditioned and thus subject to an artificial pressure regime, the storage area is not since this area is immediately adjacent to a service elevator shaft which is open to the atmosphere at the site of the hoisting machinery on the roof of the building.

Microbarograph number 3 was located in a basement storage room of a single-storey private home. Again the primary means of access to the atmosphere was via leaks around the basement windows. Care was taken to ensure that these windows were not sealed tightly.

It was judged that site number 1 afforded the least access to the atmosphere. Accordingly, tests were carried out to

determine whether the microbarograms obtained at this site were being altered by the response characteristics of the room itself. With the microbarograph operating on the ±50 microbar scale (a factor of ten more sensitive than for the observations reported in this thesis), no effect could be observed in the trace as a result of opening the windows. In a separate test, one microbarograph was left in the laboratory (site number 1) with all windows and doors closed, and another was removed to an adjacent room where the windows were opened wide. The records obtained from the two instruments were compared and no significant difference was observed.

It is therefore concluded that the microbarograms obtained in this experiment have not been significantly altered by the pneumatic behaviour of the instrument sites.

REFERENCES

Atlas, D. (1963). Radar analysis of severe storms. Meteor. Monographs, 5, 27, 177-220

Baker, D.M., and Davies, K. (1969). F2-region acoustic waves from severe weather. J. Atmos. Terrestr. Phys. 31, 1345-1352

Beer, T. (1972). Atmospheric waves and the ionosphere. Contemp. Phys. 13, 247-271

Berry, F.A. Jr., Bollay, E., and Beers, N.R. (1945). Handbook of Meteorology. (McGraw-Hill, New York)

Blackman, R.B., and Tukey, J.W. (1958). The Measurement of Power Spectra. (Dover Publications, Inc., New York)

Bracewell, R.N. (1965). The Fourier Transform and its Applications. (McGraw-Hill, New York)

Bretherton, F.P. (1969). Lamb waves in a nearly isothermal atmosphere. Quart. J. Roy. Meteor. Soc. 95, 754-757

Brooks, E.M. (1954). Characteristics of thunderstorm microbarograms. Trans. Amer. Geophys. Union 35, 413-419

Brunt, D. (1927). The period of simple vertical oscillations in the atmosphere. Quart. J. Roy. Meteor. Soc. 53, 30-32

Challinor, R.A. (1968). Long period infrasonic waves in the atmosphere. J. Atmos. Terrestr. Phys. 30, 1817-1822

Cochran, W.T. et al (IEEE G-AE Subcommittee on Measurement Concepts) (1967). What is the Fast Fourier Transform?. IEEE Trans. Audio and Electroacoustics AU-15, 2, 45-55

Connes, J. (1961). Rev. d'Opt. 40, 45, 116-171. Quoted by Jacquinot and Roizen-Dossier (1964)

Cooley, J.W., and Tukey, J.W. (1965). An algorithm for the machine calculation of complex Fourier series. Math. of Computat. 19, 90, 297-301

Cunningham, R.M. (1958). Cumulus circulation. In: Recent Advances in Atmospheric Electricity. Edited by L.G. Smith (Pergamon Press, New York)

Curry, M.J. (1968). Microbarographic studies of thunderstorms. M.Sc. Thesis, University of Western Ontario

Eckart, C. (1960). Hydrodynamics of Oceans and Atmospheres. (Pergamon Press, New York)

FitzGerald, K. (1770). An account of some improvements made in a new wheel barometer. Phil. Trans. Roy. Soc. London 60, 74-79

Flauraud, E.A., Mears, A.H., Crowley, F.A. Jr., and Crary, A.P. (1954). Investigations of microbarometric oscillations in eastern Massachusetts. USAF Cambridge Research Center, Geophysical Research Paper No. 27

Forman, M.L. (1966). Fast Fourier Transform technique and its application to Fourier spectroscopy. J. Opt. Soc. Amer. 56, 978-979

Fullerton, C.M. (1966). An analytical investigation of sinusoidal microbarometric oscillations. Ph.D. Thesis, New Mexico Institute of Mining and Technology

Georges, T.M. (1967). Ionospheric effects of atmospheric waves. Institute for Environmental Research, Technical Report IER 57-ITSA 54

Georges, T.M. (1968). Short-period ionospheric oscillations associated with severe weather. In: Acoustic-gravity waves in the atmosphere. Symposium Proceedings, Boulder, Colorado, 15-17 July 1968. (U.S. Government Printing Office, Washington)

Gossard, E.E. (1960). Spectra of atmospheric scalars. J. Geophys. Res. 65, 10, 3339-3351

Gossard, E.E., and Munk, W. (1954). On gravity waves in the atmosphere. J. Meteor. 11, 4, 259-269

Herron, T.J., and Tolstoy, I. (1969). Tracking jet stream winds from ground level pressure signals. J. Atmos. Sci. 26, 266-269

Hines, C.O. (1960). Internal atmospheric gravity waves at ionospheric heights. Can. J. Phys. 38, 1441-1481

Hines, C.O. (1965). Atmospheric gravity waves: a new toy for the wave theorist. U.S. Nat. Bur. Standards, J. Res., Sec. D, Radio Science 69, 3, 375-380

Hines, C.O. (1968). A possible source of waves in noctilucent clouds. J. Atmos. Sci. 25, 5, 937-942

Hsu, H.P. (1970). Fourier Analysis. (Simon and Schuster, New York)

Jacquinot, P., and Roizen-Dossier, B. (1964). Apodisation. In: Progress in Optics, Vol. III, ed. E. Wolf (North Holland Publishing Co., Amsterdam) pp. 29-186

Jenkins, G.M., and Watts, D.G. (1969). Spectral Analysis and its Applications. (Holden-Day, Inc., San Francisco)

Jordan, A.R. (1972). Atmospheric gravity waves from winds and storms. J. Atmos. Sci. 29, 445-456

Kortschinski, J. (1964). Design and construction of a microbarograph. B.E.Sc. Project Report, University of Western Ontario

Kortschinski, J., Murty, R.C., and Curry, M.J. (1971). Microbarograph for meteorological studies: design, theory, and analysis. J. Phys. E: Sci. Instrum. 4, 307-310

Lange, F.H. (1967). Correlation Techniques. Trans. P.B. Johns. (Iliffe Books Ltd., London)

Liu, C.H., and Yeh, K.C. (1971). Excitation of acoustic-gravity waves in an isothermal atmosphere. Tellus 23, 2, 150-163

McCracken, D.D., and Dorn, W.S. (1964). Numerical Methods and FORTRAN Programming. (John Wiley and Sons, New York)

Madden, T.R., and Claerbout, J.F. (1968). Jet stream associated gravity waves and implications concerning jet stream stability. In: Acoustic-gravity waves in the atmosphere. Symposium Proceedings, 15-17 July 1968 (U.S. Government Printing Office, Washington)

Malan, D.J. (1963). Physics of Lightning. (The English Universities Press, London)

Martyn, D.F. (1950). Cellular atmospheric waves in the ionosphere and troposphere. Proc. Roy. Soc. London, Ser. A 201, 216-234

Marwitz, J.D., and Auer, A.H. Jr. (1968). Cloud nuclei spectra and updrafts beneath convective cloud bases in the high plains. J. Applied Meteor. 7, 449-451

Milne-Thomson, L.M. (1962). Theoretical Hydrodynamics. 4th Edition (MacMillan, London)

Mood, A.M., and Graybill, F.A. (1963). Introduction to the Theory of Statistics. 2nd Edition. (McGraw-Hill, New York)

Murty, R.C., and Curry, M.J. (1969). Microbarographic observation of acoustic gravity waves. Nature 224, 5215, 169-170

Naito, K. (1966). Internal gravity-shear waves in the troposphere II. Wave amplitudes. Can. J. Phys. 44, 2275-2285

Pasechnik, I.P. (1959). Long period atmospheric waves preceding thunderstorms. Akad. Nauk. SSSR, Izvestia, Ser. Geofiz. No. 3, 471-475

Petterssen, S. (1956). Weather Analysis and Forecasting. 2nd Edition. Vol. II (McGraw-Hill, New York)

Pierce, A.D. (1965). Propagation of acoustic-gravity waves in a temperature- and wind-stratified atmosphere. J. Acoust. Soc. Amer. 37, 2, 218-227

Pierce, A.D., and Coroniti, S.C. (1966). A mechanism for the generation of acoustic-gravity waves during thunderstorm formation. Nature 210, 5042, 1209-1210

Pothecary, I.J.W. (1954). Short-period variations in surface pressure and wind. Quart. J. Roy. Meteor. Soc. 80, 345, 395-401

Shaw, W.N., and Dines, W.H. (1905). The study of the fluctuations of atmospheric pressure. Quart. J. Roy. Meteor. Soc. 31, 39-52

Tolstoy, I., and Herron, T.J. (1969). A model for atmospheric pressure fluctuations in the mesoscale range. J. Atmos. Sci. 26, 270-273

Vonnegut, B. (1963). Some facts and speculations concerning the origins and role of thunderstorm electricity. Meteor. Monographs 27, 5, 224-241

Wood, J.A. (1968). Meteorites and the Origin of Planets. (McGraw-Hill, New York)

Yamamoto, R. (1955). The microbarographic oscillations produced by the explosions of hydrogen bombs in the Marshall Islands. Weather 10, 321-325

Yamamoto, R. (1968). Propagation velocity of acoustic gravity wave due to large nuclear explosion. In: Acoustic gravity waves in the atmosphere. Symposium Proceedings, Boulder, Colorado, 15-17 July 1968 (U.S. Government Printing Office, Washington)